Inertial Navigation System Algorithms for Low Cost IMU

Xiaoying Kong

Department of Mechanical and Mechatronic Engineering
The University of Sydney

August 27, 2000

August 2000
Australian Centre for Field Robotics
Department of Mechanical and Mechatronic Engineering
The University of Sydney

This thesis is submitted to The University of Sydney in fulfillment of the requirements for the degree of **Doctor of Philosophy**. The thesis is entirely my own work and, except where otherwise stated, describes my original research.

Xiaoying Kong

Abstract

This thesis describes the development of strapdown Inertial Navigation System (INS) algorithms for low cost Inertial Measurement Units (IMU). The term "low cost IMU" is used to describe an IMU built with standard low grade gyros and accelerometers which cannot conduct self-alignment. These algorithms motivated the development of the INS error models and the Global Positioning System (GPS) error models for low cost aiding in autonomous navigation.

This thesis has three principle contributions. The first is the development of strapdown INS velocity, position and attitude error propagation models for large angle errors in the computer frame approach. There are two sets of the models. The first set uses psi angles to describe attitude errors. The other uses quaternions. These models differ from other INS error models that they do not require small angle assumptions. The second contribution is the development of low cost INS algorithms using the INS error models developed in this thesis. There are two algorithms which use the two sets of INS models. The main contribution of these algorithms is the in-motion alignment approach with unknown initial conditions. The implementation of the algorithm using the psi angle model involves the Extended Kalman Filter (EKF). The quaternions algorithm uses the Distribution Approximation Filter (DAF). GPS measurements are used to aid INS. It is argued that the quaternions approach gives better accuracy and requires less computation. The third contribution is the GPS modelling in the frequency domain. The equations of GPS position errors are derived to be identical second order systems in the frequency domain. Feedback and feedforward filters for GPS error de-correlation using INS information are presented.

The theoretical work is verified by a set of experiments using real data. A standard GPS is used to verify the GPS modelling. The experimental results using a low cost IMU and an aiding DGPS have shown that position, velocity and attitude accuracy can be achieved using the algorithms presented in this thesis.

Acknowledgments

I would like to thank all the people who encouraged and supported me during the undertaking of this thesis.

Firstly I would like to thank Professor Hugh Durrant-Whyte, the leader of the Australia Centre of Field Robotics, for giving me the opportunity to pursue PhD study at the University of Sydney. Hugh's support and expertise have proved invaluable. I would like to thank my supervisor, Dr. Eduardo Nebot, for his unwavering enthusiasm and support. Eduardo's expertise and support have also been invaluable.

There are many people I would like to thank for their many and varied inputs. Thanks goes to the entire Sydney University mechatronics crowd: Kee-Choon Wong, David Rye, Gamini Dissanayake, Julio Rosenblatt, Ha Quang, Chris Mifsud, Michael Stevens, Raj Madhavan, José Guivant, Paul Newman, Som Majumder, Miguel Santos, Stefan Baiker, Monica Louda, Eric Nettleton, Keith Willis, Adrian Bonchis, Tim Bailey, Steve Clark, Mihaly Csorba, Mohamad Bozorg and Daniel Pagac. Special thanks to Steve Scheding and Stefan Williams for frequently correcting my English, to Simon Julier for discussing the filters, to Salah Sukkarieh for hardware support, to K.Y. Lee for fixing my computer, to Nguyen Hong Quang and Anh Tuan Le for being friends, and to Grace Wong and Lynda Brown for their spiritual encouragement.

I owe my greatest debt to my parents who have been looking after my baby girl overseas. I would like to express my deepest gratitude to my husband, without his love and encouragement and moral support, I could not have finished the study.

Contents

List of Figures

Chapter 1

Introduction

1.1 The Objectives of this Thesis

This thesis develops algorithms for low cost inertial navigation systems (INS) based on INS error propagation models. The algorithms are intended for use by a low cost inertial measurement unit (IMU) to provide accurate navigation information, as position, velocity and attitude, of the vehicle which carries the INS. The term "low cost IMU" is used to describe an IMU built with standard low grade gyros and accelerometers.

To achieve the goal of algorithm development, three issues are addressed in this thesis:

- Development of INS error models appropriate for low cost IMUs which determine the accuracy and behaviour of the INS.
- Designing and tuning of the filter algorithms for such INS .
- Identifying sensor models which will be used in the filter algorithms.

1.2 Common Coordinate Systems Used in Navigation

Fundamental to the process of inertial navigation is the precise definition of a number of Cartesian coordinate reference systems or frames [1]. Each frame is an orthogonal,

right handed axis set.

The following INS frames are defined and used in this thesis.

- *Inertial frame (i-frame)* is the frame in inertial space. Its origin is at the centre of the Earth and axes are non-rotating with respect to the fixed stars.
- *Earth frame (e-frame)* is an earth-fixed frame whose origin is at the Earth centre, x axis points to the north pole, y axis points to the Greenwich meridian in the equatorial plane and the z axis completes the system to a right-hand coordinate system.
- *Body frame (b-frame)* is a frame fixed to the vehicle. The accelerations and angular rates generated by the strapdown accelerometers and gyros are measured in $b-$frame.
- *Computer frame (c-frame)* is the local level frame at the INS computed position.
- *Platform frame (p-frame)* is the frame in which the transformed accelerations from the accelerometers and angular rates from the gyros are solved.
- *True frame (t-frame)* is the true local level frame at the true position.
- *Navigation frame (n-frame)* is a user defined frame for navigation output. Any frame defined above can be chosen as the navigation frame.

The schema of these frames are shown in the following chapters.

The Global Positioning System (GPS) is another navigation source used in this thesis. The World Geodetic System WGS-84 is a coordinate system for GPS. WGS-84 is an Earth-centred Earth-fixed reference frame defined as follows [2]:

Origin: Earth's centre of mass.

z-axis: Parallel to the direction of the conventional international origin for polar motion, as defined by the Bureau International De L'HEURE (BIH) on the basis of the latitudes adopted for the BIH stations.

x-axis: Intersection of the WGS-84 reference meridian plane and the plane of the mean astronomic equator, the reference meridian being parallel to the zero meridian defined by the Bureau International De L'HEURE on the basis of the longitudes adopted for the BIH stations.

y-axis: Completes a right-handed Earth-centred, Earth-fixed orthogonal coordinate system, measured in the plan of the mean astronomic equator 90 degrees east of the x-axis.

1.3 INS Error Models

An IMU usually contains a set of three orthogonal-installed accelerometers and three orthogonal-installed gyros. When the accelerometers and the gyros are directly installed in the vehicle body, the INS is called a strapdown INS (SINS). An inertial navigation system is a real time algorithm to calculate the position, velocity and attitude of the vehicle which carries the INS by integrating the acceleration and rotation rate signals from an IMU.

The velocity and the position are calculated by double integration of the sum of the gravitational acceleration and the non-gravitational acceleration from the three accelerometers. For a strapdown INS, these integrations are performed in the coordinate system in which the three accelerometers are installed. By integrating the rotation rate signals from three gyros, the angular orientation of the three accelerometers is determined. The calculated acceleration, velocity and position are transformed into the desired navigation coordinate system by this orientation information.

Figure 1.1 shows the INS process. There are two main phases for INS operation: the alignment phase and the navigation phase. The integration sequence starts from the initial velocity, position and attitude. The process for determining these INS initial conditions is called alignment. Any INS has to undergo this initial alignment phase before it starts to navigate.

Any errors in either the alignment phase or the navigation phase will be integrated

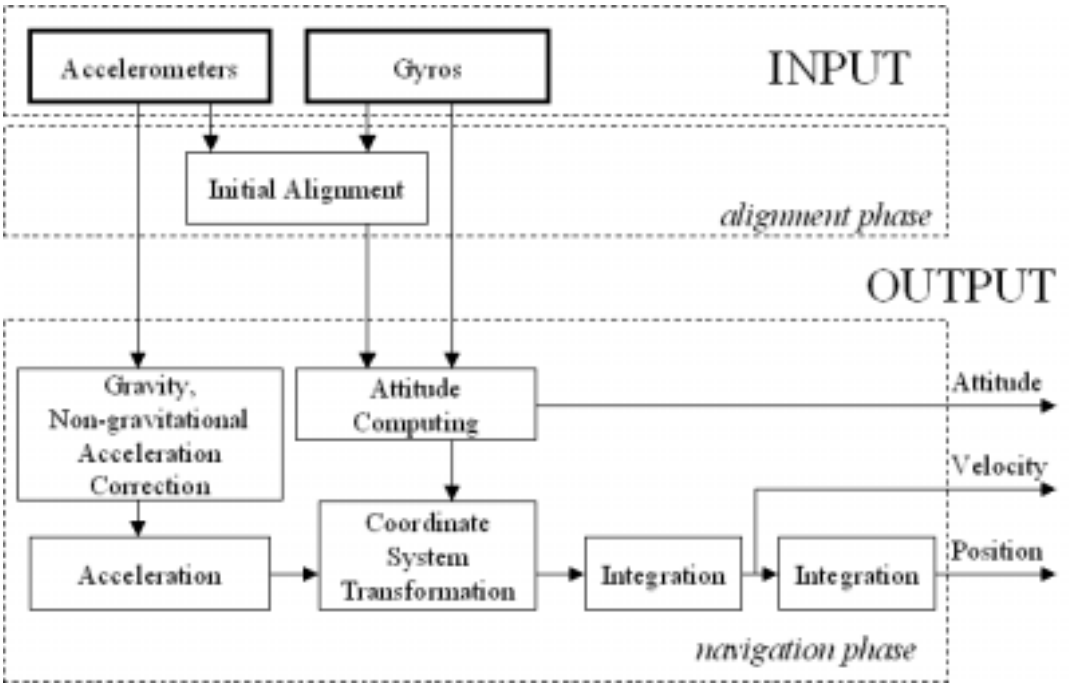

Figure 1.1: Inertial Navigation System

and will propagate over time. These errors determine the performance and the navigation accuracy of the INS. Error analysis is based on error models. Error models also serve for real-time failure detection and for the implementation of a data fusion filter in the INS algorithms [3].

Most of the literature on INS is concerned with INS error propagation analysis and models. There are two approaches to the derivation of INS error models [4]. One is known as the phi-angle approach or the true frame approach. The other is known as the psi-angle approach or the computer approach. The phi-angle approach perturbs the INS equations in the local-level north-pointing Cartesian coordinate system that corresponds to the true geographic location of the INS. The psi-angle approach perturbs the INS equations in the computer frame which is the local-level north-pointing coordinate system that corresponds to the geographic location computed by the INS. It has been shown that the models from these two approaches are equivalent and yield identical results [5, 6, 7]. Modelling procedures and the perturbation rules have been

unified in reference [3].

Most of the literature for INS modelling makes the assumption that all perturbation attitude errors are small angles. The coordinate transformation in the modelling is therefore presented by some approximation matrices.

However, in many cases, this small angle assumption will not hold. IMUs with low accuracy cannot measure the earth rate which is the key vector for INS alignment. The initial heading will be unknown. The corresponding attitude error in both the phi-angle model and the psi-angle model could be up to ± 180 degrees making the small angle approximation not valid.

In recent literature, attempts to model INS propagation errors with an unknown heading were presented. Stepanov *et al.* presented a model considering a large heading error and small tilt errors using the true frame [8]. Scherzinger developed a modified psi angle model with arbitrary heading and small tilt errors using the psi-angle approach [9, 10]. Four states are used to describe three psi angles. The psi angle ψ_z which represents the correspondent heading error is split into two states $\sin(\psi_z)$ and $\cos(\psi_z)$.

Other INS models related to land vehicles and robotics applications are presented in references [11, 12].

So far, an accurate psi angle model for three large error angles has not been discussed in the literature. *Development of such a psi angle model for all large attitude errors using three single psi angles is one of the main contributions of this thesis.*

An INS may compute the attitude using Euler angles, the direction cosine matrix or the quaternions. The quaternions method is advantageous since it requires less computation, gives better accuracy and avoids singularity [13]. Some INS error models using quaternions have been developed using the infinitesimal angle assumption [13, 14, 15].

Error models using quaternions for three large errors have not been discussed in the literature. *The development of a quaternion based INS error propagation model for large errors is another contribution of this thesis.*

1.4 Integrated INS Algorithms Using Error Models

The purpose of INS error modelling is to develop a model for INS algorithms. *Based on the two sets of models developed in this thesis, two INS algorithms are developed for low cost IMU.*

The term "low cost INS" in this thesis is used to describe an INS built with low cost IMU components whose sensitivity is not enough to measure the earth rate. The earth rate is a key input to INS initial alignment using gyrocompassing. In a case when the earth rate cannot be measured by an INS, the alignment will not be performed properly. To obtain the initial attitude, external sensors have to be used [16]. An in-motion alignment algorithm makes use of other navigation information to determine the attitude of the IMU. The Global Positioning System and other navigation sensors are commonly used as aiding information for INS alignment purposes. The Kalman filter is the most commonly used algorithm for fusing INS and other navigation data in both INS alignment and navigation phases.

The Kalman filter is a linear statistical algorithm used to recursively estimate the states of interest [17]. In INS algorithms, the states of interest usually consist of the errors of the vehicle velocity, position, attitude, IMU sensor biases, errors from other navigation systems and other relevant vehicle parameters. To aid in the estimation of the states, the Kalman filter requires two models: the process model and the observation model. The process model describes the propagation of the states. The observation model describes the information supplied by a sensor as a function of the states, together with a model of measurement noise. INS error propagation models are the main process models used in most of the literature.

Many common processes cannot be represented adequately using linear models. The psi angle model and the quaternions model developed in this thesis are based on nonlinear models. The Extended Kalman Filter (EKF) is the most widely used approach for a nonlinear filter algorithm [18]. The EKF predicts the states of the system under the assumption that its process model and observation model are locally linear.

The filter models are expanded using Jacobians. However, there are some problems with the EKF [19]. The implementation difficulty of Jacobians is one shortcoming of the EKF. The problems of the EKF motivated the development of a new filter algorithm called the Distribution Approximation Filter (DAF) [19, 20, 21, 22, 23].

In this thesis, the EKF and DAF are used for the two INS algorithms respectively. The algorithm with the psi angle model as the process model will use the EKF. The quaternions model algorithm will use the DAF.

INS provides high frequency information and is considered a dead reckoning sensor with an error that grows unbounded with time. External navigation sensors commonly aid INS. GPS can provide low frequency navigation information without drift over time. The integration of INS and GPS has been widely used for navigation. In this thesis, GPS is used for observation to aid the INS.

There are important error sources in GPS measurement. GPS errors should be modelled and estimated in the filter. This thesis presents new GPS shaping filters which describe the GPS frequency characters.

1.5 Main Contributions of this Thesis

The main contributions of this thesis are:

- The development of psi angle models in computer frame for large attitude errors.
- The development of quaternion models for large attitude errors.
- GPS modelling in the frequency domain.
- The development of an INS algorithm for low cost IMU using the psi angle approach.
- The development of an INS algorithm for low cost IMU using the quaternion approach.

These contributions are verified by a set of experimental implementations using a low cost IMU and a GPS.

1.6 The Structure of this Thesis

This thesis does not have one central literature review. Rather, the literature relevant to a particular topic will be cited at the beginning of each chapter.

Chapter 2 addresses the first two contributions of this thesis: development of generic INS error propagation models for large attitude errors in the psi angle approach and the quaternion approach.

The INS error models in the literature are reviewed at the beginning of this chapter. The psi angle approach, the phi angle approach and the quaternion model in the literature are also discussed. None of the models assumes three large attitude errors.

The INS error propagation models for large errors in the psi angle approach are developed in this chapter. There are three models: the velocity error model, the position error model and the attitude model. The models in three large errors, one large heading error and two tilts errors, and three small errors are also examined.

Another set of INS models in quaternions for large errors is derived. The computer approach is also used in these models. The quaternions and the frames used in this approach are discussed. The quaternion error propagation models for large misalignment of the platform frame and the computer frame are extended.

Chapter 3 details the modelling of the GPS errors in the frequency domain. GPS is the aiding navigation source for the INS algorithm. The chapter begins by reviewing the previous work on GPS modelling in the frequency domain.

A GPS position error model is derived. It is proved that the transfer function of the GPS position error in any frame has the identical poles and zero as the pseudo-range error. The modelling method using power spectral density of the noise is detailed.

The de-correlation of the GPS coloured noise is also described. A shaping filter is introduced to take into account the coloured noise. An example is also presented using

feedforward and feedback filters.

Chapter 4 addresses the design of an INS algorithm for low cost IMUs with unknown initial conditions using the psi angle approach in the computer frame.

The analytic coarse alignment method and gyrocompassing, which are the major methods for self-alignment, are discussed. A new in-motion alignment is proposed.

In this chapter, a new algorithm is developed in the computer frame using the psi angle approach with an unknown initial attitude using a low cost INS aided by a GPS.

The coarse alignment on ground for raw data process and IMU turn-on biases estimation is discussed. A method to determine the coarse initial cosine direction matrix is also presented.

Chapter 5 develops an INS algorithm for low cost IMUs in the computer frame using quaternions. Quaternions errors are exploited using the misalignment of the computer frame and the platform frame. The entire filter process model structure and the process noise are discussed. The process noise vectors are reconstructed by a linear combination of the white noise on the accelerometers and gyros in the body frame.

The Distribution Approximation Filter (DAF) is used to implement this algorithm. The principle and the benefit of the DAF are briefly described.

Chapter 6 presents the experimental results for the INS algorithms using the psi angle approach and the quaternion approach and GPS modelling.

Results of GPS modelling in the frequency domain are discussed. Modelling results are shown. Power spectral density (PSD) of raw GPS position data and the calculated PSDs by using the model parameters are compared by using a set of figures from the experiments using a GPS receiver. The GPS model is validated with a set of plots in the frequency domain and the time domain using the feed back de-correlation filter.

The experimental results are presented to verify the psi angle models, the quaternion models and the INS algorithms for low cost IMU. The experiment uses a low cost IMU aided by a DGPS. The results show how the heading errors are corrected from $\pm 180^{\circ}$ to $\pm 0.1^{\circ}$.

Finally, **Chapter 7** summarizes the main contributions of this study and provides

suggestions for further research.

Chapter 2

INS Error Propagation Models

2.1 Introduction

This chapter develops generic INS error propagation models for large attitude errors using the psi angle approach and the quaternion approach.

Two approaches have been adopted in the literature: the psi angle approach and the phi angle approach. The psi angle model and the phi error model are reviewed briefly in Sections 2.2.4 and 2.2.5. In recent years, some models have been developed for large heading errors in different frames. So far, there are no generic error propagation models for large attitude errors. All quaternion error models in the literature use the small angle assumption.

The INS error propagation models for large errors in the psi angle approach are developed in Section 2.3. There are three models: the velocity error model, the position error model and the attitude model. The velocity error model is developed in Section 2.3.1. The position error model has no difference between small angles and large angles. Section 2.3.3 presents the psi angle model with all large error angles. The models for three large errors, one large heading error and two tilt errors, and three small errors are also discussed.

Another type of INS model using quaternions for large errors is developed in Section 2.4. The computer approach is also used in these models. The quaternions and the

frames used in this approach are discussed in Section 2.4.1. The velocity error model in the quaternion approach is developed in Section 2.4.2. The quaternion error propagation models for large misalignment of the $p-$frame and the $c-$frame are extended in Section 2.4.4.

2.2 INS Error Models Review

2.2.1 INS Error Models Review

In the design and operation of an INS, navigation errors determine INS performance and accuracy.

Error models are developed by perturbing the nominal differential equations whose solution yields the INS output of velocity, position and orientation. The nominal equations are based on Newton's law. The basic equations can be expressed in different coordinate systems or frames. In 1992, Goshen-Meskin and Bar-Itzhack presented a unified approach and systematic methodology for developing INS error models [3]. It was demonstrated that the error models developed in the different forms are equivalent. A developer's tool was presented in their work which indicated the model developing steps to follow. Their INS error models had methodologies that produced equivalent results [3].

In 1988, Bar-Itzhack and Berman approached the analysis of INS from a control theory point of view [4]. The differential equations that describe INS error behaviour were divided into equations describing the propagation of the translatory errors and equations describing the propagation of the attitude errors. Both the translatory and attitude error equations can be expressed in two different ways that yield two versions of the translatory error equations and two versions of the attitude error equations. The two versions of the translatory equations depend on whether the equations are position error components or velocity error components. The two versions of the attitude equations depend on whether the equation variables are components of the platform to computer frame attitude difference, or components of the platform to true frame

attitude difference. All of these versions are equivalent [6, 7].

These two approaches for INS error analysis are known as the phi angle approach and the psi angle approach. The phi angle approach is also called the perturbation approach or true frame approach. In the phi angle approach, the navigation equations and error models are solved in the true frame ($t-$frame). The psi angle approach is also called the computer frame approach and solves the navigation equations in the computer frame ($c-$frame).

Benson [5] derived error equations for INS using the perturbation approach and the psi angle approach. This work shows the underlying assumptions and allows direct comparison of the two methods. The two approaches are equivalent and yield identical results.

The psi-angle error equation in the strapdown INS developed by Bar-Itzhack [24] proved that apart from a sign change, the psi-angle differential equation in the error analysis of the strapdown INS is identical to the one used in a conventional gimbled INS.

There are some other INS error models but all are based on the assumption that the angle errors are small [25, 26, 27].

2.2.2 INS Error Models for Azimuth Uncertainty

Both the psi angle and the phi angle approaches assume that the INS attitude errors are small.

Analytic coarse alignment and gyrocompassing based on the measurement of the gravity vector and the earth rate vector are the main principles for INS alignment. High quality IMUs with high resolution can measure the earth rate. This aids the INS initial alignment to reduce the initial attitude error to satisfy the small angle assumption. This method cannot be used with low cost IMUs because they are not sensitive enough to determine the earth rate. External heading sensors and tilt sensors have to be employed to obtain the INS initial attitude.

A general error model for large attitude errors in all dimensions is required to avoid

the use of external heading and tilt sensors.

So far, only a few works have attempted to model large angle errors and to consider, for example, large heading uncertainty of IMU orientation.

Pham introduced a Kalman filter mechanization for the INS airstart system in 1992 [28]. This approach used two nonlinear states to describe one heading angle. The attitude errors were not modelled. Dmitriyev, Stepanov and Shepel [8] presented an INS error model considering large heading uncertainty and small tilt misalignment errors using a true frame perturbation approach. The heading uncertainty is solved with a piecewise-Gaussian approximation of a posterior density function. The error model is built in the true frame with the assumption of two small tilt misalignments and one large misalignment. The nonlinear characteristic of the problem is considered in a short period. As a result, the heading misalignment rate is assumed to be zero. In the misalignment error models, the rates of misalignment angles are coupled with the velocity errors and the velocity errors are coupled with misalignment angles.

An approximate extended psi-angle model with large heading misalignment is presented in [9, 10] by Scherzinger using four states to describe the three psi-angles. The model extension is very involved.

In Scherzinger's model, an extended misalignment vector Ψ_e is defined as:

$$\Psi_e = [\psi_x, \psi_y, \sin\psi_z, \cos\psi_z - 1]^T \tag{2.1}$$

with the psi angle $[\psi_x, \psi_y, \psi_z]^T$ being the misalignment of the computer frame and the platform frame.

The psi angle model for large azimuth misalignment is derived as:

$$\dot{\overline{\Psi_e}} = -\begin{bmatrix} (\overline{\omega_{ic}^c})_{e+} \\ --- \\ 0_{1\times 4} \end{bmatrix} \times \overline{\Psi_e} + \begin{bmatrix} 0_{2\times 1} \\ \omega_x\psi_y - \omega_y\psi_x \\ 0 \end{bmatrix} - \begin{bmatrix} \overline{\varepsilon^p} \\ --- \\ 0 \end{bmatrix} \tag{2.2}$$

where $(\overline{\omega_{ic}^c})_{e+}$ is the extended 1×4 vector of the rate between the computer frame. $\overline{\varepsilon^p}$ is gyro error in p-frame and the inertial frame. $[\omega_x, \omega_y, \omega_z]^T$ is the vector of the

misalignment angular rate. For small azimuth misalignment, the error model turns to:

$$\dot{\overline{\Psi}_e} = -\begin{bmatrix} (\overline{\omega_{ic}^c})_{e+} \\ - - - \\ 0_{1\times 4} \end{bmatrix} \times \overline{\Psi}_e - \begin{bmatrix} \overline{\varepsilon^p} \\ - - - \\ 0 \end{bmatrix} \tag{2.3}$$

which has a similar form to the psi angle model developed in the literature by Benson [5] and Bar-Ithzack [24].

General INS error propagation models for all large angles have not been investigated in the past. Models in the quaternion form have not been thoroughly investigated either.

In this chapter, general error models for three large attitude errors will be developed. Two approaches are used in the error models: the psi angle approach and the quaternion approach.

2.2.3 Quaternion Error Models Review

INS attitude calculation is based on the methods of Euler angles, direction cosine matrix and quaternions. The psi angle model is applicable to the Euler angles and direction cosine matrix methods. The quaternion method is more effective as it provides more accuracy, requires less computation and avoids singularity in computation.

Error models in quaternions are consequently important when quaternion methods are used.

Friedland [14] presented a number of models for a strapdown INS based on quaternions including dynamics and error propagation models. Small attitude errors assumption is implied. Vathsal [15] derived error equations for quaternion propagation in spacecraft navigation also with the small angle assumption. Roumeliotis and Sukhatme [29] modelled quaternions in attitude as a constant plus a white noise using the infinitesimal angle assumption. Another quaternion error differential equation was developed by Crassidis and Markley [30] where the Riccati trajectories were introduced into error quaternion trajectories. A numerical solution form of the quaternion error was given by Lovren and Pieper [25]. The scale, skew and drift errors of INS were presented in the numerical quaternion form.

In 1998, Lee, Roh and Park [13] proposed equivalent tilt error models which were applicable to the analysis of the terrestrial strapdown inertial navigation system based on quaternions. In this work the computer approach was used. To derive the velocity and the attitude error models, small angle assumptions were considered to satisfy equivalent tilt angle definition.

In situations where initial attitudes are unknown or large attitude perturbation occurs, the previous INS error models will not satisfy the small angle assumption. So far, to the best of the author's knowledge there are no large error models employing quaternions.

In this chapter, an INS velocity error model, a position error model and an attitude error model are developed in the quaternion method in the computer frame. The velocity error propagation is presented using quaternions. Attitude errors are presented by the misalignment of the computer frame and the platform frame. Quaternion errors are solved in the computer frame. No small angle assumption is made in the model development. The models are suitable for both three small and large attitude errors cases.

2.2.4 Psi Angle Approach Review

In the psi angle approach introduced by Benson [5], the navigation equations are solved in the computer frame ($c-$frame). Error propagation models are derived from perturbation of the $c-$frame solution. See Figure 2.1.

The computer frame ($c-$frame) is defined as the local level frame located at the INS computed position. The platform frame ($p-$frame) is the frame in which the transformed accelerations and angular rates from the accelerometers and gyros are resolved. Psi-angle (ψ) is the angle between the $c-$frame and the $p-$frame. $\psi = [\psi_x, \psi_y, \psi_z]^T$.

The velocity and attitude error models of the psi angle approach for small angles are briefly introduced here.

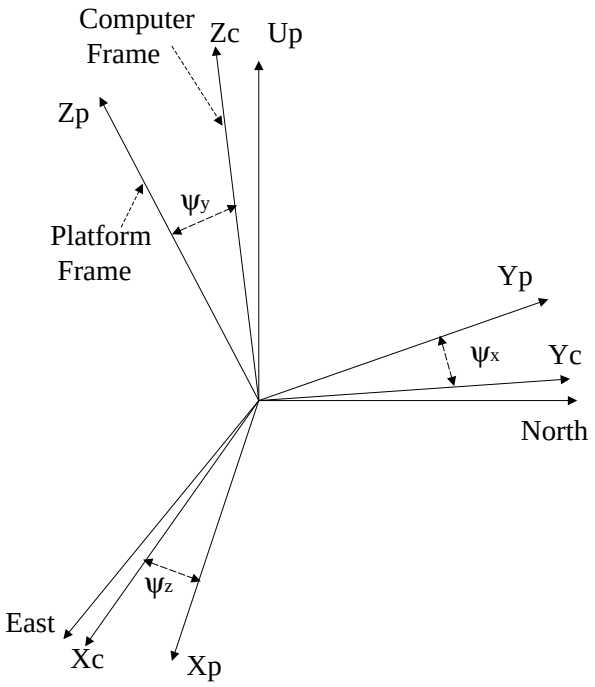

Figure 2.1: Computer frame, platform frame and three psi angles.

Velocity Error Model

The true INS velocity equation in the $c-$frame is given by:

$$\dot{V_t^c} = f_t^c + g_t^c - (2\Omega_{ie}^c + \Omega_{ec}^c)V_t^c \tag{2.4}$$

where $V_t^c = [V_{tx}^c, V_{ty}^c, V_{tz}^c]^T$ is the true velocity in the c-frame, f_t^c is the true specific force in the c-frame, g_t^c is the true gravity in the c-frame, Ω_{ie}^c is the earth rate in the c-frame and Ω_{ec}^c is the rotation rate from the c-frame to the earth frame. In the following $\widehat{\ }$ represents observation and Δ represents error.

Ω_{ie}^c and Ω_{ec}^c are the skew symmetric matrices of ω_{ie}^c and ω_{ec}^c. In the east-north-up frame with the local latitude φ :

$$\omega_{ie}^c = \begin{bmatrix} 0 \\ \omega_{ie}\cos(\varphi) \\ \omega_{ie}\sin(\varphi) \end{bmatrix} \tag{2.5}$$

$$\omega_{ec}^{c} = \begin{bmatrix} -V_y^c/R_y \\ V_x^c/R_x \\ V_x^c tg(\varphi)/R_x \end{bmatrix} \tag{2.6}$$

where $V^c = [V_x^c, V_y^c, V_z^c]^T$ is the INS velocity in the computer frame. $R = [R_x, R_y, R_z]^T$ is the vector from the earth centre to the vehicle position.

The INS solves the following velocity $\hat{V}^c$:

$$\dot{\hat{V}}^{c} = f_t^p + \nabla^p + \hat{g}^c - (2\Omega_{ie}^c + \Omega_{ec}^c)\hat{V}^c \tag{2.7}$$

where f_t^p is the true specific force in the p-frame and ∇^p is the specific force error due to accelerometers' errors.

Assuming the psi angles are small, the velocity errors are solved in the c-frame by subtracting (2.7) from (2.4) :

$$\Delta\dot{V}^c = -\Psi \times f_t^c + \nabla^p + \Delta g^c - (2\Omega_{ie}^c + \Omega_{ec}^c)\Delta V^c \tag{2.8}$$

Ψ is the skew symmetric matrix of ψ angles given by:

$$\Psi = \begin{bmatrix} 0 & -\psi_z & \psi_y \\ \psi_z & 0 & -\psi_x \\ -\psi_y & \psi_x & 0 \end{bmatrix} \tag{2.9}$$

The gravity vector error is given by:

$$\Delta g^c = [-\omega_s^2 \Delta R_x^c, -\omega_s^2 \Delta R_y^c, -\omega_s^2 \Delta R_y^c] \tag{2.10}$$

ω_s is the Schuler frequency defined as $\omega_s = \sqrt{g/r_e}$, being g the gravity constant and r_e the earth radius.

Position Error Model

The position error model in the c-frame is derived from the velocity error model and is given by Benson [5]:

$$\Delta\dot{R}^c = -\Omega_{ec}^c \Delta R^c + \Delta V^c \tag{2.11}$$

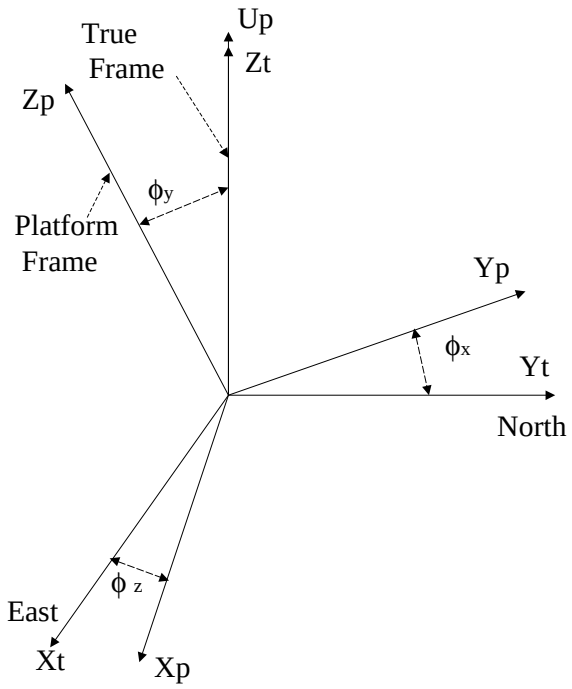

Figure 2.2: True frame and platform frame.

Attitude Error Model - Psi Angle Model

The psi angle model was introduced by Benson [5] and Bar-Itzhack [24]:

$$\dot{\psi^p} = -\omega_{ip}^p \times \psi^p + \epsilon^p \tag{2.12}$$

where $\dot{\psi^p}$ is the angular velocity of the $p-$frame with respect to the c-frame, ϵ^p is the gyro drift rate in the platform frame. ω_{ip}^p is the angular velocity of the $p-$frame in the $p-$frame with respect to the inertial frame ($i-$frame).

2.2.5 Phi Angle Approach

In the phi angle approach, see Figure 2.2, the frame in which the navigation equations are solved is the true frame (t-frame).

The true frame is the true local level frame at the true position.

The phi angle $\phi = [\phi_x, \phi_y, \phi_z]^T$ is the angle between the true frame and the platform frame.

Velocity Error Model

Similar to the navigation equations in the computer frame, the true velocity equation in the true frame is:

$$\dot{V}_t^t = f_t^t + g_t^t - (2\Omega_{ie}^t + \Omega_{et}^t)V_t^t \tag{2.13}$$

where $V_t^t = [V_x^t, V_y^t, V_z^t]^T$ is the true velocity in the t-frame, f_t^t is the true specific force in the t-frame, g_t^t is the true gravity in the t-frame, Ω_{ie}^t is the earth rate in the t-frame and Ω_{ec}^t is the rotation rate from the c-frame with respect to the earth frame. Also Ω_{ie}^t and Ω_{ec}^t are the skew symmetric matrices of ω_{ie}^t and ω_{ec}^t.

Considering the same sources of errors, the INS velocity is:

$$\dot{\hat{V}}^t = (f_t^p + \nabla^p) + \widehat{g} - (2\Omega_{ie}^t + \Omega_{et}^t)\hat{V}^t \tag{2.14}$$

The skew symmetric matrix Φ of the phi angle is:

$$\Phi = \begin{bmatrix} 0 & -\phi_z & \phi_y \\ \phi_z & 0 & -\phi_x \\ -\phi_y & \phi_x & 0 \end{bmatrix} \tag{2.15}$$

For small phi angles, the direction cosine matrix between the $p-$frame and the $t-$frame holds the relationship:

$$C_p^t = \begin{bmatrix} 1 & -\phi_z & \phi_y \\ \phi_z & 1 & -\phi_x \\ -\phi_y & \phi_x & 1 \end{bmatrix} = I_{3\times 3} - \Phi \tag{2.16}$$

where $I_{3\times 3}$ is the 3×3 identity matrix.

The velocity error model for small phi angles is then derived by subtracting (2.13) from (2.14):

$$\Delta\dot{V}^t = -\Phi \times f_t^p + \nabla^p + \Delta g^t - (2\Omega_{ie}^t + \Omega_{ec}^t)\Delta V^t \tag{2.17}$$

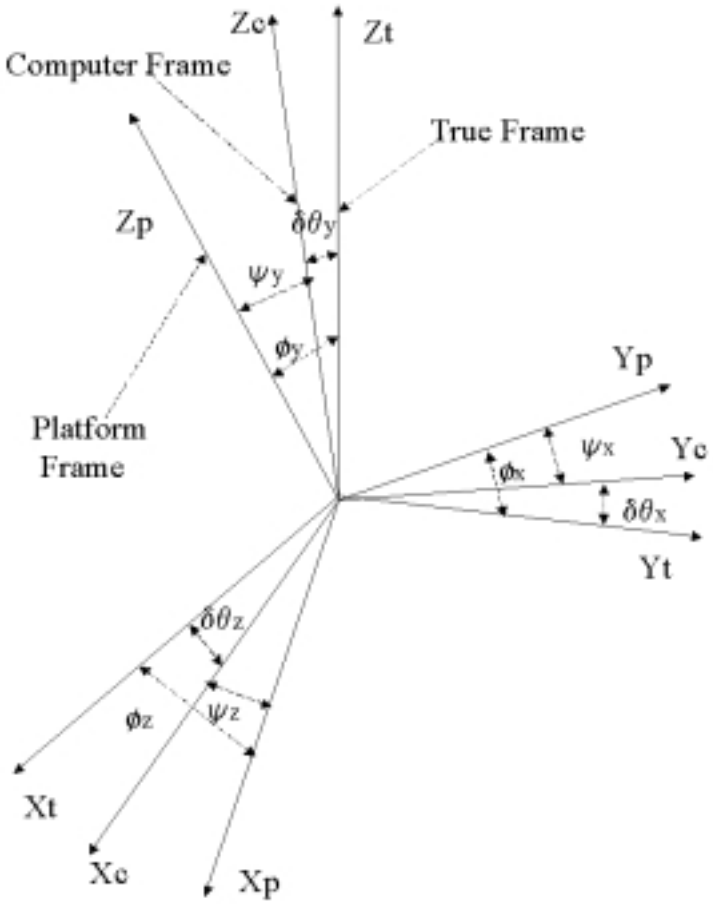

Figure 2.3: Computer frame, platform frame and true frame.

Attitude Error Model - Phi Angle Model

Let ω_{tp}^{p} be the angular velocity of the platform frame with respect to the true frame and let $\dot{\phi}$ be the small angle approximation of ω_{tp}^{p} and define the difference of the psi angle ψ and the phi angle ϕ as $\delta\theta = [\delta\theta_x, \delta\theta_y, \delta\theta_z]^T$. See Figure 2.3.

$$\delta\theta = \phi - \psi \tag{2.18}$$

Identify $\delta\omega$ as:

$$\delta\omega = \delta\theta + \omega_{it}^{t} \times \delta\theta \tag{2.19}$$

The phi angle equation is given by [5, 3, 9]:

$$\omega_{tp}^{p} = \dot{\phi} = -\omega_{ip}^{p} \times \phi + \delta\omega + \varepsilon^{p} \tag{2.20}$$

where ε^{p} is the gyro drift in the $p-$frame.

Compared with the psi angle model (2.12), the phi angle model (2.20) contains the item $\delta\omega = \delta\theta + \omega_{it}^{t} \times \delta\theta$.

Considerable comparison of the psi angle model and the phi angle model has been conducted in the literature [6, 7, 3, 5]. The equivalence of these two models has been proven by Benson and other authors in [6, 7, 3, 5].

2.2.6 Summary

The INS error models have been categorized into two identical approaches: the psi angle approach and the phi angle approach. Most of the models make the small angle assumption. Recently, there has been some work on error models assuming small tilts and large heading errors. To the best of the author's knowledge, INS error propagation models with three large attitude errors have not been presented before. The goal of this chapter is to develop an INS velocity error propagation model, a position error propagation model and a psi angle error model in the computer frame for all large attitude errors. The error models in quaternion form will also be developed in this chapter. The applications of these models will be discussed in the following chapters.

2.3 Development of Psi Angle Model for Large Errors

The INS velocity and position error models and the psi angle model for large angle errors in the computer approach will be developed in this section using the computer frame (c-frame) and the platform frame (p-frame).

2.3.1 Velocity Error Propagation Model

The true velocity equation in the c-frame is given by:

$$\dot{V}_t^c = f_t^c + g_t^c - (2\Omega_{ie}^c + \Omega_{ec}^c)V_t^c \tag{2.21}$$

The INS computer solves the following velocity $\hat{V}^c$:

$$\dot{\hat{V}}^c = f_t^p + \nabla^p + \hat{g}^c - (2\Omega_{ie}^c + \Omega_{ec}^c)\hat{V}^c \tag{2.22}$$

where f_t^p is the true specific force in the p-frame and ∇^p is the specific force error due to the errors of the accelerometers.

Subtracting (2.22) by (2.21), the velocity error $\Delta V^c = \hat{V}^c - V_t^c$ solved in the c-frame is given by

$$\Delta\dot{V}^c = f_t^p - f_t^c + \nabla^p + \Delta g^c - (2\Omega_{ie}^c + \Omega_{ec}^c)\Delta V^c \tag{2.23}$$

The specific forces in the c-frame (f_t^c) and the p-frame (f_t^p) have the following relationship:

$$f_t^c = C_p^c \times f_t^p \tag{2.24}$$

$$f_t^p = C_c^p \times f_t^c \tag{2.25}$$

where C_p^c is the direction cosine matrix (DCM) between the p-frame and the c-frame and $C_c^p = (C_p^c)^{-1}$. Therefore the velocity error model is:

$$\Delta\dot{V}^c = (C_c^p - I_{3\times3})f_t^c + \nabla^p + \Delta g^c - (2\Omega_{ie}^c + \Omega_{ec}^c)\Delta V^c \tag{2.26}$$

$$= (I_{3\times3} - C_p^c)f_t^p + \nabla^p + \Delta g^c - (2\Omega_{ie}^c + \Omega_{ec}^c)\Delta V^c \tag{2.27}$$

Let

$$s_x = \sin(\psi_x), c_x = \cos(\psi_x) \tag{2.28}$$

$$s_y = \sin(\psi_y), c_y = \cos(\psi_y)$$

$$s_z = \sin(\psi_z), c_z = \cos(\psi_z)$$

For large ψ angle the matrix C_p^c is given by:

$$C_p^c = \begin{bmatrix} c_y c_z - s_y s_x s_z & -c_x s_z & s_y c_z + c_y s_x s_z \\ c_y s_z + s_y s_x c_z & c_x c_z & s_y s_z - c_y s_x c_z \\ -s_y c_x & s_x & c_y c_x \end{bmatrix} \tag{2.29}$$

The specific force is transferred to the $p-$frame using (2.27) instead of (2.26).

Equations (2.27) and (2.29) present the general velocity error propagation model for large attitude errors.

In the case when ψ_x, ψ_y and ψ_z are all small, C_p^c can be simplified.

$$\begin{aligned} s_x &= \sin(\psi_x) = \psi_x, c_x = \cos(\psi_x) = 1 \\ s_y &= \sin(\psi_y) = \psi_y, c_y = \cos(\psi_y) = 1 \\ s_z &= \sin(\psi_z) = \psi_z, c_z = \cos(\psi_z) = 1 \end{aligned} \tag{2.30}$$

and

$$\sin(\psi_x)\sin(\psi_y) = \sin(\psi_y)\sin(\psi_z) = \sin(\psi_z)\sin(\psi_x) = 0 \tag{2.31}$$

Thus:

$$C_p^c = I_{3\times 3} + \Psi \tag{2.32}$$

$$C_c^p = I_{3\times 3} - \Psi \tag{2.33}$$

where the skew symmetric matrix Ψ is given by (2.9).

Under the three small angles assumption, the velocity error Equation (2.27) becomes

$$\begin{aligned} \Delta\dot{V}^c &= (I_{3\times 3} - C_p^c) f_t^p + \nabla^p + \Delta g^c - (2\Omega_{ie}^c + \Omega_{ec}^c)\Delta V^c \\ &= \Psi \times f_t^p + \nabla^p + \Delta g^c - (2\Omega_{ie}^c + \Omega_{ec}^c)\Delta V^c \qquad (2.34) \\ &= -\Psi \times f_t^c + \nabla^p + \Delta g^c - (2\Omega_{ie}^c + \Omega_{ec}^c)\Delta V^c \qquad (2.35) \end{aligned}$$

Equations (2.34) or (2.35) and (2.32) or (2.33) are identical to the velocity error model usually presented in the literature.

It is important to study the case of large uncertainties in heading and low uncertainties in tilt angles, that is large ψ_z and small ψ_x and ψ_y angles. With this assumption, C_p^c in (2.27) can be approximated by [31]:

$$C_p^c = \begin{bmatrix} c_z & -s_z & \psi_y c_z + \psi_x s_z \\ s_z & -c_z & \psi_y s_z - \psi_x c_z \\ -\psi_y & \psi_x & 1 \end{bmatrix} \tag{2.36}$$

Then the matrix $I_{3\times 3} - C_p^c$ in the velocity error model is given by:

$$I_{3\times 3} - C_p^c = \begin{bmatrix} 1-\cos\psi_z & \sin\psi_z & -\psi_x \sin\psi_z - \psi_y \cos\psi_z \\ -\sin(\psi_z) & 1-\cos(\psi_z) & +\psi_x \cos(\psi_z) - \psi_y \sin(\psi_z) \\ \psi_y & -\psi_x & 0 \end{bmatrix} \tag{2.37}$$

The velocity error model with large heading error and small tilt errors is:

$$\begin{aligned} \Delta\dot{V}^c = & \begin{bmatrix} 1-\cos(\psi_z) & \sin(\psi_z) & -\psi_x \sin(\psi_z) - \psi_y \cos(\psi_z) \\ -\sin(\psi_z) & 1-\cos(\psi_z) & +\psi_x \cos(\psi_z) - \psi_y \sin(\psi_z) \\ \psi_y & -\psi_x & 0 \end{bmatrix} f_t^p \\ & + \nabla^c + \Delta g^c - (2\Omega_{ie}^c + \Omega_{ec}^c)\Delta V^c \end{aligned} \tag{2.38}$$

2.3.2 Position Error Propagation Model

The position error model is the same as for the small angle case:

$$\Delta\dot{R}^c = -\Omega_{ec}^c \Delta R^c + \Delta V^c \tag{2.39}$$

2.3.3 Psi Angle Error Model

A new general psi-angle model that can be used with large angle errors is derived in this section.

The true transformation matrix C_b^c, which is the direction cosine matrix from the b-frame to the c-frame, is obtained from [27]:

$$\dot{C}_b^c = C_b^c \Omega_{ib}^b - \Omega_{ic}^c C_b^c \tag{2.40}$$

The INS solves C_b^p , which is the direction cosine matrix from the b-frame to the p-frame, using measured gyro rates $\hat{\Omega}_{ib}^b$ provided by the IMU:

$$\dot{C_b^p} = C_b^p \hat{\Omega}_{ib}^b - \Omega_{ic}^c C_b^p \tag{2.41}$$

The rates $\hat{\Omega}_{ib}^b$ contain gyro drift errors $\in^b$:

$$\hat{\Omega}_{ib}^b = \Omega_{ib}^b + \in^b \tag{2.42}$$

$\in^b$ is the skew symmetric matrix of the gyro drift vector $[\epsilon_x^b, \epsilon_y^b, \epsilon_z^b]^T$ in the body frame:

$$\in^b = \begin{bmatrix} 0 & -\epsilon_z^b & \epsilon_y^b \\ \epsilon_z^b & 0 & -\epsilon_x^b \\ -\epsilon_y^b & \epsilon_x^b & 0 \end{bmatrix} \tag{2.43}$$

Let

$$\Delta C = C_b^p - C_b^c \tag{2.44}$$

Then

$$\begin{aligned} \Delta C &= C_b^p - C_b^c && (2.45) \\ &= C_b^p - C_p^c C_b^p \\ &= (I_{3\times 3} - C_p^c) C_b^p && (2.46) \end{aligned}$$

$\dot{\Delta C}$ can be derived from (2.46) and (2.41). Differentiating equation (2.46), we have:

$$\begin{aligned} \dot{\Delta C} &= (I_{3\times 3} - C_p^c)\dot{C_b^p} - \dot{C_p^c} C_b^p && (2.47) \\ &= (I_{3\times 3} - C_p^c)(C_b^p \hat{\Omega}_{ib}^b - \Omega_{ic}^c C_b^p) - \dot{C_p^c} C_b^p \\ &= C_b^p \hat{\Omega}_{ib}^b - \Omega_{ic}^c C_b^p - C_p^c C_b^p \hat{\Omega}_{ib}^b + C_p^c \Omega_{ic}^c C_b^p - \dot{C_p^c} C_b^p \end{aligned}$$

$\dot{\Delta C}$ can also be obtained directly from $\Delta C = C_b^p - C_b^c$. Differentiating C_b^p and C_b^c we get:

$$\begin{aligned} \dot{\Delta C} &= \dot{C_b^p} - \dot{C_b^c} && (2.48) \\ &= C_b^p \hat{\Omega}_{ib}^b - \Omega_{ic}^c C_b^p - C_b^c \Omega_{ib}^b + \Omega_{ic}^c C_b^c \\ &= C_b^p \hat{\Omega}_{ib}^b - \Omega_{ic}^c C_b^p - C_p^c C_b^p \Omega_{ib}^b + \Omega_{ic}^c C_p^c C_b^p && (2.49) \end{aligned}$$

Substituting (2.47) and (2.48):

$$C_b^p\hat{\Omega}_{ib}^b - \Omega_{ic}^c C_b^p - C_p^c C_b^p\hat{\Omega}_{ib}^b + C_p^c\Omega_{ic}^c C_b^p - \dot{C}_p^c C_b^p$$
$$= C_b^p\hat{\Omega}_{ib}^b - \Omega_{ic}^c C_b^p - C_p^c C_b^p\Omega_{ib}^b + \Omega_{ic}^c C_p^c C_b^p$$

Therefore

$$\dot{C}_p^c C_b^p + C_p^c C_b^p\hat{\Omega}_{ib}^b - C_p^c\Omega_{ic}^c C_b^p - C_p^c C_b^p\Omega_{ib}^b + \Omega_{ic}^c C_p^c C_b^p = 0$$

Consider

$$\hat{\Omega}_{ib}^b = \Omega_{ib}^b + \in^b \tag{2.50}$$

post multiply both sides by C_p^b gives:

$$\dot{C}_p^c + C_p^c C_b^p \in^b C_b^p - C_p^c\Omega_{ic}^c + \Omega_{ic}^c C_p^c = 0 \tag{2.51}$$

Let $\in^p$ and $\in^c$ be the skew symmetric matrices of the gyro drift error vector in the platform frame and the computer frame respectively:

$$\in^p = \begin{bmatrix} 0 & -\epsilon_z^p & \epsilon_y^p \\ \epsilon_z^p & 0 & -\epsilon_x^p \\ -\epsilon_y^p & \epsilon_x^p & 0 \end{bmatrix}, \quad \in^c = \begin{bmatrix} 0 & -\epsilon_z^c & \epsilon_y^c \\ \epsilon_z^c & 0 & -\epsilon_x^c \\ -\epsilon_y^c & \epsilon_x^c & 0 \end{bmatrix} \tag{2.52}$$

The computed skew symmetric matrix $\widehat{\Omega}_{pb}^p$ is the sum of the true Ω_{pb}^p and $\in^p$:

$$\widehat{\Omega}_{pb}^p = \Omega_{pb}^p + \in^p \tag{2.53}$$

And the computed $\widehat{\Omega}_{pb}^b$ is the sum of the true Ω_{pb}^b and $\in^b$:

$$\widehat{\Omega}_{pb}^b = \Omega_{pb}^b + \in^b \tag{2.54}$$

For the computed $\widehat{\Omega}_{pb}^p$ and $\widehat{\Omega}_{pb}^b$ we have [27]:

$$\widehat{\Omega}_{pb}^p = C_b^p\widehat{\Omega}_{pb}^b C_p^b \tag{2.55}$$

Substituting (2.54) and (2.53) into (2.55) :

$$\Omega_{pb}^p + \in^p = C_b^p(\Omega_{pb}^b + \in^b)C_p^b \tag{2.56}$$

For the true Ω^p_{pb} and Ω^b_{pb} we also have:

$$\Omega^p_{pb} = C^p_b \Omega^b_{pb} C^b_p \tag{2.57}$$

Subtracting (2.57) from (2.56):

$$\in^p = C^p_b \in^b C^b_p \tag{2.58}$$

Similarly, it can also be proved that:

$$\in^p = C^p_c \in^c C^c_p \tag{2.59}$$

Pre multiplying C^c_p to the above equation, we have:

$$C^c_p \in^p = C^c_p (C^p_c \in^c C^c_p) = \in^c C^c_p \tag{2.60}$$

Replacing the term $C^c_p C^p_b \in^b C^p_b$ in (2.51) with (2.59) and (2.60):

$$\begin{aligned} C^c_p C^p_b \in^b C^p_b = & \\ &= C^c_p (C^p_b \in^b C^p_b) \\ &= C^c_p \in^p \\ &= \in^c C^c_p \end{aligned} \tag{2.61}$$

Consequently (2.51) can be simplified as:

$$\dot{C}^c_p + \in^c C^c_p - C^c_p \Omega^c_{ic} + \Omega^c_{ic} C^c_p = 0 \tag{2.62}$$

Replacing $\dot{C}^c_p = C^c_p \Omega^p_{cp}$, and left multiplying C^p_c (2.48) gives:

$$C^c_p \Omega^p_{cp} + \in^c C^c_p - C^c_p \Omega^c_{ic} + \Omega^c_{ic} C^c_p = 0 \tag{2.63}$$

$$\Omega^p_{cp} + C^p_c \in^c C^c_p - \Omega^c_{ic} + C^p_c \Omega^c_{ic} C^c_p = 0 \tag{2.64}$$

Notice that in (2.64):

$$C^p_c \in^c C^c_p = \in^p \tag{2.65}$$

And

$$C_c^p \Omega_{ic}^c C_p^c = \Omega_{ic}^p \tag{2.66}$$

Then (2.64) changes to:

$$\Omega_{cp}^p + \in^p - \Omega_{ic}^c + \Omega_{ic}^p = 0 \tag{2.67}$$

$\Omega_{cp}^p + \in^p - \Omega_{ic}^c + \Omega_{ic}^p$ are the sum of skew symmetric matrices of $\omega_{cp}^p + \epsilon^p - \omega_{ic}^c + \omega_{ic}^p$. Equation (2.67) can then be written in the following 3×1 vector form:

$$\omega_{cp}^p + \epsilon^p - \omega_{ic}^c + \omega_{ic}^p = 0 \tag{2.68}$$

with $\omega_{ic}^p = C_c^p \omega_{ic}^c$:

$$\omega_{cp}^p + \epsilon^p - \omega_{ic}^c + \omega_{ic}^p = \omega_{cp}^p + \epsilon^p - (I_{3\times 3} - C_c^p)\omega_{ic}^c \tag{2.69}$$

$$= 0 \tag{2.70}$$

That is:

$$\omega_{cp}^p = (I_{3\times 3} - C_c^p)\omega_{ic}^c - \epsilon^p \tag{2.71}$$

with $\omega_{cp}^p = \dot{\psi}$ being the angular rate between the $c-$frame and the $p-$frame solved in the $p-$frame. Therefore:

$$\dot{\psi} = (I_{3\times 3} - C_c^p)\omega_{ic}^c - \epsilon^p \tag{2.72}$$

Equation (2.72) is the general psi-angle error model that can be used for large or small angle errors.

When ψ_x, ψ_y and ψ_z are all small,

$$C_c^p = \begin{bmatrix} 1 & \psi_z & -\psi_y \\ -\psi_z & 1 & \psi_x \\ \psi_y & -\psi_x & 1 \end{bmatrix} \tag{2.73}$$

Equation (2.71) can be converted to small psi-angle model which is usually presented in the literature:

$$\dot{\psi} = \Psi \times \omega_{ic}^c - \epsilon^p \tag{2.74}$$

As can be seen, it is a special approximation of the more general form given by equation (2.72).

Another important case to consider is when ψ_x, ψ_y are small and ψ_z is large, $I_{3\times 3} - C_c^p$ is simplified to :

$$I_{3\times 3} - C_c^p = I_{3\times 3} - (C_p^c)^{-1} \tag{2.75}$$

$$= \begin{bmatrix} 1-c_z & -s_z & \psi_y \\ s_z & 1-c_z & -\psi_x \\ -\psi_x s_z - \psi_y c_z & +\psi_x c_z - \psi_y s_z & 0 \end{bmatrix} \tag{2.76}$$

In this case, the psi-angle model is given by:

$$\dot{\psi} = -\epsilon^p + \tag{2.77}$$

$$+ \begin{bmatrix} 1-c_z & -s_z & \psi_y \\ s_z & 1-c_z & -\psi_x \\ -\psi_x s_z - \psi_y c_z & +\psi_x c_z - \psi_y s_z & 0 \end{bmatrix} \omega_{ic}^c$$

where ω_{ic}^c is given by:

$$\omega_{ic}^c = \begin{bmatrix} -V_y^c/R_y \\ V_x^c/R_x + \omega_{ie}\cos(\varphi) \\ V_x^c tg(\varphi)/R_x + \omega_{ie}\sin(\varphi) \end{bmatrix} \tag{2.78}$$

In this section, the INS propagation error models in velocity, position and attitude for large attitude errors have been developed in the computer frame in the psi angle approach. The models are identical to their corresponding small angle models when the attitude errors are all small. INS error models using the quaternion approach will be developed in the next section.

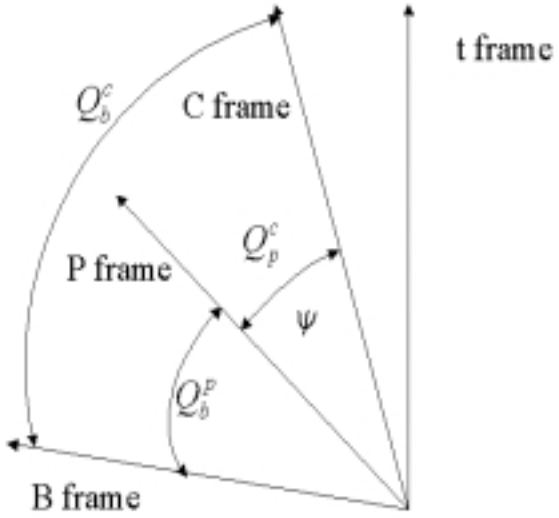

Figure 2.4: Quaternions and frames.

2.4 Development of INS Error Models Using the Quaternion Approach

2.4.1 Quaternions and Coordinate Systems

In this section, INS error models for large attitude errors will be developed using quaternions. The computer approach is used here. The coordinate systems used in these models are the computer frame, the body frame and the platform frame. The body frame is at the IMU whose axes are the IMU body axes. See Figure 2.4.

INS navigation computes the attitude transformation from the body frame to the platform frame. Quaternion $Q_b^p = [q_{b0}, q_{b1}, q_{b2}, q_{b3}]^T$ represents this rotation from the body frame to the platform frame. Direct accelerometer outputs in the body frame are transformed to the platform frame by left multiplying $C(Q_b^p)$ to the accelerations in the body frame.

$$C(Q_b^p) = \begin{bmatrix} q_{b0}^2 + q_{b1}^2 - q_{b2}^2 - q_{b3}^2 & 2(q_{b1}q_{b2} - q_{b0}q_{b3}) & 2(q_{b1}q_{b3} + q_{b0}q_{b2}) \\ 2(q_{b1}q_{b2} + q_{b0}q_{b3}) & q_{b0}^2 - q_{b1}^2 + q_{b2}^2 - q_{b3}^2 & 2(q_{b2}q_{b3} - q_{b0}q_{b1}) \\ 2(q_{b1}q_{b3} - q_{b0}q_{b2}) & 2(q_{b2}q_{b3} + q_{b0}q_{b1}) & q_{b0}^2 - q_{b1}^2 - q_{b2}^2 + q_{b3}^2 \end{bmatrix} \quad (2.79)$$

Q_b^p is normalized in each computation at INS sampling time. The four elements satisfy the constraint [32]:

$$q_{b0}^2 + q_{b1}^2 + q_{b2}^2 + q_{b3}^2 = 1 \tag{2.80}$$

The computer frame is the local level frame at the INS computed position. The rotation from the platform frame to the computer frame is represented by quaternion Q_p^c :

$$Q_p^c = [q_0, q_1, q_2, q_3]^T \tag{2.81}$$

The transformation from the platform frame to the computer frame is given by the matrix $C(Q_p^c)$:

$$C(Q_p^c) = \begin{bmatrix} q_0^2 + q_1^2 - q_2^2 - q_3^2 & 2(q_1q_2 - q_0q_3) & 2(q_1q_3 + q_0q_2) \\ 2(q_1q_2 + q_0q_3) & q_0^2 - q_1^2 + q_2^2 - q_3^2 & 2(q_2q_3 - q_0q_1) \\ 2(q_1q_3 - q_0q_2) & 2(q_2q_3 + q_0q_1) & q_0^2 - q_1^2 - q_2^2 + q_3^2 \end{bmatrix} \tag{2.82}$$

The transformation from the body frame to the computer frame is represented by the quaternion Q_b^c. This rotation can be considered as two consecutive rotations from the body frame to the platform frame, then to the computer frame. Thus:

$$Q_b^c = Q_p^c \otimes Q_b^p \tag{2.83}$$

where $\otimes$ represents the quaternion multiplication. The transformation matrix $C(Q_b^c)$ is equal to the product of two transformation matrices.

$$C(Q_b^c) = C(Q_p^c) \times C(Q_b^p) \tag{2.84}$$

The inconsistencies of the platform frame and the computer frame cause the navigation quaternion error Q_b^p. Likewise the psi angles which are the misalignment angles between the platform frame and the computer frame, quaternion Q_p^c consequently stands for the inconsistency of the $p-$frame and the $c-$frame. The attitude error model is therefore transferred to the modelling of the quaternion Q_p^c.

2.4.2 Velocity Error Propagation Model

In the computer approach, INS velocity is solved in the computer frame. The true velocity in the computer frame V_t^c is given by:

$$\dot{V}_t^c = f_t^c + g_t^c - (2\Omega_{ie}^c + \Omega_{ec}^c)V_t^c \tag{2.85}$$

where f_t^c is the true specific force resolved in the computer frame, g_t^c is the gravity vector resolved in the computer frame, Ω_{ie}^c is the matrix of the earth rate resolved in the computer frame and Ω_{ec}^c is the matrix representing the rotation from the computer frame to the earth frame.

Due to the existence of the error sources, the INS computes the following velocity:

$$\dot{\hat{V}}_t^c = (f_t^p + \nabla^p) + \hat{g}^c - (2\Omega_{ie}^c + \Omega_{ec}^c)\hat{V}_t^c \tag{2.86}$$

where f_t^p is the true specific force resolved in the platform frame. ∇^p is the bias of the accelerometers in the platform frame and $\hat{g}^c$ is the computed gravity vector.

Let $\Delta V^c = \hat{V}_t^c - V_t^c$ be the velocity error. The velocity error propagation model is obtained by subtracting (2.85) from (2.86):

Then:

$$\begin{aligned}
\Delta\dot{V}^c &= \dot{\hat{V}}_t^c - \dot{V}_t^c \qquad (2.87)\\
&= [(f_t^p + \nabla^p) + \hat{g}_t^c - (2\Omega_{ie}^c + \Omega_{ec}^c)\hat{V}_t^c] - [f_t^c + g_t^c - (2\Omega_{ie}^c + \Omega_{ec}^c)V_t^c]\\
&= (f_t^p - f_t^c) - (2\Omega_{ie}^c + \Omega_{ec}^c)\Delta V^c + (\hat{g}_t^c - g_t^c) + \nabla^p\\
&= (I_{3\times 3} - C(Q_p^c))f_t^p - (2\Omega_{ie}^c + \Omega_{ec}^c)\Delta V^c + \nabla^p + \Delta g^c
\end{aligned}$$

where $\Delta g^c = (\hat{g}^c - g_t^c)$ and $f_t^c = C(Q_p^c)f_t^p$. The transformation quaternion matrix $C(Q_p^c)$ is shown in (2.82). Therefore the velocity error model in quaternion form is

$$\Delta\dot{V}^c = (I_{3\times 3} - C(Q_p^c))f_t^p - (2\Omega_{ie}^c + \Omega_{ec}^c)\Delta V^c + \nabla^p + \Delta g^c \tag{2.88}$$

This model is applicable to the full range of misalignment angles without small angle errors assumption.

2.4.3 Position Error Propagation Model

The position error model is de-coupled from the attitude errors [5]. It has the same general form as the psi angle form. The psi angle and the quaternions do not appear directly in the position error equation:

$$\Delta \dot{R}^c = -\Omega^c_{ec} \Delta R^c + \Delta V^c \tag{2.89}$$

2.4.4 Quaternion Error Propagation Model

Modelling the quaternion error is required to correct and update the navigation quaternions in real time at the sampling time.

The inconsistencies of the platform frame and the computer frame cause the navigation quaternion error Q^p_b. The quaternion error is modelled using Q^c_p which represents the misalignment of the platform frame and the computer frame.

The quaternion Q^c_p satisfies the following differential equation:

$$\dot{Q}^c_p = \frac{1}{2} \Omega^{*p}_{cp} Q^c_p \tag{2.90}$$

where the 4×4 matrix Ω^{*p}_{cp} is a function of ω^p_{cp} which is the rotation rate between the $c-$frame and the p-frame solved in the p-frame. $\omega^p_{cp} = [\dot{\psi}_x, \dot{\psi}_y, \dot{\psi}_z]^T$. And the psi angle $\psi = [\psi_x, \psi_y, \psi_z]^T$ is the angle between the p-frame and the c-frame.

$$\Omega^{*p}_{cp} = \begin{bmatrix} 0 & -\dot{\psi}_x & -\dot{\psi}_y & -\dot{\psi}_z \\ \dot{\psi}_x & 0 & \dot{\psi}_z & -\dot{\psi}_y \\ \dot{\psi}_y & -\dot{\psi}_z & 0 & \dot{\psi}_x \\ \dot{\psi}_z & \dot{\psi}_y & -\dot{\psi}_x & 0 \end{bmatrix} \tag{2.91}$$

Extending (2.90) :

$$\begin{aligned}
\dot{Q}_p^c &= \frac{1}{2}\Omega_{cp}^{*p} Q_p^c \\
&= \frac{1}{2}\begin{bmatrix} 0 & -\dot{\psi}_x & -\dot{\psi}_y & -\dot{\psi}_z \\ \dot{\psi}_x & 0 & \dot{\psi}_z & -\dot{\psi}_y \\ \dot{\psi}_y & -\dot{\psi}_z & 0 & \dot{\psi}_x \\ \dot{\psi}_z & \dot{\psi}_y & -\dot{\psi}_x & 0 \end{bmatrix} \begin{bmatrix} q_0 \\ q_1 \\ q_2 \\ q_3 \end{bmatrix} \\
&= \frac{1}{2}\begin{bmatrix} -\dot{\psi}_x q_1 - \dot{\psi}_y q_2 - \dot{\psi}_z q_3 \\ \dot{\psi}_x q_0 + \dot{\psi}_z q_2 - \dot{\psi}_y q_3 \\ \dot{\psi}_y q_0 - \dot{\psi}_z q_1 + \dot{\psi}_x q_3 \\ \dot{\psi}_z q_0 + \dot{\psi}_y q_1 - \dot{\psi}_x q_2 \end{bmatrix} \\
&= \frac{1}{2}\begin{bmatrix} -q_1 & -q_2 & -q_3 \\ q_0 & -q_3 & q_2 \\ q_3 & q_0 & -q_1 \\ -q_2 & q_1 & q_0 \end{bmatrix} \begin{bmatrix} \dot{\psi}_x \\ \dot{\psi}_y \\ \dot{\psi}_z \end{bmatrix}
\end{aligned} \tag{2.92}$$

Let

$$B = \frac{1}{2}\begin{bmatrix} -q_1 & -q_2 & -q_3 \\ q_0 & -q_3 & q_2 \\ q_3 & q_0 & -q_1 \\ -q_2 & q_1 & q_0 \end{bmatrix} \tag{2.93}$$

Then

$$\dot{Q}_p^c = B \begin{bmatrix} \dot{\psi}_x \\ \dot{\psi}_y \\ \dot{\psi}_z \end{bmatrix} = B\dot{\psi} \tag{2.94}$$

The general psi angle model when all the psi angles are large is given by:

$$\dot{\psi} = (I - C_c^p)\omega_{ic}^c - \epsilon^p \tag{2.95}$$

The direction cosine matrix C_c^p which is the transformation matrix from the computer frame to the platform frame can be converted into the quaternions form as $C(Q_c^p)$:

$$C(Q_c^p) = \begin{bmatrix} q_0^2+q_1^2-q_2^2-q_3^2 & 2(q_1q_2+q_0q_3) & 2(q_1q_3-q_0q_2)) \\ 2(q_1q_2-q_0q_3) & q_0^2-q_1^2+q_2^2-q_3^2 & 2(q_2q_3+q_0q_1) \\ 2(q_1q_3+q_0q_2) & 2(q_2q_3-q_0q_1) & q_0^2-q_1^2-q_2^2+q_3^2 \end{bmatrix} \tag{2.96}$$

Therefore, the quaternion model is derived from the psi angle model:

$$\begin{aligned} \dot{Q}_p^c &= B\dot{\psi} \\ &= B[(I - C(Q_c^p))\omega_{ic}^c - \epsilon^p] \end{aligned} \tag{2.97}$$

That is

$$\dot{Q}_p^c = B(I - C(Q_c^p))\omega_{ic}^c - B\epsilon^p \tag{2.98}$$

Equations (2.98), (2.96) and (2.93) give the general quaternion error model without small angle assumption. The term ϵ^p is the gyro error resolved in the platform frame, ω_{ic}^c is given by:

$$\omega_{ic}^c = \begin{bmatrix} 0 \\ \omega_{ie}\cos(\varphi) \\ \omega_{ie}\sin(\varphi) \end{bmatrix} + \begin{bmatrix} -V_y^c/R_y \\ V_x^c/R_x \\ V_x^c tg(\varphi)/R_x \end{bmatrix} \tag{2.99}$$

with ω_{ie} being the earth rate, φ the local latitude. R_x and R_y are the earth radius elements in the east and north direction in the c-frame. The INS velocity vector $[V_x^c, V_y^c, V_z^c]^T$ is resolved in the computer frame.

In this section, the INS velocity, position and attitude error propagation models for large attitude errors were developed in the quaternion approach in the computer frame.

2.5 Summary

In this chapter INS error propagation models of velocity, position and attitude for large attitude errors were developed. The models proposed are based on the psi angle

method and the quaternion method. The error models using psi angles are for the navigation using the direction cosine matrix. The quaternion models are for navigation using quaternions.

There were no small angle assumptions in the development of these two sets of models. These models become essential when the INS attitude errors are large. In the later chapters, two INS algorithms using these models for INS in-motion alignment and calibration are presented.

Chapter 3

GPS Modelling in Frequency Domain

3.1 Introduction

The calibration and alignment of low cost IMUs requires an external aiding sensor. GPS is an attractive sensor to aid INS in outdoor environment. To improve the operation of the full system, it is important to model the main sources of GPS errors. This chapter presents the determination of the GPS error model in the frequency domain. The frequency domain is an appropriate method to capture, model and understand the correlated errors that arise in GPS systems.

The navigation problem is generally split into two components: creating a process model of the host vehicle and understanding or modelling the sensors to be used. The process model of a navigation system describes the prediction of states which are typically the position, velocity, attitude and related parameters affecting these variables. The INS error propagation models developed in this thesis are process models.

Section 3.2 overviews previous work on GPS modelling in the frequency domain. GPS position error models are derived in Section 3.3. It is also proved in this section that the transfer function of the GPS position error in any frame has identical poles and zeros to the pseudo range error model. The modelling method using power spectral

density of noise is described in Section 3.4. Section 3.5 describes the de-correlation of GPS coloured noise. A shaping filter is introduced to facilitate the de-correlation task using an additional sensor. Different types of feedforward and feedback filter structures are proposed and the results are presented in the frequency and time domains.

3.2 GPS Frequency Domain Modelling Review

The Global Positioning System provides three-dimensional position and velocity information to users anywhere in the world. Position determination is based on the measurement of the transit time of signals from at least four satellites. Accuracy in the order of $1cm$-$100m$ may be achieved depending on the type of GPS configuration. The baseline constellation operates in 12-hour orbits. It provides visibility of 6 to 11 satellites at 5 degrees or more above the horizon to users. Signals are transmitted at two L-band frequencies to permit corrections to be made for ionospheric delays in signal propagation time. The signals are modulated with two codes: P, which provides for precision measurement of time, and C/A, which provides for easy lock-on to the desired signal [33]. Four satellites are normally required for navigation purposes, and the four offering the best geometry can be selected using ephemeris information transmitted by the satellites. Ranges to the four satellites are determined by scaling the signal transit time by the speed of light. The transmitted message contains ephemeris parameters that enable users to calculate the position of each satellite at the time of transmission of the signal. Operation of the system requires precise synchronization of space vehicle clocks with "GPS system time". The requirement for users to be equipped with precision clocks is eliminated by the use of range measurements from four satellites. The four satellites permit an estimate of the user's clock error. The user position equations contain four unknowns consisting of position in three dimensions and the error in the user's imprecise clock.

The measurement of range to the satellites is called "pseudo range". It is defined

as

$$R = \varrho + c \times \Delta t + n \tag{3.1}$$

where R is the pseudo range to the satellite, ϱ is the true range, c is the speed of light, Δt is the receiver clock error and n is the correlated noise. Errors contained in the pseudo range measurement can be divided into the following main categories [33]: space vehicle clock errors, atmospheric delays, group delay, ephemeris errors, multipath, receiver noise and resolution, receiver vehicle dynamics. The Differential GPS (DGPS) is a method to correct the effects of measurement errors. This method can help increase receiver accuracy from 100 metres to metres. The differential corrections are calculated at a base station away from the user receiver. In a case where the DGPS correction is unavailable or in between the correction update time, it is necessary for the characteristics of the errors to be modelled. Some error modelling methods have appeared in the literature [34, 35, 36, 37, 38, 39, 40, 41, 42, 43, 44]. To the best of the author's knowledge, there is no GPS error modelling theory using the receiver position directly in the frequency domain.

3.2.1 GPS Receiver Clock Offset Model

The accuracy of the GPS range measurement relies on the accuracy of the transmitted time measurement. Each GPS satellite clock is monitored and constantly adjusted to be synchronous with GPS time. Each GPS receiver uses a low cost quartz oscillator as its timing reference. The receiver clock offset is usually modelled by users. Cooper [45] modeled this offset using a constant velocity model, because the receiver clock has a reasonably constant frequency:

$$\begin{bmatrix} c\Delta\dot{t}(t) \\ c\ddot{\Delta}t(t) \end{bmatrix} = \begin{bmatrix} 0 & 1 \\ 0 & 0 \end{bmatrix} \begin{bmatrix} c\Delta t(t) \\ c\dot{\Delta}t(t) \end{bmatrix} + \begin{bmatrix} 1 & 0 \\ 0 & 1 \end{bmatrix} \begin{bmatrix} w_p(t) \\ w_v(t) \end{bmatrix} \tag{3.2}$$

where c is the light speed, $\Delta t(t)$ is the receiver clock offset at time t, $w_p(t)$ and $w_v(t)$ are process noise.

3.2.2 GPS Correlated Error Model

Cooper and Durrant-Whyte introduced a modelling technique in the frequency domain [45]. The correlated error in the pseudo range is modelled using power spectral density (PSD). It was shown that all the satellites have the same correlated noise (or coloured noise) statistics. The power spectral density $\Psi_i(s)$ of the correlated noise of each satellite has the form of a fourth order system:

$$\Psi_i(s) = [\frac{r(s+\beta)}{s^2+2\alpha k s+\alpha^2}]^2 \tag{3.3}$$

The transfer function (3.3) can be converted to state space form so that the correlated noise can be estimated along with the original filter states. For a single satellite, the correlated noise in the pseudo range at time t is estimated as:

$$\begin{bmatrix} \dot{x}_1(t) \\ \dot{x}_2(t) \end{bmatrix} = \begin{bmatrix} -2\alpha k & 1 \\ -\alpha^2 & 0 \end{bmatrix} \begin{bmatrix} x_1(t) \\ x_2(t) \end{bmatrix} + \begin{bmatrix} r \\ r\beta \end{bmatrix} w_r(t) \tag{3.4}$$

where $x_1(t)$ is the state of interest, $x_2(t)$ is the augmented state, $w_r(t)$ is a white noise series, α, k, r and β are the model parameters in (3.3).

Hence, the GPS error propagation model for a single satellite is:

$$\dot{x}(t) = F_r x(t) + G_r u_r(t) \tag{3.5}$$

where

$$x(t) = \begin{bmatrix} c\Delta t(t) \\ c\dot{\Delta} t(t) \\ x_1(t) \\ x_2(t) \end{bmatrix}, \; F_r = \begin{bmatrix} 0 & 1 & 0 & 0 \\ 0 & 0 & 0 & 0 \\ 0 & 0 & -2\alpha k & 1 \\ 0 & 0 & -\alpha^2 & 0 \end{bmatrix} \tag{3.6}$$

and

$$G_r = \begin{bmatrix} 1 & 0 & 0 \\ 0 & 1 & 0 \\ 0 & 0 & r \\ 0 & 0 & r\beta \end{bmatrix}, \; u_r(t) = \begin{bmatrix} w_p(t) \\ w_v(t) \\ w_r(t) \end{bmatrix} \tag{3.7}$$

In the example an INS was used as an external sensor, the INS indicated position was converted into "inertial-pseudo-range" by calculating the expected range to each satellite using the inertially indicated position and the known satellite locations. The converted inertial measurement $R_{ins}(t)$ is given by:

$$R_{ins}(t) = \sqrt{(X_{sat}(t) - X_{ins}(t))^2 + (Y_{sat}(t) - Y_{ins}(t))^2 + (Z_{sat}(t) - Z_{ins}(t))^2} \quad (3.8)$$

where

$[X_{sat}(t), Y_{sat}(t), Z_{sat}(t)]$ is the satellite position in WGS-84 reference.

$[X_{ins}(t), Y_{ins}(t), Z_{ins}(t)]$ is the INS indicated vehicle position in WGS-84 reference.

The GPS uses the World Geodetic System WGS-84 as a reference. WGS-84 is an earth fixed global reference frame, including an earth model. It is defined by a set of parameters which define the shape of an earth ellipsoid, its angular velocity, the earth mass which is included in the ellipsoid reference and a detailed gravity model of the earth [46].

There are a number of shortcomings with this modelling method. The first is the need to model the receiver's clock offset. Further, all the pseudo ranges to all the satellites in use have to be modelled. Assuming that a maximum of ten satellites may be tracked at a given time, the total error model can add an additional twenty two states to the process model used in the fusion filter. Finally, the measurement of other sensors has to be converted into an equivalent pseudo range to match the GPS parameters.

These problems motivated the development of an improved modelling method by using the position measurement directly without modelling the receiver's clock offset and the pseudo ranges of all the tracked satellites. The measurement of other sensors may be used as position information without the need to convert into the equivalent pseudo range. The number of the model states will be reduced to six. The improved method is introduced in the following sections.

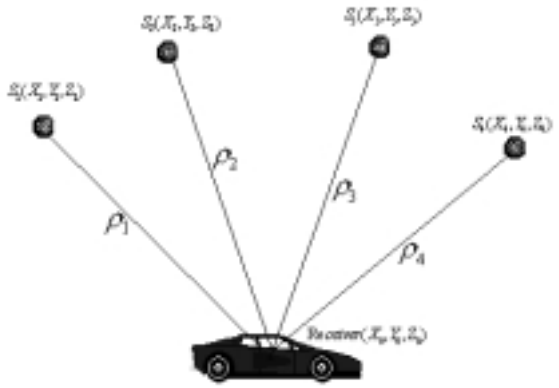

Figure 3.1: Satellites, receiver and ranges.

3.3 GPS Position Model

In this chapter the theory that the correlated position errors in any Cartesian coordinates system have an identical model structure is presented . They can be represented with a second order system driven by a white noise similar to Equation (3.3).

As shown in Figure 3.1, at time t the coordinates of four visible satellites S_1, S_2, S_3 and S_4 in WGS-84 frame are (X_1, Y_1, Z_1), (X_2, Y_2, Z_2), (X_3, Y_3, Z_3) and (X_4, Y_4, Z_4). The three axes of the WGS-84 frame are x, y and z. The position of the receiver in the WGS-84 frame is (X_0, Y_0, Z_0) and the true ranges from each satellite to the receiver are ρ_1 , ρ_2 , ρ_3 and ρ_4 with

$$\rho_i = \sqrt{(X_i - X_0)^2 + (Y_i - Y_0)^2 + (Z_i - Z_0)^2}, \ i = 1, 2, 3, 4 \tag{3.9}$$

The measured pseudo ranges R_i $(i = 1, 2, 3, 4)$ are the combinations of the true range, satellite clock offset range, receiver clock bias range and the correlated noise n_i. See Figure 3.2.

$$R_i = \rho_i + c \times (Dt_i - Dt_0) + n_i, \ i = 1, 2, 3, 4 \tag{3.10}$$

where c is the light speed, Dt_i $(i = 1, 2, 3, 4)$ is the satellite clock bias and Dt_0 is the unknown receiver clock bias.

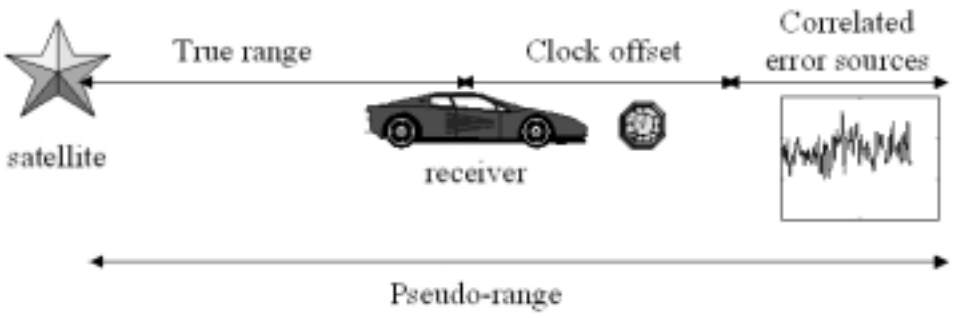

Figure 3.2: GPS pseudo range and errors.

Assume the calculated receiver position from the pseudo ranges is $(\widetilde{X}, \widetilde{Y}, \widetilde{Z})$.

$$\widetilde{X} = X_0 + D_x, \quad \widetilde{Y} = Y_0 + D_y, \quad \widetilde{Z} = Z_0 + D_z \tag{3.11}$$

where (D_x, D_y, D_z) is the correlated position error.

The pseudo range R_i $(i = 1, 2, 3, 4)$ at the receiver true position $(X_{0,}Y_{0,}Z_0)$ with increment (D_x, D_y, D_z) is:

$$R_i = \rho_i - \frac{X_i - X_0}{\rho_i} D_x - \frac{Y_i - Y_0}{\rho_i} D_y - \frac{Z_i - Z_0}{\rho_i} D_z \tag{3.12}$$

Let

$$a_i = -\frac{X_i - X_0}{\rho_i}, \quad b_i = -\frac{Y_i - Y_0}{\rho_i}, \quad c_i = -\frac{Z_i - Z_0}{\rho_i} \tag{3.13}$$

Subtracting Equation (3.12) from (3.10) and leaving the terms containing position errors on the left side:

$$a_i D_x + b_i D_y + c_i D_z = c(Dt_i - Dt_0) + n_i \tag{3.14}$$

For the four individual satellites, we have

$$a_1 D_x + b_1 D_y + c_1 D_z = c(Dt_1 - Dt_0) + n_1 \tag{3.15}$$

$$a_2 D_x + b_2 D_y + c_2 D_z = c(Dt_2 - Dt_0) + n_2 \tag{3.16}$$

$$a_3 D_x + b_3 D_y + c_3 D_z = c(Dt_3 - Dt_0) + n_3 \tag{3.17}$$

$$a_4 D_x + b_4 D_y + c_4 D_z = c(Dt_4 - Dt_0) + n_4 \tag{3.18}$$

Subtracting Equation (3.15) from (3.16), (3.17) and (3.18) respectively, the receiver clock bias Dt_0 is removed:

$$(a_1 - a_2)D_x + (b_1 - b_2)D_y + (c_1 - c_2)D_z = c(Dt_1 - Dt_2) + (n_1 - n_2) \tag{3.19}$$

$$(a_1 - a_3)D_x + (b_1 - b_3)D_y + (c_1 - c_3)D_z = c(Dt_1 - Dt_3) + (n_1 - n_3) \tag{3.20}$$

$$(a_1 - a_4)D_x + (b_1 - b_4)D_y + (c_1 - c_4)D_z = c(Dt_1 - Dt_4) + (n_1 - n_4) \tag{3.21}$$

The position error (D_x, D_y, D_z) is consequently obtained from (3.19), (3.20) and (3.21) with linear combination of satellite clock bias terms and range measurement correlated noise n_i ($i = 1, 2, 3, 4$).

Let

$$d = \begin{vmatrix} a_1 - a_2, & b_1 - b_2, & c_1 - c_2 \\ a_1 - a_3, & b_1 - b_3, & c_1 - c_3 \\ a_1 - a_4, & b_1 - b_4, & c_1 - c_4 \end{vmatrix} \tag{3.22}$$

$$d_{12=} \frac{\begin{vmatrix} b_1 - b_3, & c_1 - c_3 \\ b_1 - b_4, & c_1 - c_4 \end{vmatrix}}{d} \tag{3.23}$$

$$d_{13=} \frac{\begin{vmatrix} b_1 - b_2, & c_1 - c_2 \\ b_1 - b_4, & c_1 - c_4 \end{vmatrix}}{d}, \quad d_{14=} \frac{\begin{vmatrix} b_1 - b_2, & c_1 - c_2 \\ b_1 - b_3, & c_1 - c_3 \end{vmatrix}}{d} \tag{3.24}$$

where d, d_{12}, d_{13} and d_{14} are related to the true ranges and true positions which can be considered constants at that time.

Consider D_x first, then at time t:

$$\begin{aligned} D_x(t) = {} & d_{12}c(Dt_1(t) - Dt_2(t)) - d_{13}c(Dt_1(t) - Dt_3(t)) + \\ & + d_{14}c(Dt_1(t) - Dt_4(t)) + d_{12}(n_1(t) - n_2(t)) \\ & - d_{13}(n_1(t) - n_3(t)) + d_{14}(n_1(t) - n_4(t)) \end{aligned} \tag{3.25}$$

The satellite clock bias ranges $c(Dt_1(t) - Dt_2(t))$, $c(Dt_1(t) - Dt_3(t))$ and $c(Dt_1(t) - Dt_4(t))$ are provided by the satellite ephemeris data in GPS message. After removing

these main clock bias ranges, the remaining error $D_x\_cor(t)$ is the linear combination of correlated noise $(n_1(t) - n_2(t)), (n_1(t) - n_3(t))$ and $(n_1(t) - n_4(t))$:

$$D_x\_cor(t) = d_{12}(n_1(t) - n_2(t)) - d_{13}(n_1(t) - n_3(t)) + d_{14}(n_1(t) - n_4(t)) \tag{3.26}$$

In frequency domain:

$$D_x\_cor(s) = d_{12}(n_1(s) - n_2(s)) - d_{13}(n_1(s) - n_3(s)) + d_{14}(n_1(s) - n_4(s)) \tag{3.27}$$

The correlated noise of the pseudo range of all the satellites has an identical second order model structure [45]. The model for each satellite has identical poles and zeros. Therefore the linear combination of any of these correlated noises will not change the poles and zeros. The position error will have an identical model structure with the identical poles and zeros as the pseudo range model. The gain, however, is different and can be obtained using the following method.

Assuming that the correlated noise $n_i(s)$ $(i = 1, 2, 3, 4)$ of the pseudo range has the following transfer function which is a second order system driven by a white noise series ω_i $(i = 1, 2, 3, 4)$ with unit strength:

$$n_i(s) = \frac{r_i(s + \beta)}{s^2 + 2\alpha k s + \alpha^2}\omega_i \tag{3.28}$$

where α, k, β are identical to all the satellites. The gain r_i is different for each satellite and is related to the gain of the transfer function.

Then

$$\begin{aligned}
D_x_cor(s) &= d_{12}(\frac{r_1(s+\beta)}{s^2+2\alpha k s+\alpha^2}\omega_1 - \frac{r_2(s+\beta)}{s^2+2\alpha k s+\alpha^2}\omega_2) - \\
&- d_{13}(\frac{r_1(s+\beta)}{s^2+2\alpha k s+\alpha^2}\omega_1 - \frac{r_3(s+\beta)}{s^2+2\alpha k s+\alpha^2}\omega_3) + \\
&+ d_{14}(\frac{r_1(s+\beta)}{s^2+2\alpha k s+\alpha^2}\omega_1 - \frac{r_4(s+\beta)}{s^2+2\alpha k s+\alpha^2}\omega_4) \\
&= \frac{(s+\beta)}{s^2+2\alpha k s+\alpha^2}[(r_1\omega_1 - r_2\omega_2)d_{12} - \\
&- (r_1\omega_1 - r_3\omega_3)d_{13} + (r_1\omega_1 - r_4\omega_4)d_{14}] \\
&= \frac{(s+\beta)}{s^2+2\alpha k s+\alpha^2}[\omega_1 r_1(d_{12} - d_{13} + d_{14}) - \\
&- \omega_2 r_2 d_{12} + \omega_3 r_3 d_{13} - \omega_4 r_4 d_{14}]
\end{aligned} \tag{3.29}$$

We know that a linear combination of white noise is also white noise. Hence in (3.29) $[\omega_1 r_1(d_{12} - d_{13} + d_{14}) - \omega_2 r_2 d_{12} + \omega_3 r_3 d_{13} - \omega_4 r_4 d_{14}]$ is still a white noise series with strength G_{ainx} :

$$\begin{aligned} G_{ainx} &= E\{[\omega_1 r_1(d_{12} - d_{13} + d_{14}) - \omega_2 r_2 d_{12} + \\ &+ \omega_3 r_3 d_{13} - \omega_4 r_4 d_{14}]^T \times [\omega_1 r_1(d_{12} - d_{13} + d_{14}) - \\ &+ \omega_2 r_2 d_{12} + \omega_3 r_3 d_{13} - \omega_4 r_4 d_{14}]\} \\ &= r_1^2 (d_{12} - d_{13} + d_{14})^2 + r_2^2 d_{12}^2 + r_3^2 d_{13}^2 + r_4^2 d_{14}^2 \end{aligned}$$

Therefore $D_x\_cor(s)$ has the identical second order model structure

$$D_x\_cor(s) = \frac{s + \beta}{s^2 + 2\alpha k s + \alpha^2} \omega_{cor} \tag{3.30}$$

driven by a white noise series ω_{cor} with strength G_{ainx}.

The position errors in y and z also have a similar model with the same poles and zeros and different gains.

The latitude and the longitude of the receiver can be linearly transferred from the receiver's coordinates in axes x, y and z of the WGS-84 frame. Their correlated error models also have identical structures. The position in any other Cartesian coordinate system can be transferred to the WGS-84 frame by multiplying a direction cosine matrix. Hence, it can be concluded that in any other Cartesian coordinate system, the position correlated errors have identical error models.

Therefore, the correlated error of positions can be modelled independently without modelling the correlated errors of the pseudo ranges of an individual satellite and the receiver clock error.

In this thesis, PSD techniques are used to model the error in x, y and z position information provided by GPS.

3.4 GPS Position Error Modelling Using PSD

3.4.1 Power Spectral Density and Autocorrelation of Signals

Correlated signals can be examined in either the time domain or the frequency domain. Frequency characteristics are shown in the power spectral density of the signals. Time information is contained in the autocorrelation.

For an ergodic signal $x(t)$ the expected value of $x(t)x(t+\tau)$ is given by [47]:

$$E\{x(t)x(t+\tau)\} = \Phi_{xx}(\tau) = \lim_{T\to\infty} \frac{1}{2T} \int_{-T}^{T} x(t)x(t+\tau)dt \tag{3.31}$$

where $\Phi_{xx}(\tau)$ is called the *autocorrelation function* . τ is defiend as the delay variable.

The expected value of $x(t)$ $y(t+\tau)$ is given by

$$E\{x(t)y(t+\tau)\} = \Phi_{xy}(\tau) = \lim_{T\to\infty} \frac{1}{2T} \int_{-T}^{T} x(t)y(t+\tau)dt \tag{3.32}$$

where $\Phi_{xy}(\tau)$ is called the *crosscorrelation function* and yields information as to the dependence or correlation of $x(t)$ to $y(t)$. $y(t)$ is a second random signal.

Assuming that the time functions given by (3.31) and (3.32) are Fourier transformable, the Fourier transform of the autocorrelation and the crosscorrelation functions are defined as

$$\Psi_{xx}(j\omega) = \frac{1}{2\pi} \int_{-\infty}^{\infty} \Phi_{xx}(\tau)e^{-j\omega\tau}dt \tag{3.33}$$

$$\Psi_{xy}(j\omega) = \frac{1}{2\pi} \int_{-\infty}^{\infty} \Phi_{xy}(\tau)e^{-j\omega\tau}dt \tag{3.34}$$

where $\Psi_{xx}(j\omega)$ is called the power spectral density (PSD) function and is $\Psi_{xy}(j\omega)$ called the cross power spectral density function.

The autocorrelation is the Inverse Fourier Transform (IFT) of its PSD.

Consider the following linear time-invariant system with transfer function $g_1(t)$:

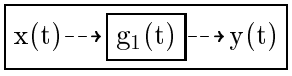

(3.35)

where the input and output are related by

$$y(t) = \int_{-\infty}^{\infty} x(t-\eta)g_1(\eta)d\eta \tag{3.36}$$

The power spectral density function $\Psi_{xx}(j\omega)$ of the input $x(t)$ and the power spectral density function $\Psi_{yy}(j\omega)$ of the output $y(t)$ have the following relationship:

$$\Psi_{yy}(j\omega) = \mid G_1(j\omega) \mid^2 \Psi_{xx}(j\omega) \tag{3.37}$$

with $G_1(j\omega)$ being the transfer function of this system in the frequency domain.

The transfer function of the correlated error model of GPS position has the structure:

$$G_1(s) = \frac{r(s+\beta)}{s^2 + 2\alpha k s + \alpha^2} \tag{3.38}$$

The PSD $\Psi_{cor}(s)$ of the correlated error $X_s(s)$ can be created by passing white noise $\omega(s)$ with a constant PSD Ψ_{white_noise} through the transfer function $G_1(s)$:

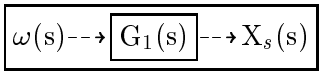

(3.39)

And

$$\Psi_{cor}(s) = \mid G_1(s) \mid^2 \Psi_{white\_noise} \tag{3.40}$$

$G_1(s)$ can be used to create a shaping filter for use as an estimation error model.

3.4.2 Error Modelling Using PSD and Autocorrelation

The GPS correlated errors are modelled by the transfer function (3.38). The poles, zeros and the gain of $G_1(s)$ are determined using the PSD and the autocorrelation of the GPS noise signals. In this section, the modelling techniques are presented.

To identify the GPS noise, raw data are collected from a known true position. For example, Figure 3.3 shows the raw data in axis x collected during 12 hours at a fixed position. At least 50 groups of data have to be collected to obtain an average PSD.

The noise data are obtained by removing the true position data from the raw data as shown in Figure 3.4. It can be seen that the noises of standard GPS position output are within 100 metres.

The Hanning window is applied to the noise data before the calculation of its power spectral density and autocorrelation [48].

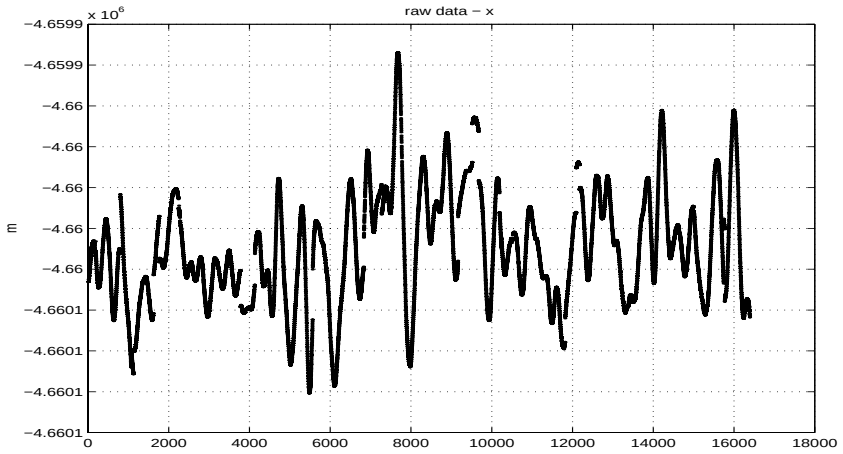

Figure 3.3: Raw data of GPS position in x-axis.

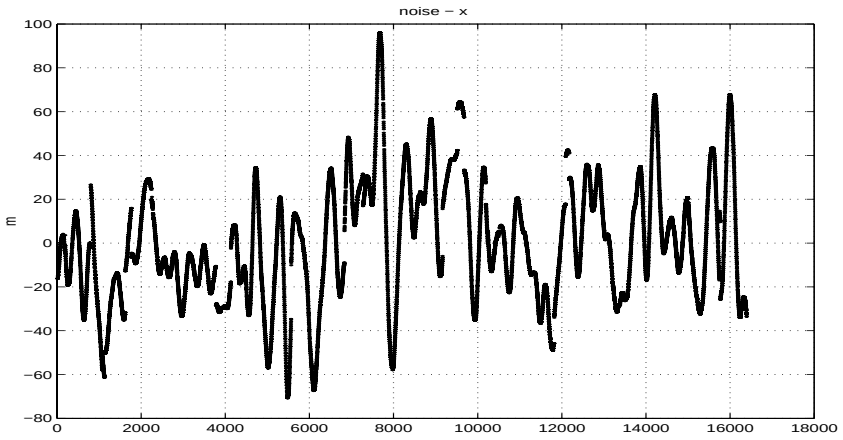

Figure 3.4: GPS correlated noise in x-axis

Least Square Method

Once the PSDs are obtained, a least square fit method can be used to identify the parameters of the transfer function.

Assume that the GPS correlated noise X_s is driven by a white noise of unit strength. From Equation (3.40), in the frequency domain the PSD Ψ_{X_s} of the noise X_s has the following relation with the model:

$$\mid \Psi_{X_s}(j\omega) \mid = \mid \frac{r(j\omega+\beta)}{(j\omega)^2+2\alpha k(j\omega)+\alpha^2} \mid^2 \tag{3.41}$$

with the frequency series $\omega \subset \{0, +\infty\}$.

Obtaining the logarithm base 10 of the elements of (3.41):

$$\begin{aligned} 10\lg \mid \Psi_{X_s}(j\omega) \mid &= 20\lg \mid \frac{r(j\omega+\beta)}{(j\omega)^2+2\alpha k(j\omega)+\alpha^2} \mid \\ &= 10\lg \frac{r(\omega^2+\beta^2)}{[(\omega+\alpha\sqrt{1-k^2})^2+\alpha^2k^2][(\omega-\alpha\sqrt{1-k^2})^2+\alpha^2k^2]} \end{aligned} \tag{3.42}$$

Set $k_1 = \sqrt{1-k^2}$, and

$$f_w = \frac{r(\omega^2+\beta^2)}{[(\omega+\alpha\sqrt{1-k^2})^2+\alpha^2k^2][(\omega-\alpha\sqrt{1-k^2})^2+\alpha^2k^2]} \tag{3.43}$$

Then

$$\begin{aligned} f_w &= \frac{r(\omega^2+\beta^2)}{(\omega^2+\alpha^2+2\omega\alpha k_1)(\omega^2+\alpha^2-2\omega\alpha k_1)} \\ &= \frac{r(\omega^2+\beta^2)}{(\omega^2+\alpha^2)^2-4\omega^2\alpha^2k_1^2} \end{aligned} \tag{3.44}$$

Equation (3.42) can be simplified as

$$\omega^2 r + y - pf_w - 2q\omega^2 f_w + 4u\omega^2 f_w = f_w\omega^4 \tag{3.45}$$

when

$$\begin{aligned} &y = r\beta^2,\ z_w = (\omega^2+\alpha^2)^2,\ u = \alpha^2k_1^2 \\ &p = \alpha^4,\ q = \alpha^2 \end{aligned} \tag{3.46}$$

That is:

$$\begin{bmatrix} \omega^2 & 1 & -f_w & -2\omega^2 f_w & 4\omega^2 f_w \end{bmatrix} \times \begin{bmatrix} r \\ y \\ p \\ q \\ u \end{bmatrix} = f_w \omega^4 \tag{3.47}$$

The least square equation (3.47) can be used to obtain the parameters r, y, p, q, u which can be transformed to α, k, r, β by (3.46). Back to (3.43) and (3.42), f_w can be obtained from the PSD of raw data $10 \lg \mid \Psi_{X_s}(j\omega) \mid$:

$$f_w = \frac{10 \lg \mid \Psi_{X_s}(j\omega) \mid}{10} \tag{3.48}$$

Curve Fitting Method

Curve fitting can also be used to obtain the parameters of the model.

Figure 3.5 shows the PSD plot of GPS correlated noise in axis x given in the WGS-84 frame. The curve has a cut-off frequency at approximately 0.0018Hz. The roll-off rate after this cut-off is about $-40dB/decade$. This roll-off shows that there are two poles in the transfer function of the error model. There is also a slope change to $-20dB/decade$ at the frequency 0.01Hz which indicates that there is a zero in the transfer function. In the end of the curve, there is some white noise. This PSD curve shows the character of the 2nd order system:

$$G_1(s) = \frac{r(s+\beta)}{s^2 + 2\alpha k s + \alpha^2} \tag{3.49}$$

The PSD plot characteristics are identical to the system (3.30).

The parameters in (3.49) therefore can also be obtained from curve fitting manually.

To model the errors accurately, 50 groups of raw data were collected to average the PSD evaluation. Each group must contain the consecutive raw data for at least 30 minutes. The PSD mean curve which is the average PSD of these 50 groups of data is shown in Figure 3.6. Also shown in this figure is the PSD curve using the estimated

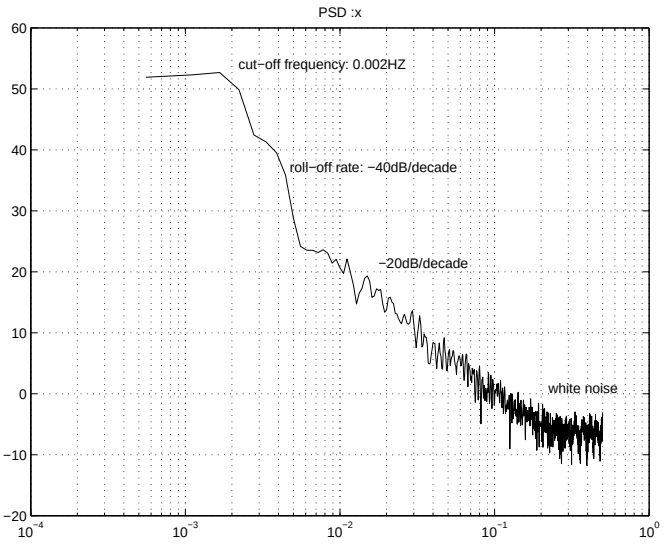

Figure 3.5: PSD curve : x

parameters. The parameters are adjusted until the curve of the estimated PSD best fits the raw PSD curve.

The best fitting PSD curve is obtained by manually adjusting these curves and visual inspection. The model parameters are consequently the best fitted α, β, k and r in that curve. This PSD curve fitting technique can be applied to any position correlated noise in any axis in any frame. Once the model is determined, a traditional shaping filter can be introduced using the transfer function (3.49).

3.5 De-correlate GPS Noise Using INS

3.5.1 Shaping Filter

A shaping filter models a correlated noise as a linear system driven by white noise [49]. The output of the shaping filter is the observed measurement error. The PSD model of GPS correlated noise can be expressed in block diagram form in Figure 3.7 as a shaping filter.

The input of this shaping filter is a unity white noise $\omega_{sp}(t)$. The output $X_s(t)$ is

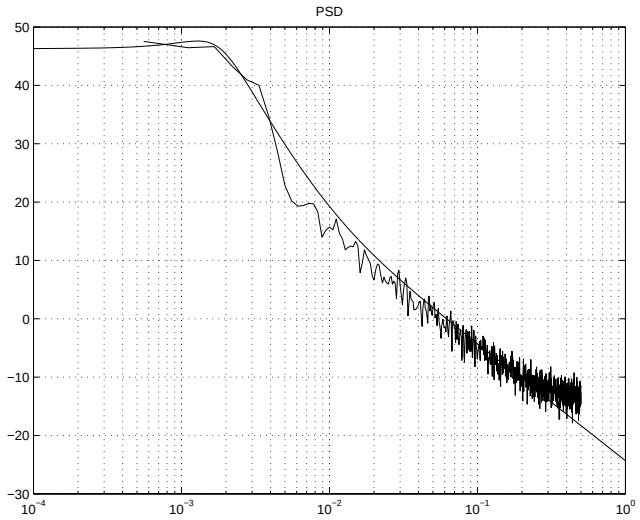

Figure 3.6: PSD curve fitting.

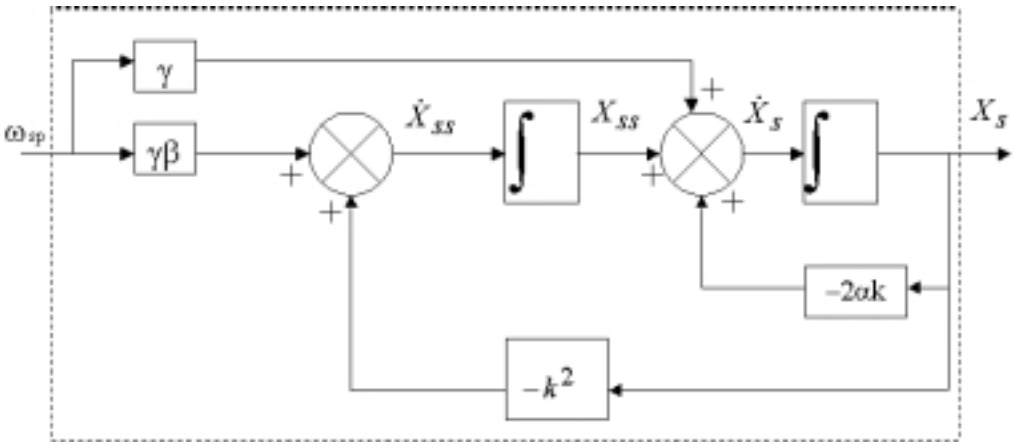

Figure 3.7: Shaping filter.

the GPS correlated noise. Its state space form is given by:

$$\dot{X}_s(t) = -2\alpha k X_s(t) + X_{ss}(t) + r\omega_{sp}(t) \tag{3.50}$$
$$\dot{X}_{ss}(t) = -\alpha^2 X_s(t) + r\beta\omega_{sp}(t)$$

That is:

$$\begin{bmatrix} \dot{X}_s(t) \\ \dot{X}_{ss}(t) \end{bmatrix} = \begin{bmatrix} -2\alpha k & 1 \\ -\alpha^2 & 0 \end{bmatrix} \begin{bmatrix} X_s(t) \\ X_{ss}(t) \end{bmatrix} + \begin{bmatrix} r \\ r\beta \end{bmatrix} \omega_{sp}(t) \tag{3.51}$$

Suppose there is a system with $m \times 1$ state vector $x(t)$ and $p \times 1$ measurement vector $z(t)$:

$$\dot{x}(t) = F(t)x(t) + G(t)\omega(t) \tag{3.52}$$
$$z(t) = H(t)x(t) + n_s(t) + v(t)$$

The system process noise $\omega(t)$ is a $q \times 1$ white noise vector. The measurement is corrupted by white noise $v(t)$ and nonwhite correlated noise $n_s(t)$ with:

$$n_s(t) = X_s(t) \tag{3.53}$$

Define the augmented state vector process $x_a(t)$ as:

$$x_a(t) = \begin{bmatrix} x(t) \\ X_s(t) \\ X_{ss}(t) \end{bmatrix} \tag{3.54}$$

The augmented state process model can be written as

$$\dot{x}_a(t) = \begin{bmatrix} \dot{x}(t) \\ \dot{X}_s(t) \\ \dot{X}_{ss}(t) \end{bmatrix}_{(m+2)} \tag{3.55}$$
$$= \begin{bmatrix} F(t) & 0_{m\times 2} & 0_{m\times 2} \\ 0_{1\times m} & -2\alpha k & 1 \\ 0_{1\times m} & -\alpha^2 & 0 \end{bmatrix} \begin{bmatrix} x(t) \\ X_s(t) \\ X_{ss}(t) \end{bmatrix} + \begin{bmatrix} G & 0_{q\times 1} \\ 0_{1\times q} & r \\ 0_{1\times q} & r\beta \end{bmatrix} \begin{bmatrix} \omega(t) \\ \omega_{sp}(t) \end{bmatrix}$$

The augmented system output can be written as:

$$z(t) = \begin{bmatrix} H(t) & I_p 0_p \end{bmatrix} \begin{bmatrix} x(t) \\ X_s(t) \\ X_{ss}(t) \end{bmatrix} + v(t) \tag{3.56}$$
$$= H_a(t) \times x_a(t) + v(t)$$

with

$$H_a(t) = \begin{bmatrix} H(t) & 0_{p\times 2} \end{bmatrix} \tag{3.57}$$

The augmented system with shaping filter is depicted in Figure 3.8. It is noted that the only driving noise in the augmented system is white noise. It consequently satisfies the basic assumption for the Kalman filter that the non-model dynamics noise is white.

The coloured noise $n_s(t)$ will only be de-correlated from the GPS measurement by external information.

3.5.2 De-correlation of GPS Noise Using Feedforward Filter

Description of the De-correlation Filter

When using a single GPS with correlated noise, the system will exhibit almost identical behaviour regardless of whether the GPS error has been modelled. Further sensing is needed to aid the de-correlation of the coloured noise to improve system accuracy [17]. Consider a filter in one dimension with the combination of a GPS and an INS as in Figure 3.9.

Suppose that the acceleration, velocity and position of INS outputs and the position output of GPS have been transformed into the same navigation frame. Assuming that the acceleration is corrupted by white noise $w_{ins}(t)$ only. The filter states $x(t)$ are INS position error $dr(t)$, INS velocity error $dv(t)$ and two GPS shaping states $X_s(t)$, $X_{ss}(t)$:

$$x(t) = [dr(t), dv(t), X_s(t), X_{ss}(t)]^T \tag{3.58}$$

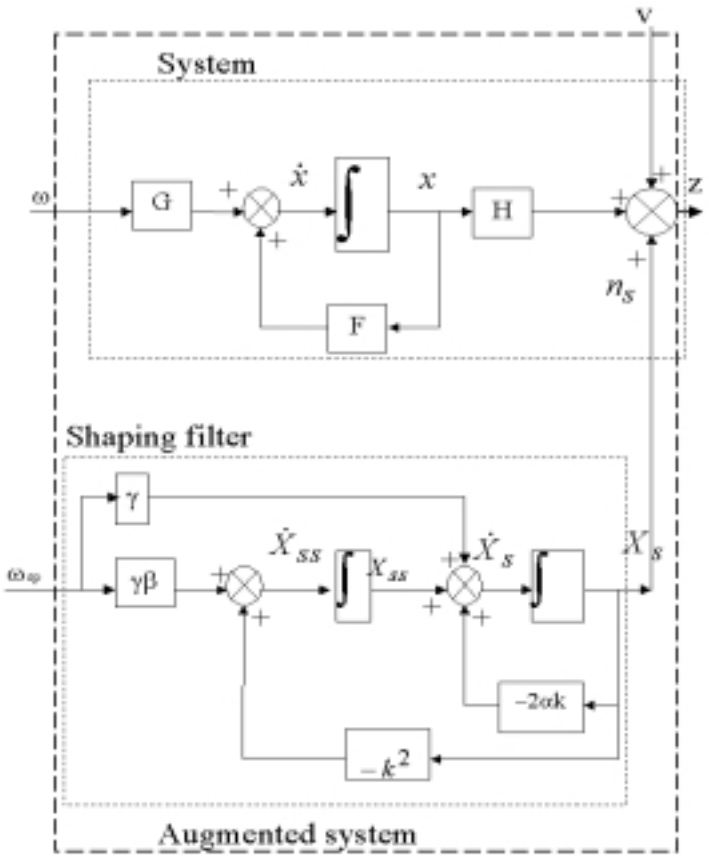

Figure 3.8: Shaping filter generating measurement corruption noise.

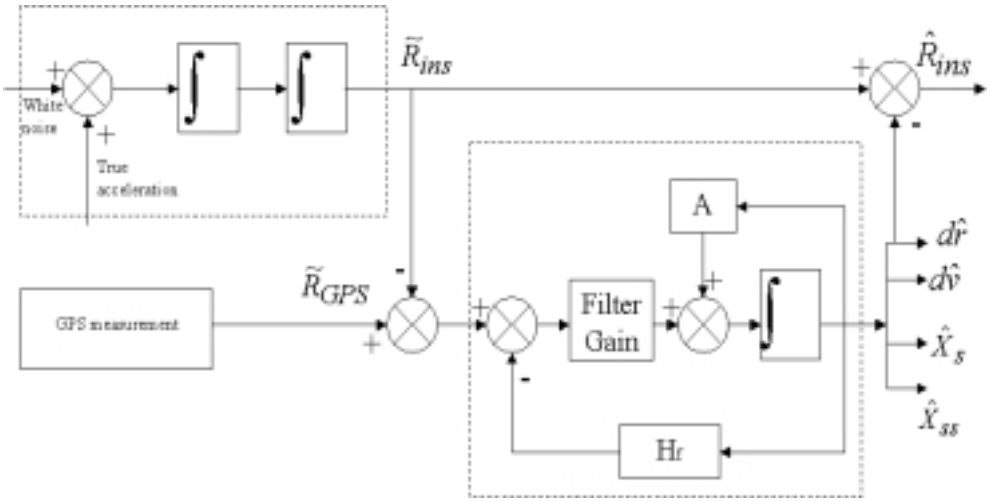

Figure 3.9: Feedforward filter with GPS and INS.

and

$$dr(t) = \widetilde{R}_{ins}(t) - R_{true}(t) \tag{3.59}$$
$$dv(t) = \widetilde{V}_{ins}(t) - V_{true}(t)$$

where $R_{true}(t)$ and $V_{true}(t)$ are the true position and true velocity in the navigation frame. $\widetilde{R}_{ins}(t)$ and $\widetilde{V}_{ins}(t)$ are the outputs of INS position and velocity. The filter measurement $z(t)$ is the difference between the GPS output $\widetilde{R}_{GPS}(t)$ and the INS output $\widetilde{R}_{ins}(t)$.

$$z(t) = \widetilde{R}_{GPS}(t) - \widetilde{R}_{ins}(t) \tag{3.60}$$

GPS outputs are corrupted by the coloured noise $X_s(t)$ and white noise $v(t)$.

We have the relation:

$$d\dot{r}(t) = dv(t) \tag{3.61}$$
$$d\dot{v}(t) = w_{ins}(t)$$

and

$$\begin{aligned} z(t) &= \widetilde{R}_{GPS}(t) - \widetilde{R}_{ins}(t) \\ &= [R_{true}(t) + X_s(t) + v(t)] - [R_{true}(t) + dr(t)] \\ &= -dr(t) + X_s(t) + v(t) \end{aligned} \tag{3.62}$$

The filter process model is given by

$$\begin{bmatrix} d\dot{r}(t) \\ d\dot{v}(t) \\ \dot{X}_s(t) \\ \dot{X}_{ss}(t) \end{bmatrix} = A \begin{bmatrix} dr(t) \\ dv(t) \\ X_s(t) \\ X_{ss}(t) \end{bmatrix} + G_f \begin{bmatrix} w_{ins}(t) \\ \omega_{sp}(t) \end{bmatrix} \tag{3.63}$$

with the process noise being a white noise sequence:

$$w(t) = \begin{bmatrix} w_{ins}(t) \\ \omega_{sp}(t) \end{bmatrix} \tag{3.64}$$

where

$$A = \begin{bmatrix} 0 & 1 & 0 & 0 \\ 0 & 0 & 0 & 0 \\ 0 & 0 & -2\alpha k & 1 \\ 0 & 0 & -\alpha^2 & 0 \end{bmatrix} \tag{3.65}$$

$$G_f = \begin{bmatrix} 0 & 0 \\ 1 & 0 \\ 0 & r \\ 0 & r\beta \end{bmatrix} \tag{3.66}$$

The observation model is given by

$$z(t) = H_f \times x(t) + v(t) \tag{3.67}$$

with

$$H_f = [-1, 0, 1, 0] \tag{3.68}$$

The process and observation noise covariance matrices are

$$Q = E[w(t)w^T(t+\tau)] = \begin{bmatrix} q_{ins}^2 & 0 \\ 0 & 1 \end{bmatrix} \delta(\tau) \tag{3.69}$$

$$R = E[v(t)v^T(t+\tau)] = \sigma_{gps}^2 \delta(\tau) \tag{3.70}$$

with the white noise variance q_{ins}^2 on the acceleration output and the variance σ_{gps}^2 on the GPS position observation.

De-correlation Feedforward Filter Performance in Frequency Domain and Time Domain

In the frequency domain, the transfer function from the observation $z(s)$ to the Kalman filter states estimate $\widehat{x}(s)$ is calculated by:

$$\frac{\widehat{x}(s)}{z(s)} = (sI_{4\times 4} - A + KH_f)^{-1}K \tag{3.71}$$

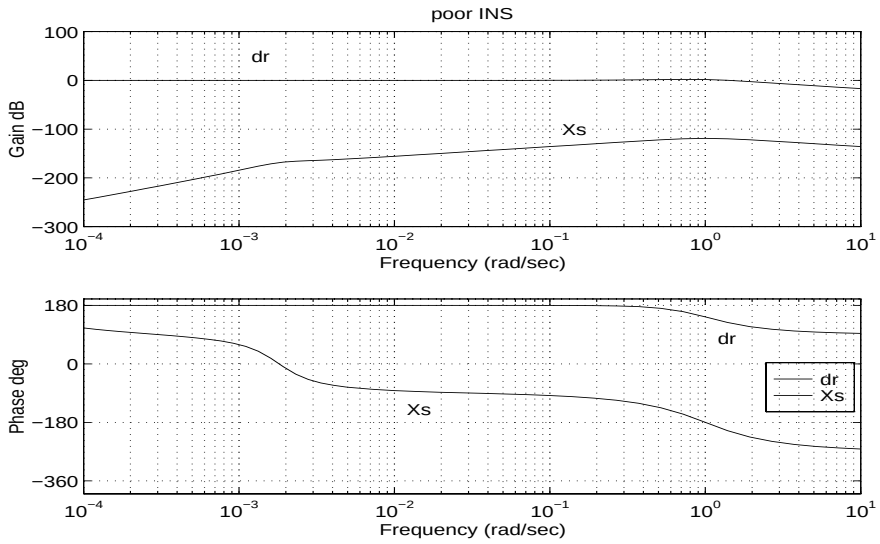

Figure 3.10: Bode plot of the feedforward filter using a poor INS.

with the filter gain K having been determined by the filter parameters and the process and observation noise.

For a single standard GPS without differential correction, the variance of position error is about $20 \times 20m^2$. The Bode plot of a low quality INS with a variance of the acceleration output of $0.1 \times 0.1(m/s^2)^2$ is shown in Figure 3.10. From the plot it can be seen that the gain for the shaping state estimate is very small. The performance of the system in the time domain is shown in Figure 3.11. The GPS position output consists of almost the entire correlated noise when the vehicle is stationary. The estimated shaping state does not follow the shape of the GPS output. The estimate position follows the INS output whose errors grow without bound due to no real-time correction in this kind of filter structure. De-correlation of GPS coloured noise fails with a poor INS of this level quality. These results were presented by Figure 3.10.

Figure 3.12 is the Bode plot of the feedforward filter using a high quality INS with a variance of $1 \times 10^{-6}(m/s^2)^2$ of the acceleration output. The gain for the shaping state estimation in frequency band $10^{-4}(rad/\sec)$ to $10^{-2}(rad/\sec)$ is $0dB$. Figure 3.13 shows the time domain performance of the system. The shaping state estimate

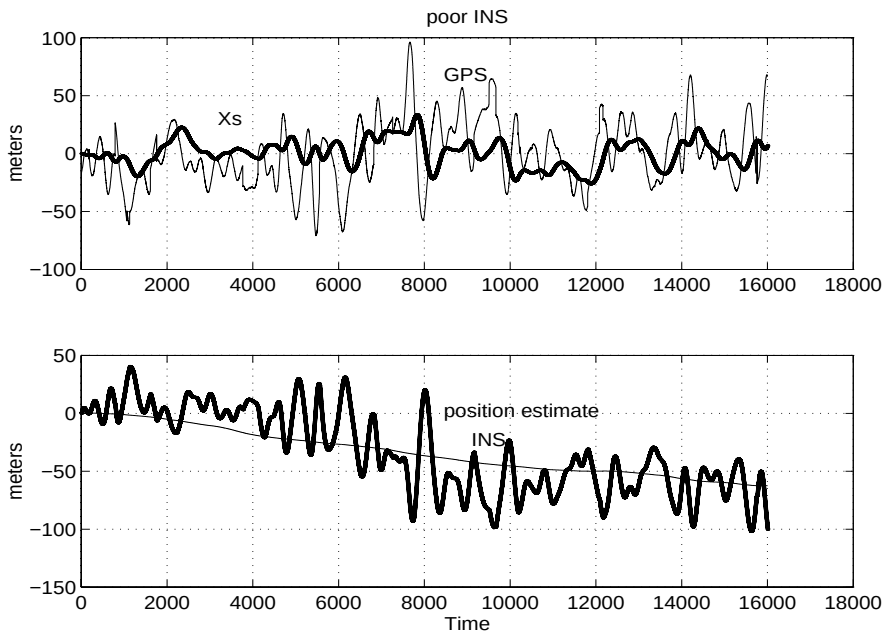

Figure 3.11: Time domain performance of the feedforward filter using a poor INS.

$\widetilde{X}_s$ has almost the same shape and magnitude as the GPS output which is almost the entire coloured noise since the observation corresponds to a fixed position. The position estimate error has been considerably reduced to $4m$ only.

Figure 3.14 shows the Bode plot of the transfer function (3.71) when the variance of the INS noise changes from $0.1 \times 0.1(m/s^2)^2$ to $1 \times 10^{-6}(m/s^2)^2$.

The essential requirement for the variance of the acceleration noise for de-correlation can be found from the Bode plot of the filter transfer function. Therefore, in order to use an indirect feedforward Kalman filter to de-correlate GPS coloured noise with an INS, the accuracy of the INS needs to be above a certain threshold which can be obtained from the Bode plot.

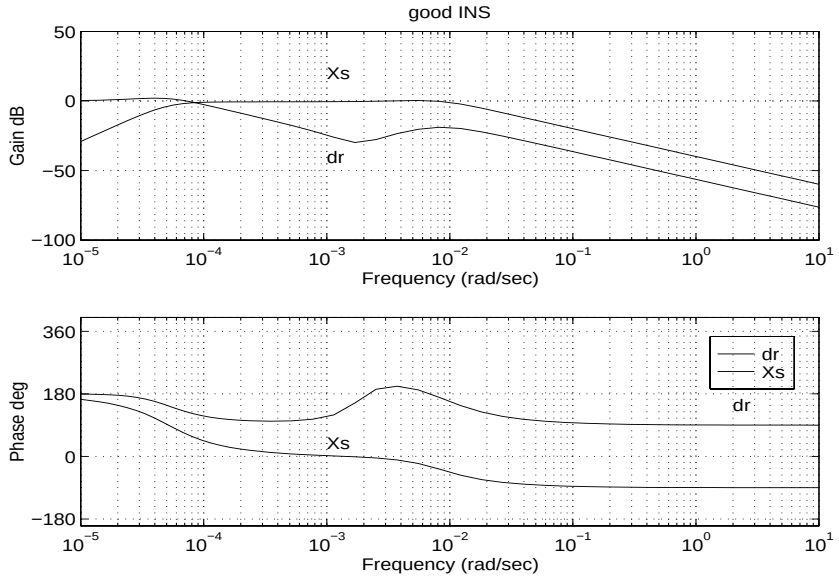

Figure 3.12: Bode plot of the feedforward filter using a good INS.

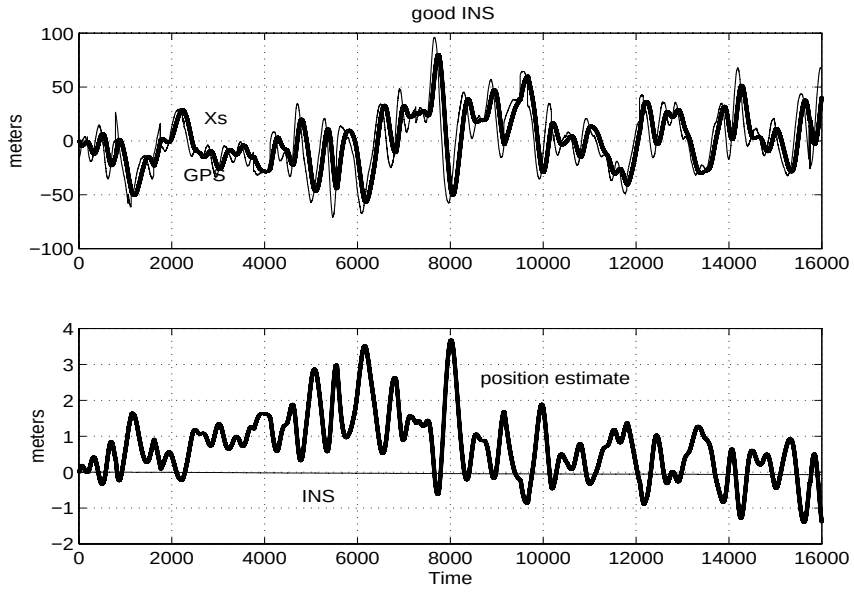

Figure 3.13: Time domain performance of the feedforward filter using a good INS.

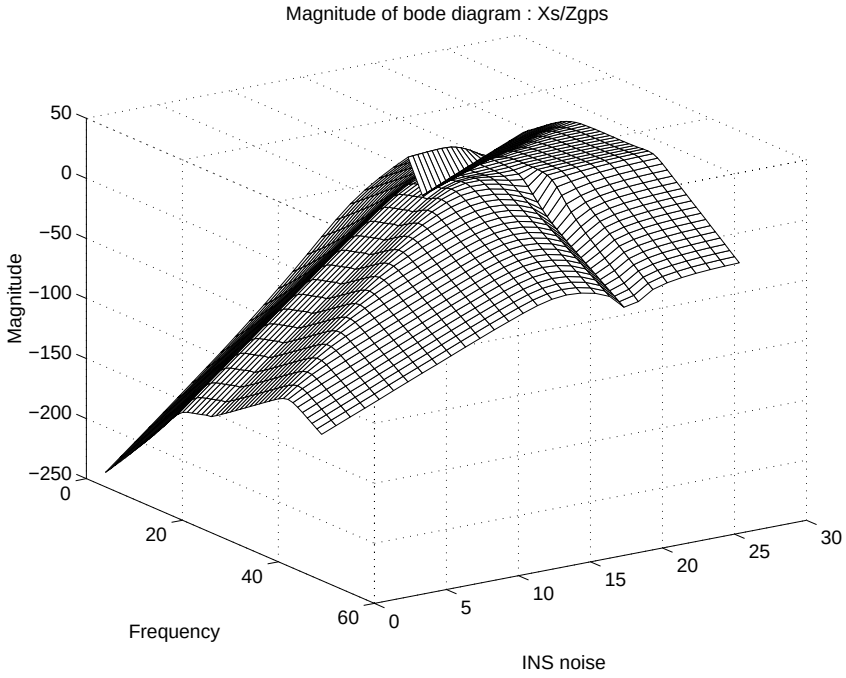

Figure 3.14: Bode plots of the transfer functions using the feedforward filter. The magnitude of the Bode plots, the frequency in rad/sec unit and the INS noise in m/s^2 unit are logarithmically scaled. The magnitude unit in the plots represent the power numbers of the logarithm units. The units for the frequency and INS noise represent the negative power numbers of the logarithm units.

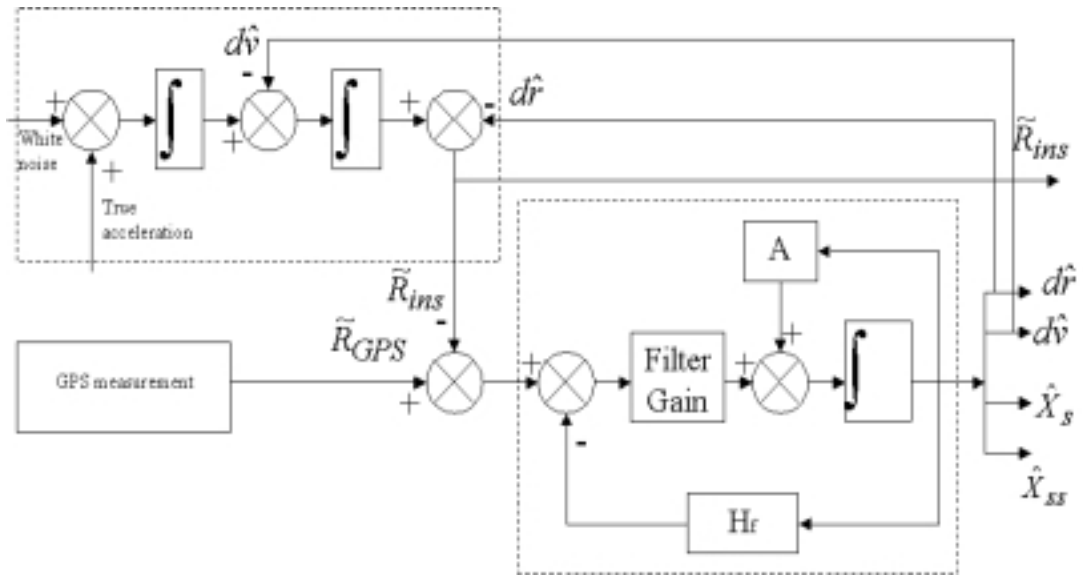

Figure 3.15: Indirect feedback filter

3.5.3 De-correlation Using Indirect Feedback Filter

Filter Description

Using a feedforward filter with INS to de-correlate GPS coloured noise can make the position error grow without bound. An indirect feedback filter can overcome this problem by using estimated INS error to correct the state. Figure 3.15 shows the filter structure.

The INS generates velocity and position at very high frequency. The filter processes the measurement difference between the GPS position and INS position at the GPS sampling time. The filter estimates the position error dr, velocity error dv and two GPS shaping states, feeds back the error estimate to the INS position and velocity to correct the INS velocity and position outputs of the filter. The INS keeps generating the output of the filter until a new GPS observation is made. The filter states are still the INS position error dr, INS velocity error dv and two GPS shaping states X_s, X_{ss}. The process model and the observation model remain the same as the indirect feedforward filter as Figure 3.9.

Filter Performance in Frequency Domain and Time Domain

The performance of the indirect feedback filter is analyzed both in the frequency domain and the time domain. It is found from the experiments that the quality of the INS still affects the de-correlation in this filter structure.

Figure 3.16 shows the Bode plot of the transfer function from the filter observation to the filter estimate using a low quality INS with a noise variance of $0.1 \times 0.1(m/s^2)^2$. From the plot it can be seen that the gain for the GPS shaping state is very low. The time domain performance is shown in Figure 3.17. The shaping state estimate does not follow the shape and the gain of the GPS measurement which is almost the entire coloured noise since the observation corresponds to a fixed position. The INS position output and position estimate are bound over time. The GPS coloured noise de-correlation does not work appropriately with this quality of INS.

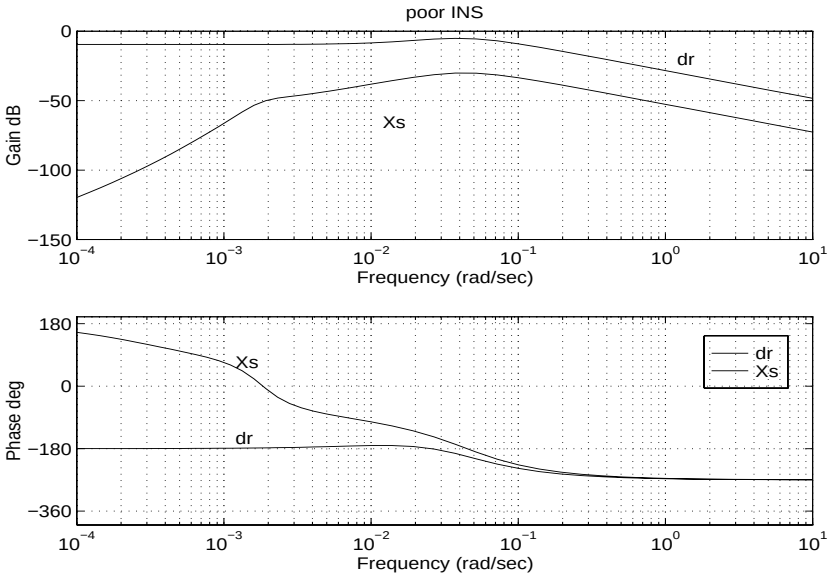

Figure 3.16: Bode plot of the feedback filter with a poor INS.

$1 \times 10^{-6}(m/s^2)^2$ is the threshold value of the noise variance of an accelerometer. The gain of the transfer function for the shaping state $\widetilde{X}_s$ is $0dB$ in the Bode plot before $10^{-2} rad/\sec$ as in Figure 3.18. This means that the shaping state estimate $\widetilde{X}_s$ tracks

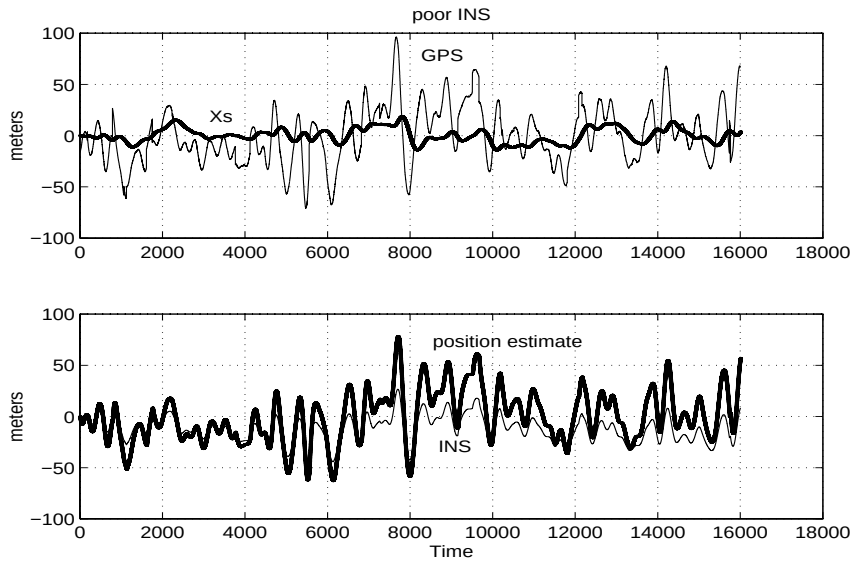

Figure 3.17: Time domain performance with a poor INS using a feedback filter.

the observation which almost entirely consists of GPS coloured noise. Figure 3.19 shows the performance in the time domain. The shaping state estimate $\widetilde{X}_s$ matches the GPS measurement observations.

In order to generate de-correlation the quality of the INS can be obtained using Figure 3.20. From the plot this essential variance requirement is still $3.16 \times 10^{-6} (m/s^2)^2$ for a standard GPS with a variance of $20 \times 20 m^2$.

Therefore, to use an indirect feedback filter to de-correlate the GPS coloured noise, the essential quality requirement of the accelerometer is the same as for the feedforward filter. The additional advantage with this approach is that the position estimate is bound.

3.6 Conclusion

This chapter has introduced an improved GPS error modelling method in the frequency domain. In previous work, the errors were modelled in the pseudo range and clock offset. The measurement from other sensors has to be converted into an equivalent

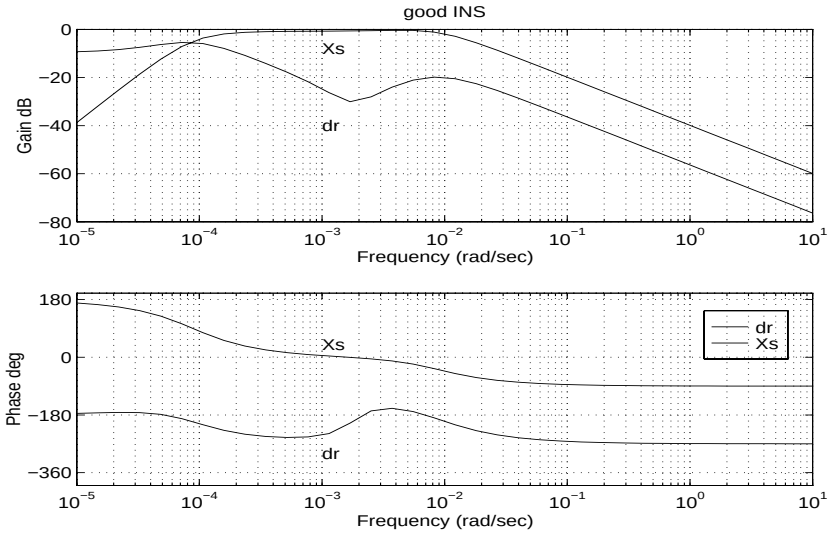

Figure 3.18: Bode plot of the indirect feedback filter with a good INS.

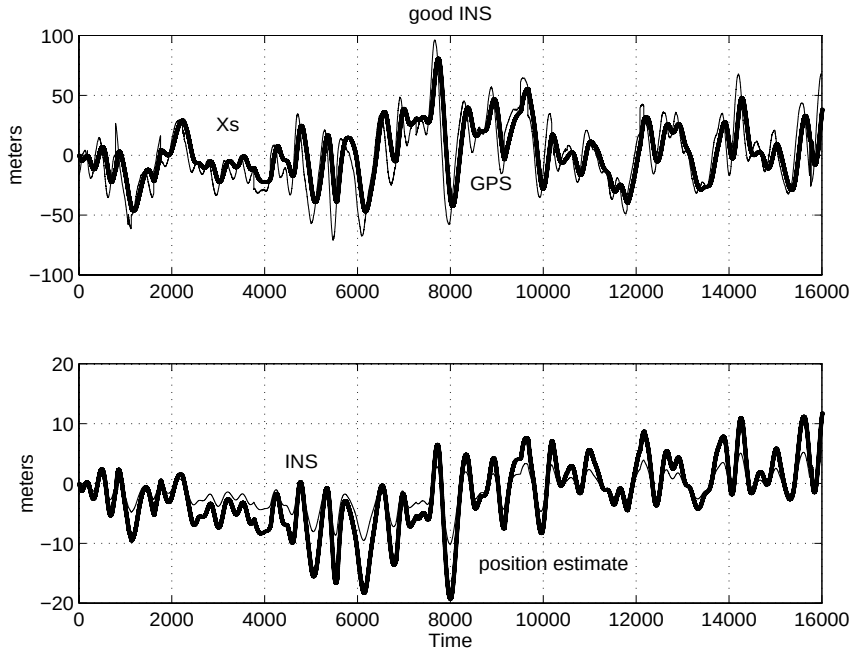

Figure 3.19: Time domain performance of the indirect feedback filter using a good INS.

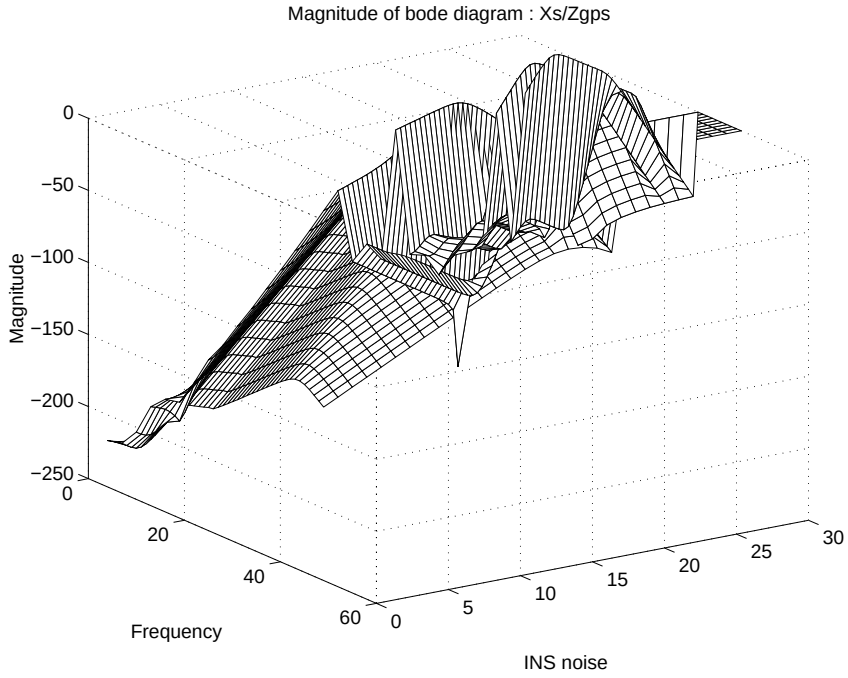

Figure 3.20: Bode plots of the transfer functions using indirect the feedback filter. The magnitude of the Bode plots, the frequency in rad/sec unit and the INS noise in m/s^2 unit are logarithmically scaled. The magnitude unit in the plots represent the power numbers of the logarithm units. The units for the frequency and INS noise represent the negative power numbers of the logarithm units.

pseudo range to match the GPS measurement.

The model of the correlated noise in a GPS position has been derived using a second order system driven by a white noise series.

The PSD model of the correlated position errors in any axis of any frame has been proved to have an identical structure. The parameters of the position error model are obtained from the PSD of the position raw data. By adjusting the poles, zero, damping ratio and the magnitude of the estimate PSD curve against the PSD curve of raw data, the best parameters can be found using the least square or the curve fitting methods.

The PSD model has been used in a shaping filter. To de-correlate the GPS error, another sensor has to be used. Two de-correlation filters using an INS have been discussed in this chapter. To use an indirect feedforward filter with an INS, the position estimate is not bound. The indirect feedback filter has better behaviour with a bound position estimate. The quality of the INS in both the de-correlate filters is required for the de-correlation. The essential variance of the INS has been found using the Bode plot of the transfer function of the de-correlation filters.

The GPS model developed in this chapter will be used in the data fusion filter whose observation contains GPS measurement.

Feedback and feedforward methods have been proposed to design a filter that de-correlates the GPS coloured noise. The minimal requirement for the external sensor is also presented.

Chapter 4

INS Algorithm for Low Cost IMU in Psi Angle Approach

4.1 Introduction

This chapter addresses the design of an INS algorithm for low cost IMUs with unknown initial conditions using the psi angle approach in the computer frame.

Previous INS alignment algorithms are reviewed in Section 4.2. Self-alignment approaches are reviewed in Section 4.2.1. Analytic coarse alignment and gyrocompassing are the major methods for self-alignment. They require measurements of the gravity vector and the earth rate by three accelerometers and three gyros. In-motion alignment is another approach for INS fine alignment which is reviewed in Section 4.2.2. Most of the published applications of in-motion alignment are based on filters with known initial attitudes. For low cost IMUs, the initial attitude errors are usually large. There are very few works that have attempted to solve the problem.

In this chapter, a new algorithm is presented that does not require initial attitudes. Section 4.3 describes the coarse alignment for raw data process and IMU turn-on biases estimation. A method to determine the initial direction cosine matrix is formulated in Section 4.3.2.

Unknown initial attitudes are solved in Section 4.4 by an in-motion alignment al-

gorithm. The filter process models and the measurement equations are developed in Section 4.4.3. The non-linear filter is implemented using the extended Kalman Filter (EKF). The discrete filter and Jacobian matrix are derived in Section 4.4.4.

Section 4.5 describes the navigation stage after the initial alignment. The continuing alignment and the calibration of the system in the navigation are briefly discussed in this section.

4.2 Overview

The INS algorithm generates velocity, position and attitude information. The inputs to the INS algorithm are the measured gyro and accelerometer outputs. The INS algorithm outputs navigation data in a desired navigation frame. The main functions executed in a strapdown INS algorithm are the integration of IMU measured angular rate into attitude and also the transformation and integration of IMU measured specific force acceleration, Coriolis acceleration and modelled gravity to the desired navigation frame [50, 51].

The INS integration assumes the initial values of velocity, position and attitude. Therefore an initial alignment phase is required before navigation begins.

Initial misalignment is one of the major error sources of the INS. During the initial alignment phase, the attitude difference between the axes of the INS coordinate systems and those of a chosen reference is estimated and removed. This attitude difference, or misalignment consists of two tilt angles and an azimuth angle which have distinct effects on the propagation errors of the INS. The Kalman filter has been successfully used to estimate the tilt and the azimuth errors of the INS. It is well known that the estimation rate of the azimuth misalignment and the final value it reaches are the two factors that determine the performance of the whole alignment process [52]. The initial alignment can be performed either when the INS is at rest on ground or while the vehicle is in motion.

4.2.1 Self-alignment Review

One of the ground alignment methods is to obtain the INS initial attitude through the use of external reference by optical techniques, magnetic heading sensors or other external means. Most ground based applications consist of two phases: leveling and azimuth alignment [53]. Two self-alignment methods have been considered: gyrocompass alignment and analytic alignment [27, 53, 54, 16, 55, 56, 57, 58, 4, 59] . The analytic method is used for coarse alignment while the gyrocompass method is used for fine alignment [58, 53].

The analytic coarse alignment method determines the transformation matrix which relates vectors in the desired navigation frame to the same vectors expressed in the geographic frame or in other equivalent frames using the knowledge of the gravity g and the earth rate vectors w_{ie}.

Define a vector v as

$$v = g \times w_{ie} \tag{4.1}$$

The alignment matrix C_g^n is given by:

$$C_g^n = \begin{bmatrix} (g^n)^T \\ (w_{ie}^n)^T \\ (v^n)^T \end{bmatrix}^{-1} \begin{bmatrix} (g^g)^T \\ (w_{ie}^g)^T \\ (v^g)^T \end{bmatrix} \tag{4.2}$$

where the gravity vector g and the earth rate w_{ie} in the desired navigation frame n and the geographic frame g are g^n , g^g, w_{ie}^n and w_{ie}^g.

Britting [27] analyzed the errors of the analytic coarse alignment scheme by taking into account the effect of instrument uncertainties and that the base motions are not readily amenable to analytic methods. This method requires the vectors g and w_{ie} to be measured.

For a gimbled INS, physical gyrocompass alignment consists of finding the coordinate transformation between local geographic axes and navigation axes by physical gyrocompassing. The transformation matrix C_g^n is physically driven to be the unit matrix.

For strapdown INS, the initial alignment matrix represents the transformation from the body frame to the navigation frame. This analytic alignment method can be used for high accuracy applications in only the most benign of environments [27], since the performance deteriorates because of angular disturbance vibrations and accelerations. The measurement of the gravity and the earth rate could also be corrupted. Some filtering is introduced in order to reduce the effects of these vibrations. When a low-pass filter is used to obtain the average values of the measured quantities, the instantaneous position of the body frame can vary considerably from its average position. A significant misalignment could exist when the system is switched to the navigation operation mode. A self-corrective alignment scheme is introduced to refine the initial estimate of the transformation matrix by using the error angles between the known reference frame and the corresponding computed frame.

Many gyrocompassing algorithms for both gimbled INSs and strapdown INSs have appeared in literature. Jurenka and Leondes developed an optimum controller for driving the alignment in 1967 [58]. Huang and White presented self-alignment techniques for an IMU considering the fine alignment of an INS platform whose base is subject to vibration and whose sensors are subject to noise in 1975 [57]. The observability of INS ground alignment was analyzed by Jiang and Lin in 1992 [53]. In the covariance analysis of strapdown INS considering gyrocompass characteristics by Heung *et al.* in 1995 [56], it was found that cross-coupling terms in gyrocompass alignment errors can significantly influence the strapdown INS error propagation. The initial heading error has a close correlation with the east component of gyro bias error, while initial level tilt errors are closely linked to the accelerometer bias error. Heung *et al.* also developed a multiposition alignment method for INS stationary alignment on ground in 1993.

Bar-Itzhack summarized INS error models for the ground alignment in 1988 [4]. All these models in the literature assume that the initial misalignments are small angles with errors of only a few degrees. The measurement of the earth rate is indispensable and an essential input for the ground alignment.

4.2.2 In-motion Alignment Review

If the initial alignment is carried out when the vehicle is in motion, the alignment is called in-motion alignment. The initial condition can be obtained by transfer alignment.

Transfer alignment is the operation of aligning a slave INS with a master INS comparing quantities computed by both INSs [60]. Direct transfer of the master INS navigation states would not account for the fact that the slave INS is not pointed in the same direction as the master INS. In the transfer alignment stage, the velocity computed by the master INS is compared with the one computed by the slave INS and the difference, which is indicative of the slave misalignment with respect to the master INS, is processed by a Kalman filter. This yields misalignment data as well as the slave gyro and accelerometer error data. There are some other inertial measurement matching methods such as velocity matching alignment and position update alignment which achieve in-motion alignment by comparing estimates of velocity and position generated by the aligning INS with estimates of the same quantities provided by the master INS [1].

There are many issues concerning the transfer alignment algorithm design [52, 60, 61]. Bar-Itzhack investigated the azimuth observability enhancement that was accomplished by subjecting the INS to accelerations generated by manoeuvres of a combat aircraft [52]. The effect of acceleration switching during INS in-motion alignment was also analyzed [62].

To obtain high accuracy and a highly robust navigation system, inertial navigation aided by other navigation references like star scanner, GPS, laser, radar, sighting devices and Doppler have been widely used [63, 64, 65]. Complementary filtering is the one mutual aiding method implemented in the frequency domain [65]. It is applied to the fusion of a compass-aided heading gyro, Doppler-inertial ground speed estimation and a baro-inertial altimeter. In the time domain, Kalman filtering with INS error models has been the main tool for the implementation of aided INS in-motion alignment, navigation and calibration stages. The assumption of small misalignment angles is implied in those

filterings and models.

4.2.3 Large Misalignment Problem Review

Ground alignment in the stationary stage using gyrocompassing, analytic alignment, aiding attitude sensors and in-motion alignment using reference navigation information have been the main methods for INS initial alignment. With the assumption of small initial misalignments, Kalman filter mechanizations using the INS error propagation models have been designed and implemented for many years.

Ground self-alignment is limited to high resolution inertial measurement units which are able to measure the vectors of gravity and the earth rate. For low cost IMUs, with resolution lower than the quantities of the gravity or the earth rate, self-alignment principles will not work. External sensors have to be employed to obtain the initial attitude [16]. If external sensors are not available, the initial misalignment will be large. Several attempts have been made to solve this problem.

Jiang and Lin [66] suggested an error estimation algorithm in the true frame for ground alignment for an arbitrary azimuth. The misalignment is estimated by a combination of leveling error rates. However the misalignment propagation was not modelled.

In 1992, Pham introduced a Kalman filter mechanization for strapdown INS airstart with an unknown azimuth [28]. He assumed two small tilt misalignment errors and one large heading error. Heading misalignment α is considered as a wander angle in a wander angle frame and separated into two states $\sin\alpha$ and $\cos\alpha$ in the filter. The earth rate is still the required input in the filter process model. The misalignment was not modelled.

In 1994 and 1996, Scherzinger developed inertial navigator error models for large heading uncertainty [9, 10]. The expected application was for alignment with an unknown heading. The computer frame approach was used. Again, two states were used to track one heading misalignment variable. An extended misalignment vector Ψ_e was

defined as:

$$\Psi_e = [\psi_x, \psi_y, \sin\psi_z, \cos\psi_z - 1] \tag{4.3}$$

where the psi angle $[\psi_x, \psi_y, \psi_z]$ is the misalignment of the computer frame and the platform frame. Scherzinger's model has a similar form of the psi angle model developed in the literature by Benson [5] and Bar-Itzhack [24].

In 1997, Dmitriyev *et al.* published a nonlinear filter method application in INS alignment which discussed the problem of coarse alignment [8]. Error equations with a nonlinear characteristic have been obtained with a considerable level of a priori coarse uncertainty. The error model is designed in the true frame with the assumption of two small tilt misalignments and one large heading misalignment. The nonlinear characteristic of the problem was considered over a short period. As a result, the heading misalignment rate was assumed to be zero. In the misalignment error models, the rates of misalignment angles were coupled with the velocity errors and the velocity errors are coupled with the misalignment angles.

In 1997, Rogers proposed another in-motion alignment method without the benefit of attitude initialization [67]. Similar to the methods of Pham and Scherzinger, Roger's filter contained two sine and cosine states of the heading error. Small tilts and large heading error were assumed.

The psi angle models and quaternion models for three large misalignment error angles in the computer frame developed in the previous chapter of this thesis provide a solution to the unknown initial attitude problem. The additional two tilt angles and one heading angle could be all large using the proposed models.

4.3 Coarse Alignment

An INS commonly uses the analytic alignment and the gyrocompass principle to perform self-alignment on ground. For a low cost IMU which cannot measure the earth rate vector, external sensors must to be used.

In this thesis, a low grade inertial measurement system, made by Watson Industry INC. is used. The resolution of gyros and accelerometers for the Watson IMU are shown in the following table:

Watson IMU	IMU-1	IMU-2
gyros	$1.0779\times10^{-4}\ rad/sec$	$4.3115\times10^{-4}\ rad/\sec$
accelerometers	$0.0024\ m/s^2$	$0.0024\ m/s^2$

Figure 4.1 shows the raw data of the Watson IMU-1 in a stationary stage.

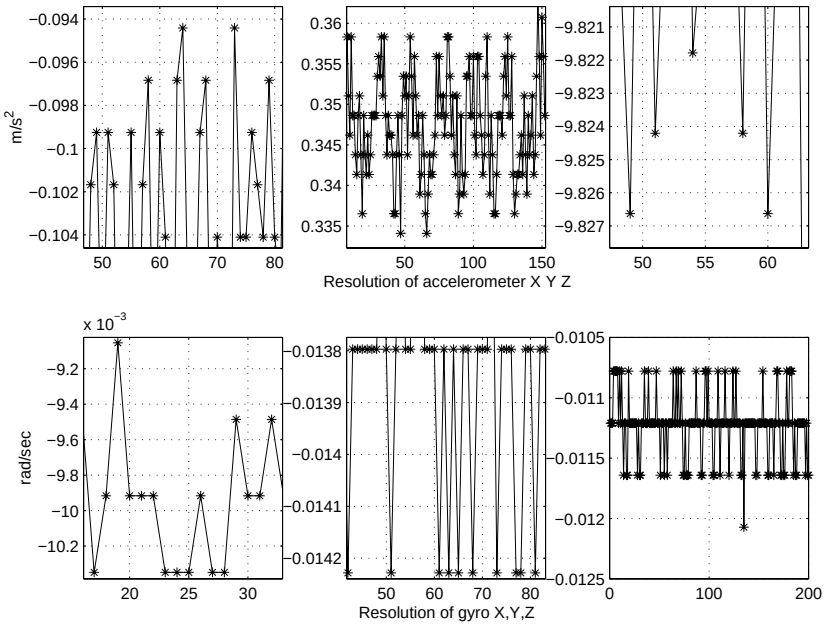

Figure 4.1: Resolution of Watson IMU-1.

The quantity of the earth rate vector is $7.2722\times10^{-5} rad/sec$. Usually, the resolution of accelerometers is high enough to measure the gravity vector. For this kind of IMU, the coarse alignment can be partly performed using the acceleration data to detect the tilt information. The coarse alignment algorithm is introduced here. The raw data process which determines the average turn-on biases of the accelerometers and gyros is included in the coarse alignment stage.

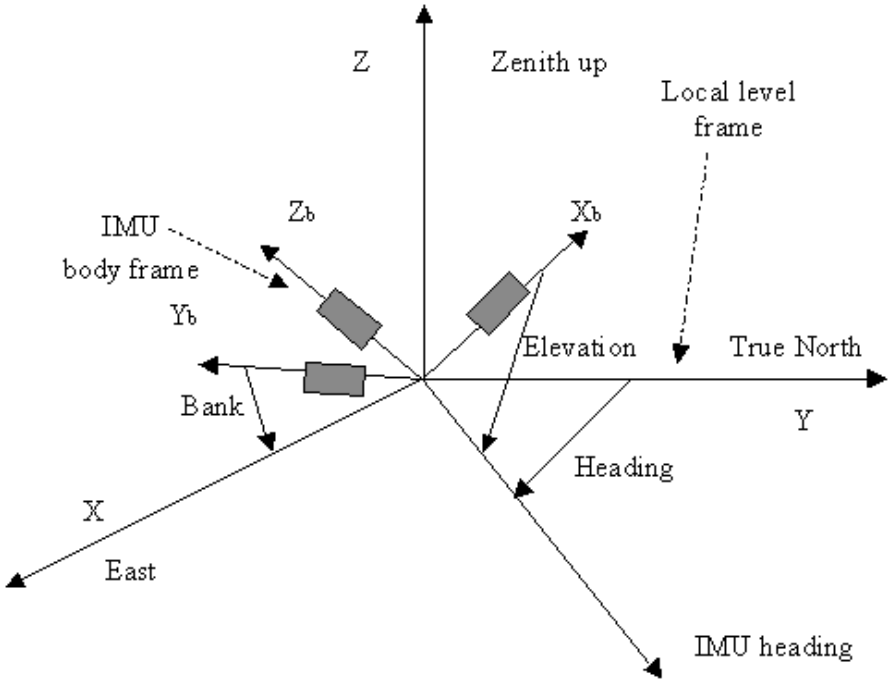

Figure 4.2: Bank and elevation of Watson IMU.

4.3.1 Raw Data Process

Once the IMU is turned on, there are random biases in the accelerometers and gyros. They have a crucial effect on attitude, velocity and position. The integration of the biases of the accelerometers cause the position errors to increase quadratically over time. The attitudes, direction cosine matrix and quaternions will also have important errors from integrating the gyro biases. Therefore, the gyro biases will accumulate the position errors over time proportional to the cube of the time index.

The following table gives examples of the effects on velocity and position by the Watson IMU.

axis (IMU body frame)	gyro bias (rad/sec)	accelerometer bias (m/sec^2)
x	0.004	0.008
y	0.008	0.2
z	0.003	0.03

Figure 4.3 shows the average biases of the three accelerometers and the three gyros

of IMU-1 installed in the body frame over a period of 34 seconds.

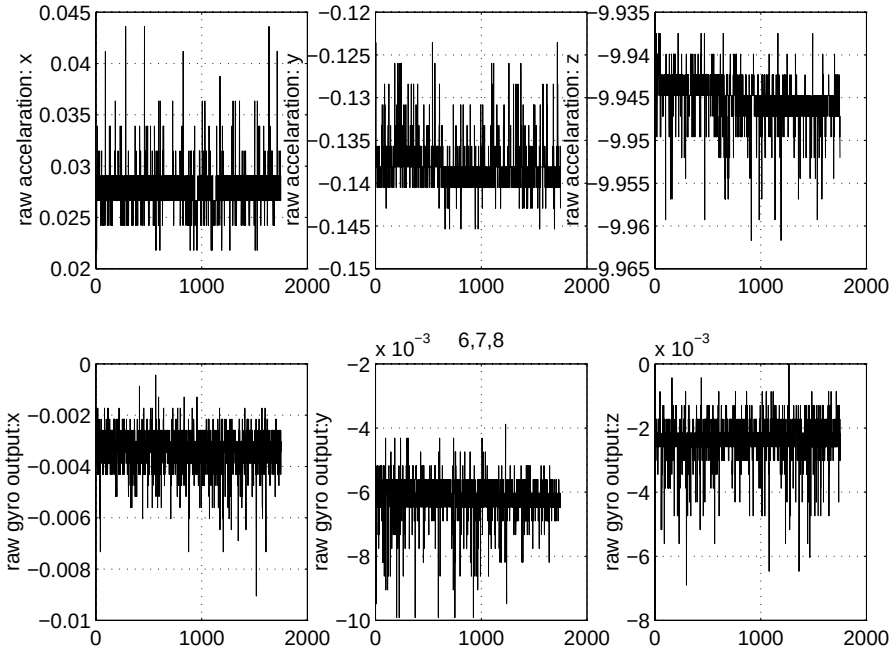

Figure 4.3: These six plots show the turn-on biases for the Waston IMU-1. The 2000 samples are taken over a period of 34 seconds. The units for the y axes in the top three plots are m/s^2. The units for the y axes in the bottom three plots are rad/s.

Figure 4.4 shows the quaternion errors due to the gyro biases in a stationary position over 28 seconds. The four curves of the four elements $[Q_0, Q_1, Q_2, Q_3]$ show linear divergence over time.

The first order, the second order and the third order effects over time of the IMU turn-on biases are shown in Figure 4.5. The acceleration "Vtx_DOT" and "Vty_DOT" of axes x and y in the platform frame show a large linear divergence over time. The velocity "V_tx" and "V_ty" show a quadratic divergence over time squared. The curves of the position coordinates "dx_WGS84" and "dy_WGS84" have a third order relationship with time.

The gyro bias of 0.008 $rad/second$ and the accelerometer bias of 0.2 $m/second^2$ will cause a velocity error of 20 m/s and a position error of $200m$ over 28 seconds.

These results demonstrate that before the raw data can be used, it is essential to

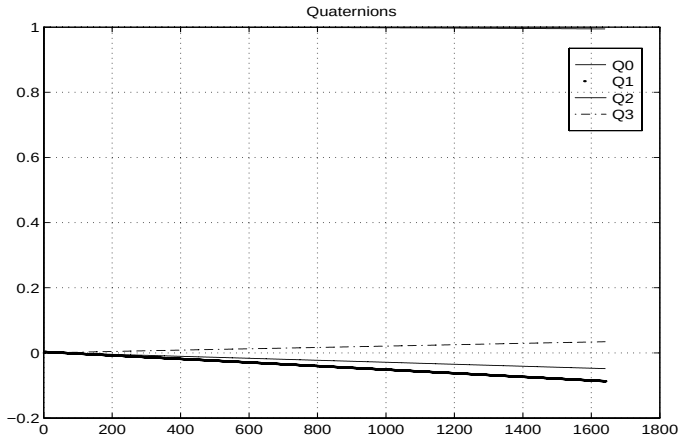

Figure 4.4: Quaternion errors due to gyro biases. The 1650 samples are taken over a period of 28 seconds. The unit for the quaternions is 1.

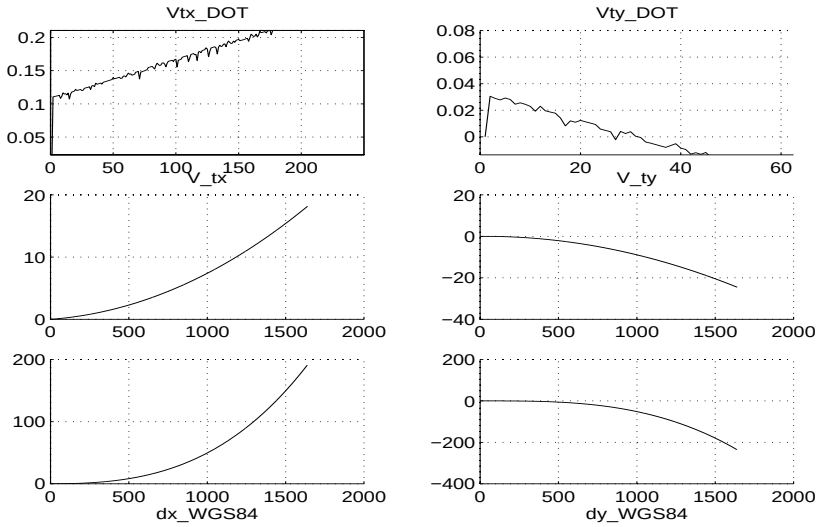

Figure 4.5: Errors of acceleration, velocity and position due to turn-on biases of IMU. The units for y axes in the top two plots, the middle two plots and the bottom two plots are m/s^2, m/s and m respectively. Along x axes are data samples over time taken at 84Hz in 20 seconds.

remove the turn on biases. The method of bias determination is discussed here.

The frames of the Watson IMU are shown in Figure 4.2. The bank and elevation information are defined as the angles with respect to the local level frame in Figure 4.2. The average tilt angles from the tilt gyros are used to generate the coarse alignment information.

Turn-on Biases of the Accelerometers

A time period during the stationary stage is selected. Define the vector of the average output of the three accelerometers in the body frame:

$$\hat{F}_b = [\hat{f}_x^b, \hat{f}_y^b, \hat{f}_z^b]^T \tag{4.4}$$

This is the sum of the true acceleration vector F_b in the body frame and the bias vector of the accelerometers $\nabla^b(0)$ in the body frame:

$$\hat{F}_b = F_b + \nabla^b(0) \tag{4.5}$$

The true acceleration vector F_b is transformed by the gravity vector in the platform frame:

$$F_b = C_p^b[0, 0, -g]^T = (C_b^p)^{-1}[0, 0, -g]^T \tag{4.6}$$

where the direction cosine matrix C_p^b is given by [68]:

$$C_b^p = \begin{bmatrix} \cos\beta\cos H - \sin\beta\sin EL\sin H & -\cos EL\sin H \\ \cos\beta\sin H + \sin\beta\sin EL\cos H & \cos EL\cos H \\ -\sin\beta\cos EL & \sin EL \end{bmatrix} \tag{4.7}$$

$$\begin{bmatrix} \sin\beta\cos H + \cos\beta\sin EL\sin H \\ \sin\beta\sin H - \cos\beta\sin EL\cos H \\ \cos\beta\cos EL \end{bmatrix}$$

where BK, EL and H are the average bank, elevation and heading information during the stationary stage and

$$\beta = \sin^{-1}(\frac{\sin BK}{\cos EL}) \tag{4.8}$$

Therefore the bias vector of the accelerometers $\nabla^b(0)$ is subtracted from (4.5):

$$\begin{aligned}\nabla^b(0) &= \hat{F}_b - F_b \\ &= [\hat{f}_x^b, \hat{f}_y^b, \hat{f}_z^b]^T - (C_b^p)^{-1}[0, 0, -g]^T \\ &= \begin{bmatrix} \hat{f}_x^b \\ \hat{f}_y^b \\ \hat{f}_z^b \end{bmatrix} - \begin{bmatrix} -\sin\beta\cos EL \\ \sin EL \\ \cos BK\cos EL \end{bmatrix} g \end{aligned} \tag{4.9}$$

The heading does not appear here.

Turn-on Biases of the Gyros

Theoretically, the turn-on biases of the gyros are derived from the earth rate. During the coarse alignment, the vehicle which is stationary, senses the earth rate only. In the platform frame, the output of the gyros $\hat{W}^p$ is the sum of the earth rate Ω_{ie} and the turn-on bias of the gyros ∇^p:

$$\hat{W}^p = \Omega_{ie} + \nabla^p \tag{4.10}$$

For the convenience of removal of the gyro biases from the raw data in the body frame, the bias vector is converted into the body frame:

$$\nabla^b = C_p^b(0)\nabla^p = C_p^b(0)(\hat{W}^p - \Omega_{ie}) \tag{4.11}$$

The earth rate term is ignored for a low cost IMU, therefore:

$$\begin{aligned}\nabla^b &= C_p^b(0)\hat{W}^p \\ &= (C_p^b(0))^{-1}(C_b^p(0)\hat{W}^b) \\ &= \hat{W}^b = \begin{bmatrix} \hat{\omega}_x^b \\ \hat{\omega}_y^b \\ \hat{\omega}_z^b \end{bmatrix} \end{aligned} \tag{4.12}$$

To remove the turn on biases of the three gyros, the average gyro measurement $\hat{W}^b = \left[\hat{\omega}_x^b, \hat{\omega}_y^b, \hat{\omega}_z^b\right]^T$ is removed from the raw data.

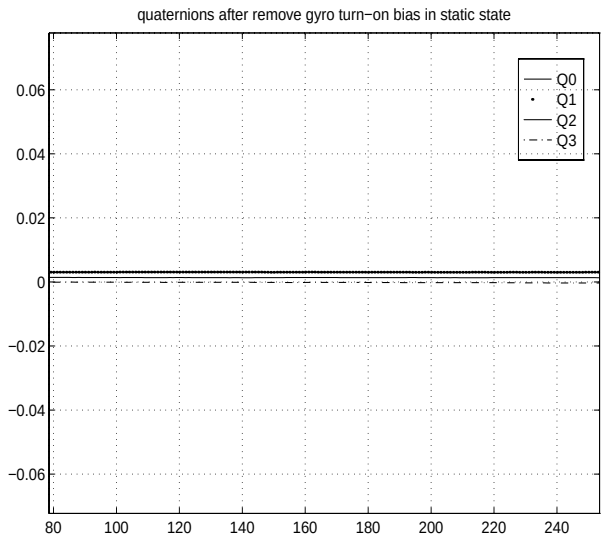

Figure 4.6: Quaternions after removal of turn on biases of gyros. The unit for the quaternions is 1. Along x axis are data samples over time taken at 84Hz.

After the removal of the turn-on biases, the raw data from the IMU can be used directly for navigation. Figure 4.6 is a plot of quaternions over 28 seconds. Compared with the Figure 4.4 before the removal of turn on biases, the four curves of the four elements $[Q_0,Q_1,Q_2,Q_3]$ are almost flat without divergence.

The errors in acceleration, velocity and position are reduced after this process. Figure 4.7 is a plot of computed acceleration, velocity and position in the platform frame while the Watson IMU was moving in an oscillation trajectory of $20cm$ around a fixed point for 320 seconds. As in Figure 4.7, the acceleration "Vtx_DOT" and "Vty_DOT" of the axes x and y in the platform frame after 300 seconds are almost zero without divergence. The velocity "V_tx", "V_ty" and position "dx_WGS84", "dy_WGS84" still have some errors but are considerably smaller. The remaining biases are modelled and will be removed by in-motion calibration algorithms.

4.3.2 Coarse Leveling - Initial Direction Cosine Matrix

The purpose of the leveling algorithm is to obtain the initial attitudes of the INS, that is the initial direction cosine matrix or the initial quaternions. The turn-on biases of

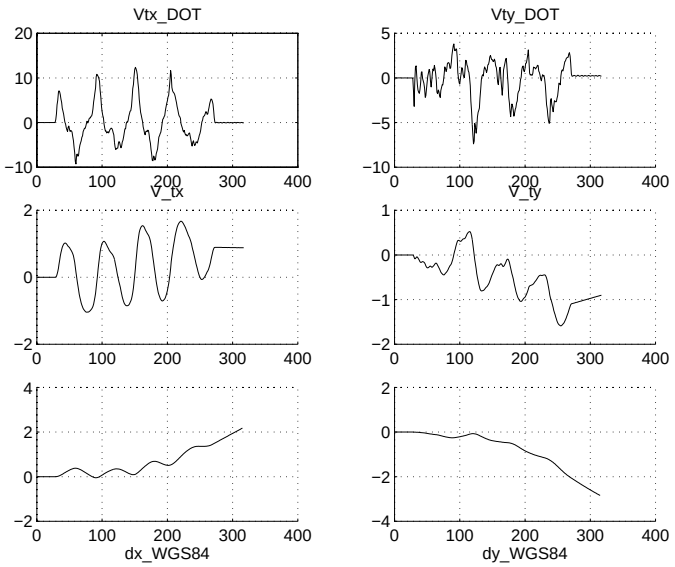

Figure 4.7: Acceleration, velocity and position after removal of turn-on biases. Along x axes are data samples over time taken at 84Hz. The units for the y axes in the top two plots, the middle two plots and the bottom two plots are m/s^2, m/s and m respectively.

the accelerometers and the gyros are also computed at this stage. The coarse leveling alignment is conducted on-ground. The inertial cosine matrix for the psi angle approach will be considered.

The direction of the axes x, y and z is defined as east-north-up of the local level frame. The initial direction cosine matrix is constructed by the initial attitude and the initial heading. In the coarse alignment mode, the vehicle remains stable for at least 15 seconds. Average bank and elevation are recorded as BK and EL. The heading is unknown for a low cost INS and will be solved by the in-motion alignment algorithm. Assuming an arbitrary heading input H, the initial direction cosine matrix C_b^p between the body frame and the platform frame is given by Equation (4.7).

The computation uses the average bank and elevation data during the stationary stage. The vehicle position may be changed from its average position. Due to the noise and the vibration of the vehicle, this estimation of leveling is only an approximation. The fine alignment will be performed during the in-motion alignment stage when the vehicle starts to move.

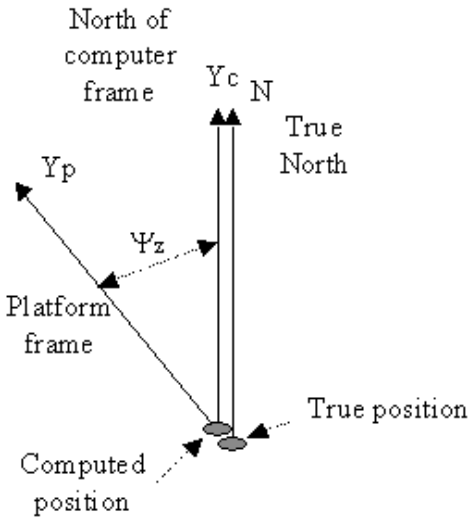

Figure 4.8: Heading error definition.

4.4 In-motion Alignment: Solution of Initial Attitude Uncertainty

4.4.1 Introduction

The coarse alignment takes about 15-20 seconds to obtain the initial values of the navigation needs except the initial heading of the IMU. The purpose of the in-motion alignment in this thesis is to solve heading uncertainty. The calibration of the direction cosine matrix or the quaternions, the correction of the velocity and the position errors and calibration of the accelerometers and the gyros are also done at this stage.

A low cost IMU cannot work alone due to the drift and nonlinearity of the inertial sensors. External velocity or position information has to be employed to aid the INS. GPS is an ideal source to aid an INS.

In this section, heading uncertainty is solved during in-motion alignment using GPS information. The psi angle model for large angle errors developed in the previous chapter is applied.

As illustrated in Figure 4.8, the true heading error is the misalignment between the

platform north and the true north of the true local level frame at the true position. The position is aided by external position reference. The position error of the computed position and the true position is small. Therefore the north of the computer frame is very close to the true north of the true local level frame at the true position. The misalignment ψ_z between the computer frame and the platform frame is approximately the heading error. The correction of ψ_z consequently becomes the goal of the heading uncertainty algorithm.

In-motion alignment commences after the coarse alignment. The initial heading entry is arbitrarily set.

When the GPS fix is not available, the INS performs vehicle navigation in the platform frame at each IMU sampling time. The gyros of the IMU output the angular rate of the vehicle in the body frame which can be used to calculate the direction cosine matrix. The accelerometers output the acceleration of the vehicle in the body frame which is transformed into the platform frame by the direction cosine matrix . The INS navigation outputs the attitude, velocity and position in the platform frame by integrating the angular rate, acceleration and velocity respectively.

When the GPS fix becomes available, the velocity and position measurements of the GPS fix are processed. A nonlinear filter based on the computer approach (the psi angle approach) estimates the psi angle errors, velocity errors and position propagation errors of the INS in the computer frame and the drift errors of the accelerometers, the gyros and the GPS errors. The nonlinearity of the filter is due to the nonlinearity of the psi angle model for large heading errors between $[-180^\circ, +180^\circ]$. The estimates of the errors are used to correct the velocity, position and attitude. The readings of the accelerometers, gyros and the GPS measurement are also compensated by the filter estimation of the sensor errors.

The algorithm runs until the errors are corrected. The three attitude errors are now all satisfied to the small angle assumption. The psi angle model can be switched to its small angle form. The algorithm is then switched from the alignment mode to the navigation mode which still employs the same filter, only the psi angle model switches

to its small angle form.

The flow chart of the algorithm is shown in Figure 4.9.

4.4.2 Filter States

The filter in the heading correction stage is performing alignment and calibration. The filter states include the propagation errors of the velocity, position and attitude errors in the computer frame. Measurement errors are contained in the shaping filter which is part of the alignment and calibration filter. X being the filter state vector, then:

$$X = [\Delta V_x^c, \Delta V_y^c, \Delta V_z^c, \Delta R_x^c, \Delta R_y^c, \Delta R_z^c, \psi_{x,}\psi_{y,}\psi_{z,} \\ \nabla_{x,}^b \nabla_{y,}^b \nabla_{z,}^b \epsilon_x^b, \epsilon_y^b, \epsilon_z^b, X_{sx}, X_{sy}, X_{sz}, X_{2x}, X_{2y}, X_{2z}]^T \tag{4.13}$$

where

$\Delta V^c = [V_x^c, \Delta V_y^c, \Delta V_z^c]^T$ is the INS velocity error vector in the computer frame.

$\Delta R^c = [\Delta R_x^c, \Delta R_y^c, \Delta R_z^c]^T$ is the INS position error vector in the computer frame.

$\psi = [\psi_{x,}\psi_{y,}\psi_z]^T$ is the psi angle vector, which is the angle between the computer frame and the platform frame.

$\nabla^b = [\nabla_{x,}^b \nabla_{y,}^b \nabla_z^b]^T$ is the vector of the accelerometer biases in the body frame.

$\epsilon^b = [\epsilon_x^b, \epsilon_y^b, \epsilon_z^b]^T$ is the vector of the gyro biases in the body frame.

$X_s = [X_{sx}, X_{sy}, X_{sz}]^T$ and $X_{ss} = [X_{2x}, X_{2y}, X_{2z}]^T$ are the shaping states of the GPS errors.

4.4.3 Filter Equations

The main filter equations are the error propagation models in the computer frame.

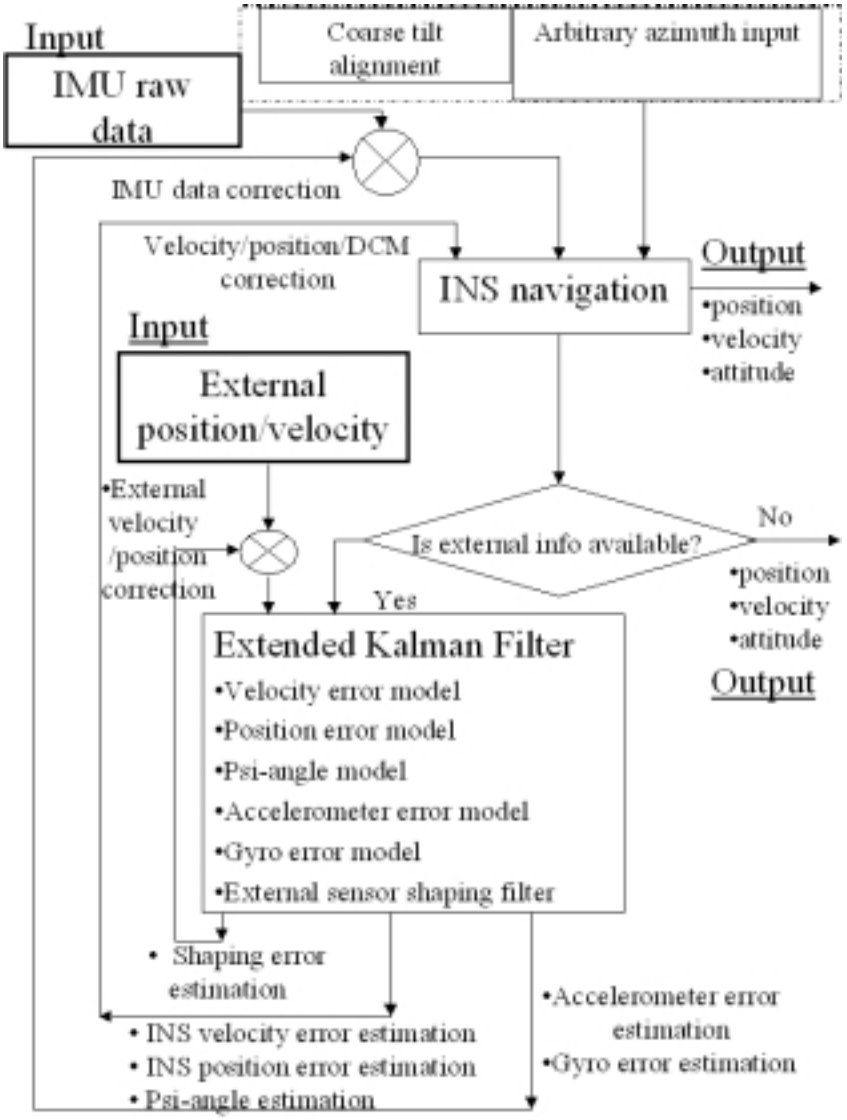

Figure 4.9: Flow chart of heading correction and filter estimation using the psi angle approach.

Velocity Error Equation

The velocity error equation has been presented in the previous chapter. In a case where the coarse alignment is not performed, there will be three large initial attitude errors. The psi angle vector will have three large elements.

$$\Delta \dot{V}^c = (I - C_p^c) f_t^p + \nabla^c + \Delta g^c - (2\Omega_{ie}^c + \Omega_{ec}^c)\Delta V^c \tag{4.14}$$

where C_p^c is given by:

$$C_p^c = \begin{bmatrix} \cos\psi_x \cos\psi_z - \sin\psi_x \sin\psi_y \sin\psi_z & -\cos\psi_y \sin\psi_z \\ \cos\psi_x \sin\psi_z + \sin\psi_x \sin\psi_y \cos\psi_z & \cos\psi_y \cos\psi_z \\ -\sin\psi_x \cos\psi_y & \sin\psi_y \end{bmatrix}$$
$$\begin{bmatrix} \sin\psi_x \cos\psi_z + \cos\psi_x \sin\psi_y \sin\psi_z \\ \sin\psi_x \sin\psi_z - \cos\psi_x \sin\psi_y \cos\psi_z \\ \cos\psi_x \cos\psi_y \end{bmatrix} \tag{4.15}$$

In most cases, when the coarse alignment has been done with an unknown azimuth, there will be two small initial tilt errors and one large heading error. The psi angle is still large.

For most low cost INSs, the area of operation is close to the earth surface. The gravity has very small variation. In this case, the gravity error model can be ignored

and the velocity error equation can be simplified to:

$$\begin{aligned}\Delta\dot{V}^c = &\begin{bmatrix} 0 & -[V_x^c tg(\varphi)/R_0 + 2\omega_{ie}\sin(\varphi)] \\ V_x^c tg(\varphi)/R_0 + 2\omega_{ie}\sin(\varphi) & 0 \\ -[V_x^c/R_0 + 2\omega_{ie}\cos(\varphi)] & -V_y^c/R_0 \end{bmatrix} \\ &\begin{bmatrix} V_x^c/R_0 + 2\omega_{ie}\cos(\varphi) \\ V_y^c/R_0 \\ 0 \end{bmatrix} \times \begin{bmatrix} \Delta V_x^c \\ \Delta V_y^c \\ \Delta V_z^c \end{bmatrix} + \\ &+ \begin{bmatrix} 1-\cos(\psi_z) & \sin(\psi_z) & -\psi_x\sin(\psi_z) - \psi_y\cos(\psi_z) \\ -\sin(\psi_z) & 1-\cos(\psi_z) & +\psi_x\cos(\psi_z) - \psi_y\sin(\psi_z) \\ \psi_y & -\psi_x & 0 \end{bmatrix} \begin{bmatrix} f_x^p \\ f_y^p \\ f_z^p \end{bmatrix} + \\ &+ \begin{bmatrix} \cos(\psi_z) & -\sin(\psi_z) & \psi_x\sin(\psi_z) + \psi_y\cos(\psi_z) \\ \sin(\psi_z) & \cos(\psi_z) & -\psi_x\cos(\psi_z) + \psi_y\sin(\psi_z) \\ -\psi_y & \psi_x & 0 \end{bmatrix} C_b^p \begin{bmatrix} \nabla_x^b \\ \nabla_y^b \\ \nabla_z^b \end{bmatrix}\end{aligned} \tag{4.16}$$

where

$V^c = [V_x^c, V_x^c, V_x^c]^T$ is the velocity vector in the computer frame.

R_0 is the earth radius. For a low cost INS, travel distance is limited and the earth radius is considered to be a constant.

ω_{ie} is the earth rate.

φ is the local latitude solved in navigation.

g is the gravity constant.

$[f_x^p, f_y^p, f_z^p]^T$ is the specific force transformed to the platform frame.

C_b^p is the direction cosine matrix with which INS actually transforms the vectors from the body frame to the platform using measured INS angular rate in navigation mode.

Position Error Equation

The position error model does not distinguish between small and large attitude errors:

$$\Delta\dot{R}^c = \Delta V^c - \Omega^c_{ec}\Delta R^c \tag{4.17}$$

The extension of the position error equation is:

$$\Delta\dot{R}^c = \begin{bmatrix} \Delta V^c_x \\ \Delta V^c_y \\ \Delta V^c_z \end{bmatrix} - \begin{bmatrix} 0 & -V^c_x tg(\varphi)/R_0 & V^c_x/R_0 \\ V^c_x tg(\varphi)/R_0 & 0 & V^c_y/R_0 \\ -V^c_x/R_0 & -V^c_y/R_0 & 0 \end{bmatrix} \begin{bmatrix} \Delta R^c_x \\ \Delta R^c_y \\ \Delta R^c_z \end{bmatrix}$$

The notation is as before.

Psi Angle Model

The attitude and heading errors are solved in the form of the psi angles. The psi angle model developed in Chapter 2 is described here in detail.

The general ψ angle model is given by equation (4.18):

$$\dot{\psi} = (I - C^p_c)\omega^c_{ic} - \epsilon^p \tag{4.18}$$

where C^p_c is given by:

$$C^p_c = \begin{bmatrix} \cos\psi_x\cos\psi_z - \sin\psi_x\sin\psi_y\sin\psi_z & & \\ -\cos\psi_y\sin\psi_z & & \\ \sin\psi_x\cos\psi_z + \cos\psi_x\sin\psi_y\sin\psi_z & & \end{bmatrix}$$
$$\begin{bmatrix} \cos\psi_x\sin\psi_z + \sin\psi_x\sin\psi_y\cos\psi_z & -\sin\psi_x\cos\psi_y \\ \cos\psi_y\cos\psi_z & \sin\psi_y \\ \sin\psi_x\sin\psi_z - \cos\psi_x\sin\psi_y\cos\psi_z & \cos\psi_x\cos\psi_y \end{bmatrix} \tag{4.19}$$

When the three initial attitudes are all unknown, or in the large perturbation case when the errors of the three attitudes are all large during the navigation stage, the ψ angle model with large angle assumption has to be used.

In most cases, the initial tilt angles can be solved within an error of 1° in the coarse alignment stage, while the heading remains unknown. In this case, ψ_x and ψ_y are small

and ψ_z is large within $[-180^\circ, +180^\circ]$. The psi angle equation in this case is extended to:

$$\dot{\psi} = \begin{bmatrix} 1-\cos(\psi_z) & -\sin(\psi_z) & \psi_y \\ \sin(\psi_z) & 1-\cos(\psi_z) & -\psi_x \\ -\psi_x\sin(\psi_z)-\psi_y\cos(\psi_z) & +\psi_x\cos(\psi_z)-\psi_y\sin(\psi_z) & 0 \end{bmatrix} \times \begin{bmatrix} -V_y^c/R_0 \\ V_x^c/R_0+\omega_{ie}\cos(\varphi) \\ V_x^c tg(\varphi)/R_0+\omega_{ie}\sin(\varphi) \end{bmatrix} - C_b^p \begin{bmatrix} \epsilon_x^b \\ \epsilon_y^b \\ \epsilon_z^b \end{bmatrix} \tag{4.20}$$

Sensor Error Equations

In both the alignment and the navigation stages, the errors of the IMU sensors and GPS can be estimated and calibrated in-motion. The error models are included in the process model of the filter.

For a low cost IMU, the drift over a long period of time can be significant. Internal temperature variation could also cause bias changes.

The biases in the gyros and the accelerometers can be modelled as [45, 69]:

$$\dot{\nabla}^b = \frac{-\nabla^b}{T_a} + \frac{a_1}{T_a} \tag{4.21}$$

$$\dot{\epsilon}^b = \frac{-\epsilon^b}{T_g} + \frac{b_1}{T_g} \tag{4.22}$$

The model parameters T_a, T_g, a_1 and b_1 are obtained experimentally.

In a case where the IMU has slow internal temperature variation, the gyro and accelerometer errors can be modelled as white noise plus a constant:

$$\dot{\nabla}^b = 0 \tag{4.23}$$

$$\dot{\epsilon}^b = 0$$

The white noise is to be added on top of these.

The error model for the GPS has been presented in the previous chapter. The

shaping states X_s and X_{ss} of the GPS position error have the following relations:

$$\dot{X}_s = -2\alpha k X_s + X_{ss} + r\omega_{sp} \tag{4.24}$$
$$\dot{X}_{ss} = -\alpha^2 X_s + r\beta\omega_{sp}$$

That is:

$$\begin{bmatrix} \dot{X}_s \\ \dot{X}_{ss} \end{bmatrix} = \begin{bmatrix} -2\alpha k & 1 \\ \alpha^2 & 0 \end{bmatrix} \begin{bmatrix} X_s \\ X_{ss} \end{bmatrix} + \begin{bmatrix} r \\ r\beta \end{bmatrix} [\omega_{sp}] \tag{4.25}$$

with the white noise ω_{sp}.

Measurement Equations

The filter observation is the difference between the GPS measurement and the INS output. It must be noted that these two different outputs are in two different frames. When the differential GPS with the position error of $2cm$ and the velocity error of $5cm/second$ is used as the navigation reference, the velocity and the position of the DGPS are considered to be solved and transformed into the true local level frame.

Let the velocity difference V_d and the position difference R_d be the difference between the INS outputs and measured GPS outputs:

$$V_d = \widehat{V}^c_{INS} - \widehat{V}^t_{GPS} \tag{4.26}$$
$$R_d = \widehat{R}^c_{INS} - \widehat{R}^t_{GPS} \tag{4.27}$$

where the superscripts c and t indicate whether the vectors are in the computer frame or in the true frame. $\widehat{R}^c_{INS}$ and $\widehat{V}^c_{INS}$ are the INS computed position and velocity. $\widehat{R}^t_{GPS}$ and $\widehat{V}^t_{GPS}$ are the GPS position and velocity outputs respectively.

When the GPS error model is proposed, the observation has the following form:

$$\begin{aligned} Z = R_d &= \widehat{R}^c_{INS} - \widehat{R}^t_{GPS} \\ &= (R^c_{true} + \Delta R^c) - (R^t_{true} + X_s + \Gamma_{gps}) \\ &= (R^c_{true} - R^t_{true}) + (\Delta R^c - X_s - \Gamma_{gps}) \\ &= (I_{3\times 3} - C^t_c) R^c_{true} + (\Delta R^c - X_s - \Gamma_{gps}) \end{aligned} \tag{4.28}$$

where $\Gamma_{gps} = [\Gamma_x, \Gamma_y, \Gamma_z]^T$ is the white noise of GPS measurement. R^t_{true} and R^c_{true} are the true position in the computer frame and the true frame respectively.

Since the position is aided, the INS computed position and the true position will have small errors. The computer frame c, which is the local level frame at the computed position, and the true local level frame t at the true position will have a small difference

in orientation. Therefore $C_c^t \approx I_{3\times3}$ in the observation equation. Consequently:

$$\begin{aligned} R_d &= \Delta R^c - X_s - \Gamma_{gps} \\ &= \begin{bmatrix} \Delta R_x^c \\ \Delta R_y^c \\ \Delta R_z^c \end{bmatrix} - \begin{bmatrix} X_{sx} \\ X_{sy} \\ X_{sz} \end{bmatrix} - \begin{bmatrix} \Gamma_x \\ \Gamma_y \\ \Gamma_z \end{bmatrix} \end{aligned} \tag{4.29}$$

$$= \begin{bmatrix} 0_{3\times3} & I_{3\times3} & 0_{3\times3} & 0_{3\times3} & 0_{3\times3} & -I_{3\times3} & 0_{3\times3} \end{bmatrix} \begin{bmatrix} \Delta V_x^c \\ \Delta V_y^c \\ \Delta V_z^c \\ \Delta R_x^c \\ \Delta R_y^c \\ \Delta R_z^c \\ \psi_x \\ \psi_y \\ \psi_z \\ \nabla_x^b \\ \nabla_y^b \\ \nabla_z^b \\ \epsilon_x^b \\ \epsilon_y^b \\ \epsilon_z^b \\ X_{sx} \\ X_{sy} \\ X_{sz} \\ X_{2x} \\ X_{2y} \\ X_{2z} \end{bmatrix} - \begin{bmatrix} \Gamma_x \\ \Gamma_y \\ \Gamma_z \end{bmatrix} \tag{4.30}$$

When the DGPS is used, the observation can be considered as corrupted by white

noise only. The observation z is:

$$Z = \begin{bmatrix} V_d \\ R_d \end{bmatrix}$$
$$V_d = \widehat{V}^c_{INS} - \widehat{V}^t_{GPS}$$
$$R_d = \widehat{R}^c_{INS} - \widehat{R}^t_{GPS} \tag{4.31}$$

And

$$\begin{aligned} V_d &= \widehat{V}^c_{INS} - \widehat{V}^t_{GPS} \\ &= (V^c_{true} + \Delta V^c) - (V^t_{true} + \Theta_{gps}) \\ &= (V^c_{true} - V^t_{true}) + (\Delta V^c - \Theta_{gps}) \\ &= (I_{3\times 3} - C^t_c)V^c_{true} + \Delta V^c - \Theta_{gps} \end{aligned} \tag{4.32}$$

where

$\Theta_{gps} = [\Theta_x, \Theta_y, \Theta_z]^T$ is the white noise of the DGPS velocity measurement.

V^c_{true} is the true velocity in the computer frame.

V^t_{true} is the true velocity in the true frame.

Again, $C^t_c \approx I_{3\times 3}$ in this case. Therefore

$$V_d = \Delta V^c - \Theta_{gps} \tag{4.33}$$

And

$$\begin{aligned} R_d &= \widehat{R}^c_{INS} - \widehat{R}^t_{GPS} \\ &= (R^c_{true} + \Delta R^c) - (R^t_{true} + \Gamma_{gps}) \\ &= (I_{3\times 3} - C^t_c)R^c_{true} + \Delta R^c - \Gamma_{gps} \\ &= \Delta R^c - \Gamma_{gps} \end{aligned} \tag{4.34}$$

The observation equation will be:

$$
\begin{aligned}
Z = \begin{bmatrix} V_d \\ R_d \end{bmatrix} &= \begin{bmatrix} \Delta V^c - \Theta_{gps} \\ \Delta R^c - \Gamma_{gps} \end{bmatrix} \\
&= \begin{bmatrix} I_{3\times3} & 0_{3\times3} & 0_{3\times3} & 0_{3\times3} & 0_{3\times3} \\ 0_{3\times3} & I_{3\times3} & 0_{3\times3} & 0_{3\times3} & 0_{3\times3} \end{bmatrix} \begin{bmatrix} \Delta V_x^c \\ \Delta V_y^c \\ \Delta V_z^c \\ \Delta R_x^c \\ \Delta R_y^c \\ \Delta R_z^c \\ \psi_x \\ \psi_y \\ \psi_z \\ \nabla_x^b \\ \nabla_y^b \\ \nabla_z^b \\ \epsilon_x^b \\ \epsilon_y^b \\ \epsilon_z^b \end{bmatrix} - \begin{bmatrix} \Theta_{gps} \\ \Gamma_{gps} \end{bmatrix}
\end{aligned} \tag{4.35}
$$

4.4.4 Discrete Filter and Jacobian Matrix

The process model of the filter in the in-motion alignment stage is nonlinear. The Kalman filtering process has been designed to estimate the state vector in a linear model. It has many successful applications in INS alignment and navigation. If the model turns out to be nonlinear, a linearization procedure is usually performed in deriving the filtering equations. The linear Taylor approximation of the process model at the previous state estimation and that of the observation model at the corresponding predicted position is usually considered [18, 70]. The Kalman filter so obtained is called the Extended Kalman Filter (EKF). Linearization is justified by the argument that the estimate maintained by the EKF is close to the true state of the system. The

expected values of the second and higher-order terms in the Taylor series expansion are small [19]. Jacobian matrices of the process and observation models have to be evaluated. The Distribution Approximation Filter which is introduced by Julier and Uhlman [19, 20, 21, 22, 23] provides another approach for nonlinear filtering.

The Extended Kalman filter is employed in this section for the psi angle approach, where for the navigation update, direction cosine matrices are used for attitude update purposes.

The update stage is performed at each data fusion step when a GPS fix is available. Usually, the INS sampling time is less than the sampling time of the GPS. For example, the sampling frequency of the Watson IMU and the Ashtech GPS are $82Hz$ and $10Hz$ respectively. During the period when a GPS fix is not available, INS computes and outputs the navigation data independently without the filter prediction.

The filter in continuous time is the combination of the equation in Section 4.4.3. The whole filter can be written as:

$$\begin{aligned} X(t) &= f_c(t, X(t)) + G(t)U(t) \\ Z(t) &= HX(t) + V(t) \end{aligned} \tag{4.36}$$

The strengths of $U(t)$ and $V(t)$ are $Q(t)$ and $R(t)$ respectively.

The discrete-time model is:

$$\begin{aligned} X(t_k) &= X(t_{k-1}) + f_c(t_k, X(t_k))dt + G(t_k)U(t_k)dt \\ Z(t_k) &= H(t_k)X(t_k) + V(t_k) \end{aligned} \tag{4.37}$$

where dt is the time interval between t_{k-1} and t_k.

This compares with the standard form of the discrete-time filter:

$$\begin{aligned} X_{k+1} &= f_k(X_k) + G_k u_k \\ Z_k &= H_k X_k + v_k \end{aligned} \tag{4.38}$$

with:

$$G_k = G(t_k)dt \tag{4.39}$$

$$u_k = U(t_k) \tag{4.40}$$

$$v_k = V(t_k) \tag{4.41}$$

The approximation is also given:

$$f_k(X_k) = X(t_{k-1}) + f_c(t_k, X(t_k))dt \tag{4.42}$$

This relationship provides a shortcut to evaluate the Jacobian matrix J_f at time t_k in discrete time by using the Jacobian matrix $J_c(t)$ at time t_k in continuous time, which can be directly derived from the filter models:

$$\begin{aligned} J_f(k) &= \frac{\partial f_k(X_k)}{\partial X_k} \\ &\approx I + \frac{\partial f_c(t_k, X(t_k))}{\partial X_k}dt \\ &= I + J_c(t_k)dt \end{aligned} \tag{4.43}$$

The derivation of the Jacobian matrix J_c of the filter at time t_k is more complicated. For example, when the noise of the accelerometers and the gyros is treated as white noise plus a constant and the DGPS is used, the Jacobian matrix in continuous time is derived as follows.

The filter can be separated into a linear part and a nonlinear part plus the noise:

$$\begin{bmatrix} \Delta\dot{V}^c \\ \Delta\dot{R}^c \\ \dot{\psi} \\ \nabla^b \\ \epsilon^b \end{bmatrix} = \begin{bmatrix} -(2\Omega_{ie}^c + \Omega_{ec}^c) & 0_{3\times3} & 0_{3\times3} & 0_{3\times3} & 0_{3\times3} \\ I_{3\times3} & -\Omega_{ec}^c & 0_{3\times3} & 0_{3\times3} & 0_{3\times3} \\ 0_{3\times3} & 0_{3\times3} & 0_{3\times3} & 0_{3\times3} & 0_{3\times3} \\ \multicolumn{5}{c}{\text{---------------------}} \\ \multicolumn{5}{c}{0_{6\times15}} \end{bmatrix} \begin{bmatrix} \Delta V^c \\ \Delta R^c \\ \psi \\ \nabla^b \\ \epsilon^b \end{bmatrix} + \begin{bmatrix} (I - C_p^c)f_t^p \\ 0_{3\times1} \\ (I - C_c^p)\omega_{ic}^c \\ 0_{6\times1} \end{bmatrix} + \begin{bmatrix} \nabla^p \\ 0_{3\times1} \\ -\epsilon^p \\ 0_{6\times1} \end{bmatrix} \tag{4.44}$$

Then the Jacobian matrix is evaluated as:

$$Jc = \begin{bmatrix} -(2\Omega_{ie}^c + \Omega_{ec}^c) & 0_{3\times3} & F_{13} & I_{3\times3} & 0_{3\times3} \\ I_{3\times3} & -\Omega_{ec}^c & 0_{3\times3} & 0_{3\times3} & 0_{3\times3} \\ 0_{3\times3} & 0_{3\times3} & F_{33} & 0_{3\times3} & I_{3\times3} \\ \hline 0_{6\times15} \end{bmatrix} \tag{4.45}$$

When only the heading is unknown, the matrix elements F_{13} and F_{33} in J_c are:

$$F_{13} = \begin{bmatrix} -\sin(\psi_z) f_z^p & -\cos(\psi_z) f_z^p \\ \cos(\psi_z) f_z^p & -\sin(\psi_z) f_z^p \\ -f_y^p & f_z^p \end{bmatrix}$$

$$\begin{bmatrix} f_x^p \sin(\psi_z) + f_y^p \cos(\psi_z) + (\psi_y \sin(\psi_z) - \psi_x \cos(\psi_z)) f_z^p \\ \sin(\psi_z) f_y^p - \cos(\psi_z) f_x^p - (\psi_x \sin(\psi_z) + \psi_y \cos(\psi_z)) f_z^p \\ 0 \end{bmatrix} \tag{4.46}$$

And

$$F_{33} = \begin{bmatrix} 0 & w_3 \\ -w_3 & 0 \\ -\sin(\psi_z) w_1 + \cos(\psi_z) w_2 & -\cos(\psi_z) w_1 - \sin(\psi_z) w_2 \end{bmatrix}$$

$$\begin{bmatrix} \sin(\psi_z) w_1 - \cos(\psi_z) w_2 \\ \cos(\psi_z) w_1 + \sin(\psi_z) w_2 \\ (\psi_y \sin(\psi_z) - \psi_x \cos(\psi_z)) w_1 - (\psi_y \cos(\psi_z) + \psi_x \sin(\psi_z)) w_2 \end{bmatrix} \tag{4.47}$$

where

$$\begin{aligned} w_1 &= -V_y^c / R_0 \\ w_1 &= V_x^c / R_0 + w_{ie} \cos(\varphi)] \\ w_3 &= V_x^c \tan(\varphi) / R_0 + w_{ie} \cos(\varphi) \end{aligned} \tag{4.48}$$

φ is the local latitude. All the variables in the Jacobian matrices above are evaluated at time t_k.

The filter noise has the following attributes:

When the IMU noise is considered as white noise plus a constant and the noise is estimated in the filter, G at time t_k is evaluated as:

$$G(t_k) = \begin{bmatrix} C_b^p(t_k) & 0_{3\times 3} \\ 0_{3\times 3} & 0_{3\times 3} \\ 0_{3\times 3} & -C_b^p(t_k) \\ \hline 0_{6\times 6} \end{bmatrix} \tag{4.49}$$

Then in the continuous-time filter:

$$G(t_k)U(t_k) = \begin{bmatrix} \nabla^p \\ 0_{3\times 1} \\ -\epsilon^p \\ \hline 0_{6\times 1} \end{bmatrix} = \begin{bmatrix} C_b^p(t_k) & 0_{3\times 3} \\ 0_{3\times 3} & 0_{3\times 3} \\ 0_{3\times 3} & -C_b^p(t_k) \\ \hline 0_{6\times 6} \end{bmatrix} \begin{bmatrix} \nabla^b \\ \epsilon^b \end{bmatrix} \tag{4.50}$$

where $C_b^p(t_k)$ is the direction cosine matrix from the body frame to the platform which is solved in navigation at time t_k.

In the discrete-time filter (4.38), u_k and v_k are white noise sequences with strength G_k and R_k. They can be approximated as [71]:

$$Q_k = G(t_k)Q(t_k)G^T(t_k)dt$$

$$R_k = R(t_k)/dt$$

4.4.5 Filter Implementation Using the EKF

The filter real time implementation can be seen in Figure 4.9. The filter state X is initially modelled as a Gaussian random variable $X_{0,0}$ at the epoch when the coarse alignment finished and the in-motion alignment starts. Take the zero-mean of the Gaussian variable for initialization. The initial X is given as $X_{0,0}$:

$$X_{0,0} = [0,0,0,0,0,0,0,0,0,0,0,0,0,0,0,0,0,0]^T \tag{4.51}$$

The initial covariance matrix $P_{0,0}$ provides a statistical measure of confidence of the states:

$$P_{0,0} = \begin{bmatrix} \sigma^2_{\Delta V} & 0_{3\times3} & 0_{3\times3} & 0_{3\times3} & 0_{3\times3} & 0_{3\times3} & 0_{3\times3} \\ 0_{3\times3} & \sigma^2_{\Delta R} & 0_{3\times3} & 0_{3\times3} & 0_{3\times3} & 0_{3\times3} & 0_{3\times3} \\ 0_{3\times3} & 0_{3\times3} & \sigma^2_{\psi} & 0_{3\times3} & 0_{3\times3} & 0_{3\times3} & 0_{3\times3} \\ 0_{3\times3} & 0_{3\times3} & 0_{3\times3} & \sigma^2_{\nabla^b} & 0_{3\times3} & 0_{3\times3} & 0_{3\times3} \\ 0_{3\times3} & 0_{3\times3} & 0_{3\times3} & 0_{3\times3} & \sigma^2_{\epsilon^b} & 0_{3\times3} & 0_{3\times3} \\ 0_{3\times3} & 0_{3\times3} & 0_{3\times3} & 0_{3\times3} & 0_{3\times3} & \sigma^2_{X_s} & 0_{3\times3} \\ 0_{3\times3} & 0_{3\times3} & 0_{3\times3} & 0_{3\times3} & 0_{3\times3} & 0_{3\times3} & \sigma^2_{X_{ss}} \end{bmatrix} \tag{4.52}$$

$P_{0,0}$ is assumed diagonal for lack of sufficient statistical information to evaluate its off-diagonal terms.

The initial dynamic process noise matrix is set as Q_0:

$$Q_0 = \begin{bmatrix} \sigma^2_{accx} & 0 & 0 & 0 & 0 & 0 \\ 0 & \sigma^2_{accy} & 0 & 0 & 0 & 0 \\ 0 & 0 & \sigma^2_{accz} & 0 & 0 & 0 \\ 0 & 0 & 0 & \sigma^2_{gyrox} & 0 & 0 \\ 0 & 0 & 0 & 0 & \sigma^2_{gyroy} & 0 \\ 0 & 0 & 0 & 0 & 0 & \sigma^2_{gyroz} \end{bmatrix} \tag{4.53}$$

The initial measurement noise matrix is set as R_0:

$$R_0 = \begin{bmatrix} r^2_{rx} & 0 & 0 & 0 & 0 & 0 \\ 0 & r^2_{ry} & 0 & 0 & 0 & 0 \\ 0 & 0 & r^2_{rz} & 0 & 0 & 0 \\ 0 & 0 & 0 & r^2_{vx} & 0 & 0 \\ 0 & 0 & 0 & 0 & r^2_{vy} & 0 \\ 0 & 0 & 0 & 0 & 0 & r^2_{vz} \end{bmatrix} \tag{4.54}$$

The diagonal terms of R_0 are the variance of the noise on INS and GPS measurements.

At time t_k, the state estimation is $X_{k,k-1}$, with the covariance matrix $P_{k,k-1}$ being available. The Jacobian matrix of f_k is then evaluated as:

$$J_f(k) = I + J_c(t_k)dt \tag{4.55}$$

The filter gain K_k is calculated by:

$$K_k = P_{k,k-1}H_k^T(H_k P_{k,k-1} H_k^T + R_k)^{-1} \tag{4.56}$$

The updated measurement is fused into the filter. The updated state estimation $X_{k,k}$ is:

$$X_{k,k} = X_{k,k-1} + K_k(Z_k - H_k X_{k,k-1}) \tag{4.57}$$

Since the errors have been compensated at each filter time, $X_{k,k-1}$ is zero. Therefore, the updated estimation of states which is used to correct navigation output and calibration sensor errors is:

$$X_{k,k} = K_k Z_k \tag{4.58}$$

The covariance update is:

$$P_{k,k} = (I - K_k H_k)P_{k,k-1} \tag{4.59}$$

For the next iteration t_{k+1}, the a priori state estimation will be:

$$X_{k+1,k} = f_k(X_{k,k}) \tag{4.60}$$

with an a priori covariance matrix:

$$P_{k+1,k} = J_f(k)P_{k,k}J_f^T(k) + G_{k+1}Q_k G_{k+1}^T \tag{4.61}$$

The estimation of the states is used to correct the system errors by subtracting each estimated error from the INS velocity, position, attitude, accelerometer output data, gyro output data and GPS position data, as shown in the flow chart in Figure 4.9.

4.5 Navigation Stage: Continue Alignment and Calibration

Once the attitude errors diminish to a few degrees, the in-motion alignment stage finishes. The velocity error model, position error model, psi angle model will be switched to their small angle approximations.

The process models are replaced to their small angle forms, the filter process model and the observation models are now all linear. A standard Kalman filter is applied to estimate the navigation state.

4.6 Summary

In this chapter, the INS algorithm for low cost IMUs is developed using psi angle models for large attitude errors. The main contribution of this algorithm is the in-motion alignment to solve the initial attitude uncertainty.

The alignment mode is separated into coarse alignment and in-motion fine alignment. Section 4.3 presented the determination of the initial direction cosine matrix, turn-on biases of the accelerometers and the gyros in the coarse alignment stage.

Section 4.4 presented the in-motion alignment approach with an unknown initial condition. The psi angle models developed in this thesis are used as the filter process models. The Extended Kalman Filter is used to implement the nonlinear filter.

Chapter 5

INS Algorithm for Low Cost IMU in Quaternion Approach

5.1 Introduction

This chapter addresses the INS algorithm design for low cost IMUs using quaternions in the computer frame.

The INS navigation equations are based on a quaternion approach. The quaternion equations are formulated and an update based on the Adams-Bashford method is presented.

The filter is composed of the INS velocity error model, the INS position error model and the quaternion error model in the computer frame. The quaternion errors are exploited using the misalignment of the computer frame and the platform frame. The entire filter process model structure and the process noise are discussed. The process noise vectors are reconstructed by a linear combination of the white noise on the accelerometers and gyros in the body frame. A Distribution Approximation Filter (DAF) is used instead of the EKF. The principle and the benefit of the DAF are briefly described.

5.2 INS Navigation Using Quaternions

5.2.1 Overview

An INS computes the current velocity, position and attitude from the initial velocity, position and attitude and the time history of the kinematic acceleration. The gyros of the IMU provide angular rates of the body frame to the inertial frame. An orientation transformation matrix is calculated using outputs of gyros to transfer the specific force measured by the accelerometers to the navigation frames. Velocity and position are consequently integrated by acceleration and velocity respectively in the navigation frame.

In the previous chapter, the vehicle attitudes, the misalignment of coordinate systems and the orientation of the coordinate frames were represented by a set of angles and the direction cosine matrix. In this chapter, they are represented by quaternions.

Quaternions were introduced by Hamilton in 1843 and are a set of four parameters that evolve in accordance with a simple differential equation. Quaternions are less amenable to direct physical interpretation. Although their elements have quadratic forms, the quaternion approach is less computationally intensive, gives better accuracy and avoids the singularity problem inherent in the Euler approach. It contains only four parameters and uses the half angular increments [72, 73, 74, 75, 76, 77, 78, 79, 80, 81, 14]. The algorithm flow chart is shown in Figure 5.1.

The INS algorithm processes the raw data to estimate the turn on biases of accelerometers and gyros. Coarse alignment is performed by setting up initial velocity, position, attitude and quaternions. Initial quaternions are evaluated by the initial attitude angles.

When external heading sensors are not available, ground coarse alignment cannot be performed accurately. The psi angle approach described in the previous chapter can be used to correct the attitude without initial attitude input. In this chapter, another approach using quaternions instead of psi angles is developed. The velocity error propagation model, position error model and quaternions propagation which are

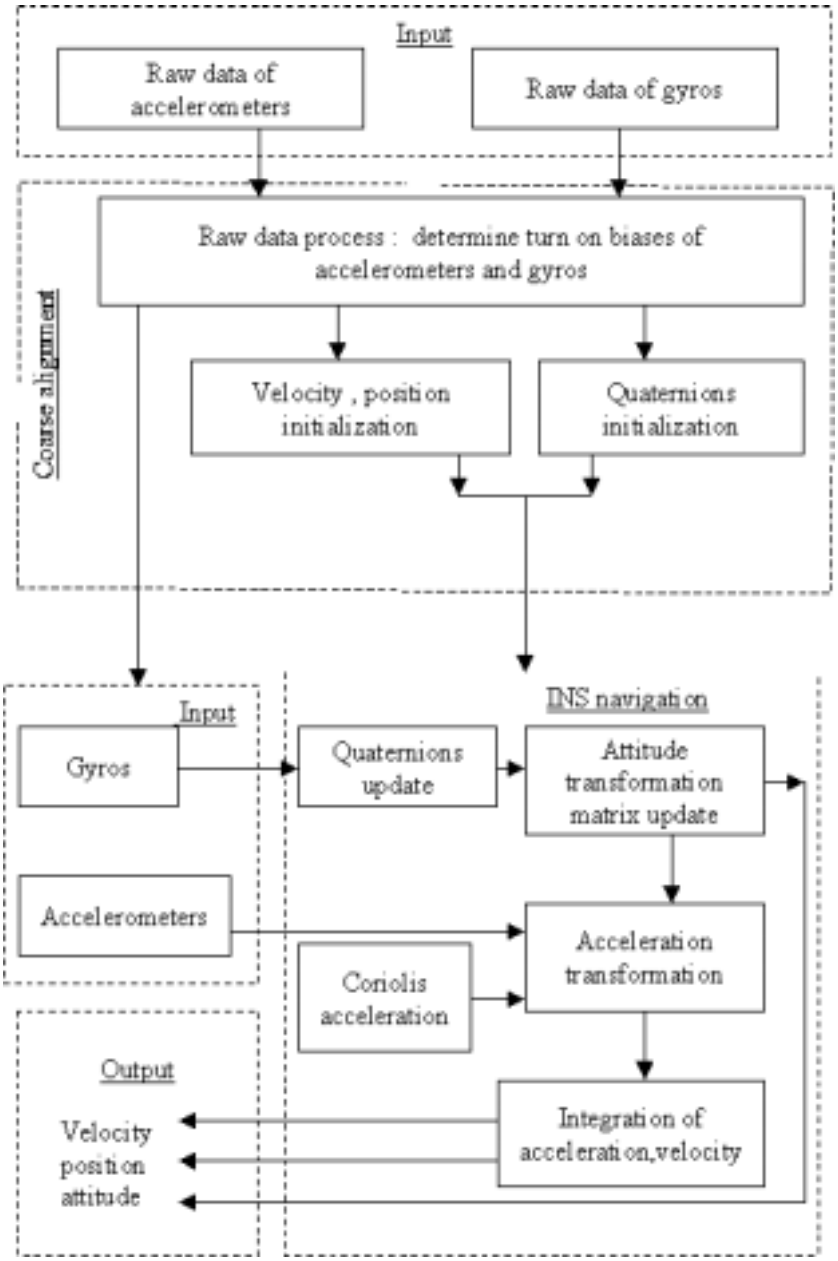

Figure 5.1: INS flow chart

developed in this thesis are applied here.

5.2.2 Raw Data Process

The IMU provides raw data of acceleration and rotation rate in the body frame. Raw data contain turn-on biases which can be estimated while stationary and removed at each navigation step as described in the previous chapter.

An example of the raw data in axis x of the body frame is shown in Figure 5.2. From time 15 seconds to 50 seconds, the vehicle is stationary. The average raw data

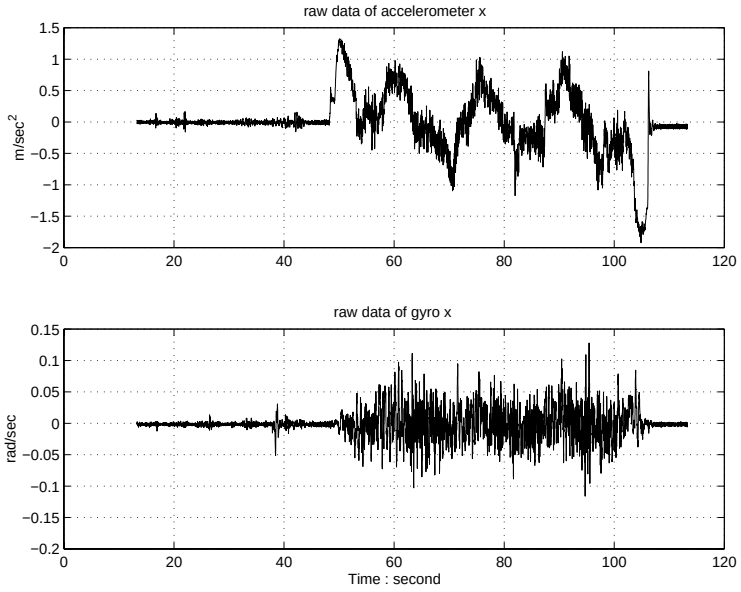

Figure 5.2: Raw data of accelerometer x and gyro x.

of accelerometers and gyros are collected during this stage. Turn-on biases of three accelerometers and three gyros are estimated and removed from the raw data. As in the raw data plot, there is perturbation noise from time 38 seconds to 39 seconds which cannot be estimated in real time. Therefore the calculated biases at this stage are not accurate. The biases will also drift over time with temperature changes. They will be estimated in the filter and removed at each update step.

5.2.3 Quaternions Initialization

To transfer the measured acceleration in the body frame to the platform frame, a rotation transfer matrix has to be calculated to get the orientation of the vehicle at each navigation step.

Quaternions are initialized while the vehicle is stationary. The initial rotation transfer matrix is calculated by averaging bank, elevation and heading. Let the transformation matrix T_0 be the initial direction cosine matrix from the body frame to the platform frame. In the case where the initial attitudes are unknown, T_0 can be set arbitrarily. If coarse tilt information can be obtained and the heading is unknown, T_0 can be set by coarse tilt and arbitrary heading.

The quaternion integrations are updated from the initial quaternion vector $Q_b^p(1) = [q_{n0}(1), q_{n1}(1), q_{n2}(1), q_{n3}(1)]^T$.

$$T_0 = \begin{bmatrix} 2(q_{n0}^2(1)+q_{n1}^2(1))-1 & 2(q_{n1}(1)q_{n2}(1)-q_{n0}(1)q_{n3}(1)) \\ 2(q_{n1}(1)q_{n2}(1)+q_{n0}(1)q_{n3}(1)) & 2(q_{n0}^2(1)+q_{n2}^2(1))-1 \\ 2(q_{n1}(1)q_{n3}(1)-q_{n0}(1)q_{n2}(1)) & 2(q_{n2}(1)q_{n3}(1)+q_{n0}(1)q_{n1}(1)) \end{bmatrix}$$
$$\begin{bmatrix} 2(q_{n1}(1)q_{n3}(1)+q_{n0}(1)q_{n2}(1)) \\ 2(q_{n2}(1)q_{n3}(1)-q_{n0}(1)q_{n1}(1)) \\ 2(q_{n0}^2(1)+q_{n3}^2(1))-1 \end{bmatrix} \tag{5.1}$$

with the constraint

$$q_{n0}^2(1)+q_{n1}^2(1)+q_{n2}^2(1)+q_{n3}^2(1) = 1 \tag{5.2}$$

Then the solutions of (5.1) are:

$$\begin{aligned} q_{n1}(1) &= \frac{1}{2}\sqrt{1+T_0(1,1)-T_0(2,2)-T_0(3,3)} \times sign(T_0(3,2)-T_0(2,3)) \\ q_{n2}(1) &= \frac{1}{2}\sqrt{1-T_0(1,1)+T_0(2,2)-T_0(3,3)} \times sign(T_0(1,3)-T_0(3,1)) \\ q_{n3}(1) &= \frac{1}{2}\sqrt{1-T_0(1,1)-T_0(2,2)+T_0(3,3)} \times sign(T_0(2,1)-T_0(1,2)) \\ q_{n0}(1) &= \sqrt{1-q_{n1}^2(1)-q_{n2}^2(1)-q_{n3}^2(1)} \end{aligned}$$

where $sign(x)$ is $+1$ when x is positive, returns -1 when x is negative.

5.2.4 Transformation Matrix Using Quaternions

At INS navigation time t, let $C(Q_b^p)$ be the rotation transformation matrix from the body frame to the platform frame represented by $Q_b^p(t) = [q_{n0}(t), q_{n1}(t), q_{n2}(t), q_{n3}(t)]^T$. Then:

$$C(Q_b^p) = \begin{bmatrix} 2(q_{n0}^2(t) + q_{n1}^2(t)) - 1 & 2(q_{n1}(t)q_{n2}(t) - q_{n0}(t)q_{n3}(t)) \\ 2(q_{n1}(t)q_{n2}(t) + q_{n0}(t)q_{n3}(t)) & 2(q_{n0}^2(t) + q_{n2}^2(t)) - 1 \\ 2(q_{n1}(t)q_{n3}(t) - q_{n0}(t)q_{n2}(t)) & 2(q_{n2}(t)q_{n3}(t) + q_{n0}(t)q_{n1}(t)) \end{bmatrix}$$
$$\begin{bmatrix} 2(q_{n1}(t)q_{n3}(t) + q_{n0}(t)q_{n2}(t)) \\ 2(q_{n2}(t)q_{n3}(t) - q_{n0}(t)q_{n1}(t)) \\ 2(q_{n0}^2(t) + q_{n3}^2(t)) - 1 \end{bmatrix} \tag{5.3}$$

The evaluation of this matrix is less computationally expensive than using the direction cosine matrix.

5.2.5 Quaternion, Velocity and Position Update

In each step, the current quaternions are integrated from the information of the current gyro outputs and the quaternions at the previous step. To update the quaternion vector Q_b^p from time t to time $t+1$, the Adams-Bashford integration is used.

At time t, Q_b^p satisfies the following differential equation [32]:

$$\dot{Q}_b^p = \frac{1}{2}\Omega_b^n \times Q_b^p \tag{5.4}$$

where the angular rate matrix Ω_b^n is:

$$\Omega_b^n = \begin{bmatrix} 0 & -w_x & -w_y & -w_z \\ w_x & 0 & w_z & -w_y \\ w_y & -w_z & 0 & w_x \\ w_z & w_y & -w_x & 0 \end{bmatrix} \tag{5.5}$$

and

$$w_{nb}^b = [w_x, w_y, w_z]^T \tag{5.6}$$

is the body frame rate with respect to the platform frame solved in the body frame. This is derived by differencing the measured body frame rates w_{ib}^b and the estimates of the components of platform frame rate w_{ip}^p. w_{ip}^p is obtained by summing the Earth rate with respect to the inertial frame w_{ie}^p and the turn rate of the platform frame to the Earth frame w_{ep}^p. These rates have the following relation [27]:

$$w_{in}^p = w_{ie}^p + w_{ep}^p \tag{5.7}$$

and

$$w_{nb}^b = w_{ib}^b - C_p^b[w_{ie}^p + w_{ep}^p] \tag{5.8}$$

Let δt be the INS update interval and $Q_b^p(t-2\delta t)$ and $Q_b^p(t-\delta t)$ be the quaternions at time $(t-2\delta t)$ and $(t-\delta t)$. The angular rate matrix of the previous two steps $(t-2\delta t)$ and $(t-\delta t)$ are $\Omega(t-2\delta t)$ and $\Omega(t-\delta t)$. To integrate the quaternion differential equation (5.4), a 2-step Adams-Bashford method [82] is used. The quaternion at the current step is given by [68]:

$$Q_b^p(t) = Q_b^p(t-\delta t) + (3\Omega(t-\delta t)Q_b^p(t-\delta t) - \Omega(t-2\delta t)Q_b^p(t-2\delta t)) \times 0.25\delta t \tag{5.9}$$

Usually the INS sampling time is a constant. If there is a variation in δt, Q_b^p and Ω are selected using the values of the last two steps. For the Watson IMU, the sampling time is 0.008 seconds.

In the algorithm presented, the quaternion vector is normalized at each update stage. Figure 5.3 is a plot of the actual norms of quaternions minus 1. The range is within 5×10^{-16}. Therefore the quaternions are normalized at each INS navigation time.

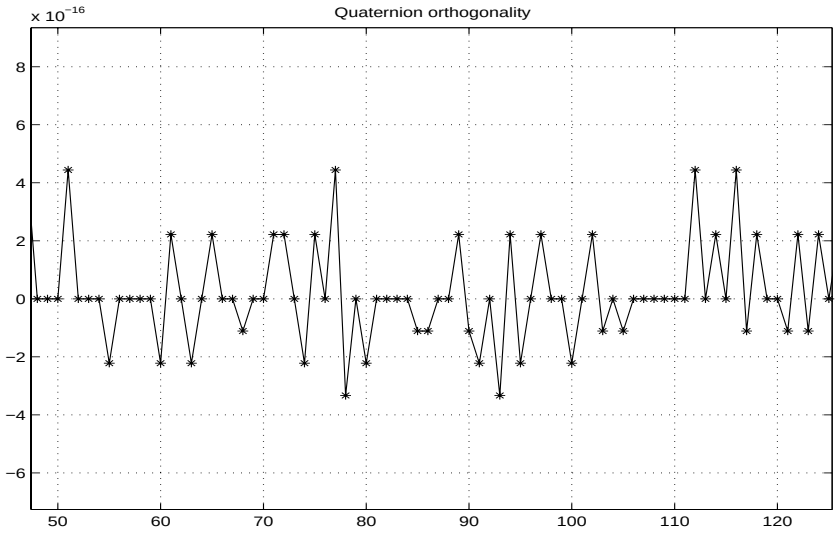

Figure 5.3: Quaternions' orthogonality

5.3 INS Algorithm for Low Cost IMU in Quaternion Approach

5.3.1 Introduction

It is argued that attitude transformation and update using quaternions can provide more accurate results than the direction cosine matrix and the Euler method.

When a low cost IMU is used, initial attitude and initial quaternions are unknown. Quaternion models for large attitude errors developed in this thesis can be used to solve the initial quaternion uncertainty without additional heading sensors.

In this section, the quaternion approach in the computer frame is applied to the INS in-motion alignment to solve large azimuth uncertainty. A Distribution Approximation Filter (DAF) instead of EKF is used to implement the nonlinear filter. One of the advantages of this approach is that it does not require the evaluation of Jacobians.

The algorithm flow chart is shown in Figure 5.4.

During the quaternion initialization, the four elements of the quaternion vector are evaluated under the assumption of an arbitrary attitude. The INS computes the

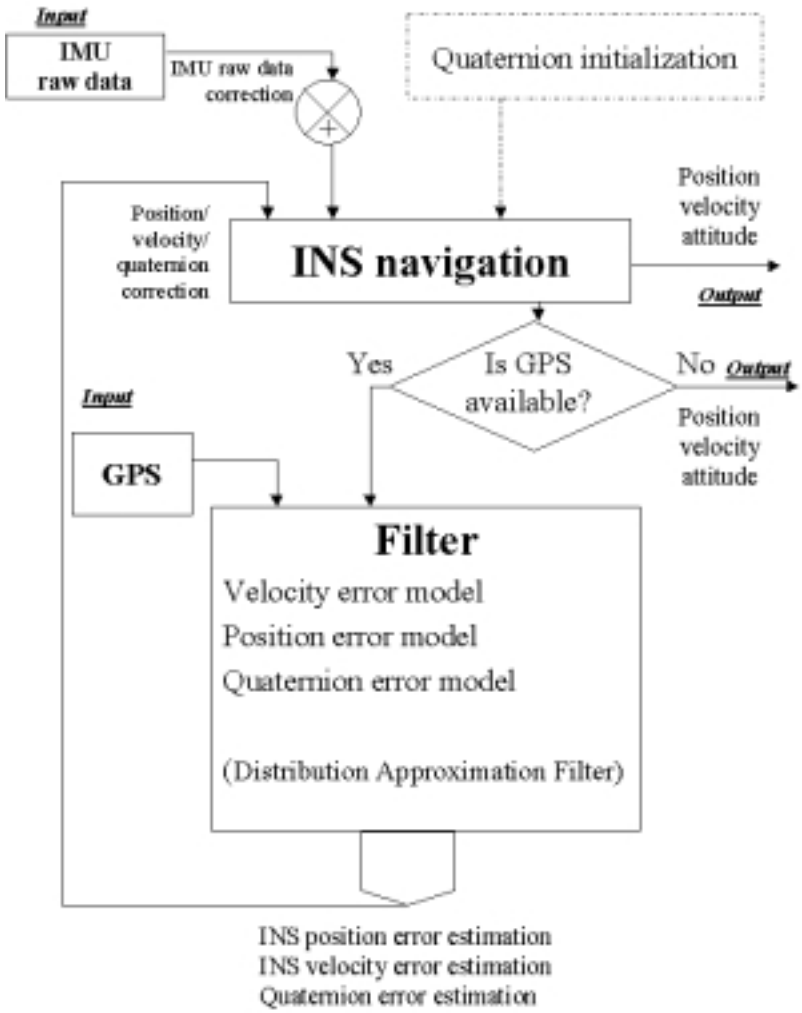

Figure 5.4: Flow chart of the quaternion approach.

navigation data at each INS sampling time starting with the first quaternion vector. When a GPS fix is available, a filter based on the velocity, position and quaternion error models updates the states. The state vector consists of the INS velocity error, the position errors, the quaternion errors in the computer frame and the IMU and GPS error states. These estimates are used to correct the INS navigation and calibrate IMU biases.

The computer frame is selected as the local level frame in east, north and up at the INS computed position.

5.3.2 Filter Models

The filter propagates the estimated errors of the INS. The filter states in this algorithm are: the INS velocity and position errors in the computer frame and the quaternion errors. To simplify the presentation of the algorithm, the accelerometer biases and the gyro biases in the body frame are considered as zero-mean white noises. The experimental data in this thesis was obtained using a DGPS system. The shaping filter was not included in this case because the magnitude of the noise due to SA with this type of differential GPS implementation was neglibe.

The state vector is:

$$X = [\Delta V_x^c, \Delta V_y^c, \Delta V_z^c, \Delta R_x^c, \Delta R_y^c, \Delta R_z^c, q_0, q_1, q_2, q_3]^T \tag{5.10}$$

where

$\Delta V^c = [V_x^c, \Delta V_y^c, \Delta V_z^c]^T$ is the INS velocity error vector in the computer frame.

$\Delta R^c = [\Delta R_x^c, \Delta R_y^c, \Delta R_z^c]^T$ is the INS position error vector in the computer frame.

$Q_p^c = [q_0, q_1, q_2, q_3]^T$ is the quaternion vector which represents the rotation between the platform frame and the computer frame.

The system model is:

$$\dot{X}(t) = f_c(X,t) + G_c u(t) \tag{5.11}$$

$$Z(t) = HX(t) + w(t) \tag{5.12}$$

where Equation (5.11) describes the continuous-time propagation equation. The filter state equations are nonlinear and $u(t)$ is white noise. The measurement equations are linear in this case and $w(t)$ is white noise. The measurement vector contains the difference between the INS velocity and position information and the GPS velocity and position information.

Velocity Error Equation

Let $\Delta V^c = \widehat{V}_t^c - V_t^c$ be the INS velocity error in the computer frame. The general velocity error model for large attitude errors in quaternion form is:

$$\Delta \dot{V}^c = (I_{3\times 3} - C(Q_p^c))f_t^p - (2\Omega_{ie}^c + \Omega_{ec}^c)\Delta V^c + \Delta g^c + \nabla^p \tag{5.13}$$

Most low cost INSs are used in level navigation applications and consequently the gravity error Δg^c can be ignored. The matrix $C(Q_p^c)$ transforms the true specific force $f_t^p = [f_x^p, f_y^p, f_z^p]^T$ in the platform frame to the computer frame. It is given by:

$$C(Q_p^c) = \begin{bmatrix} q_0^2 + q_1^2 - q_2^2 - q_3^2 & 2(q_1q_2 - q_0q_3) & 2(q_1q_3 + q_0q_2) \\ 2(q_1q_2 + q_0q_3) & q_0^2 - q_1^2 + q_2^2 - q_3^2 & 2(q_2q_3 - q_0q_1) \\ 2(q_1q_3 - q_0q_2) & 2(q_2q_3 + q_0q_1) & q_0^2 - q_1^2 - q_2^2 + q_3^2 \end{bmatrix} \tag{5.14}$$

The earth rate matrix Ω_{ie}^c and the matrix Ω_{ec}^c of the rate of the computer frame in respect to the earth frame are:

$$2\Omega_{ie}^c + \Omega_{ec}^c = \begin{bmatrix} 0 \\ V_x^c tg(\varphi)/R_x + 2\omega_{ie}\sin(\varphi) \\ -[V_x^c/R_x + 2\omega_{ie}\cos(\varphi)] \end{bmatrix} \begin{bmatrix} -[V_x^c tg(\varphi)/R_x + 2\omega_{ie}\sin(\varphi)] & V_x^c/R_x + 2\omega_{ie}\cos(\varphi) \\ 0 & V_y^c/R_y \\ -V_y^c/R_y & 0 \end{bmatrix} \tag{5.15}$$

where φ is the local latitude. The earth rate $\omega_{ie} = 7.272205 \times 10^{-5} rad/second$. The earth radius elements R_x in the east direction and R_y in the north direction can be considered as equal to $R = 6,378,393m$. The INS velocity components V_x^c and V_y^c are computed in the computer frame in east and north. Therefore the velocity error equation must include the following transformation:

$$\begin{aligned}
\Delta\dot{V}^c &= \begin{bmatrix} \Delta\dot{V}_x^c \\ \Delta\dot{V}_y^c \\ \Delta\dot{V}_z^c \end{bmatrix} \qquad (5.16)\\
&= 2\begin{bmatrix} q_2^2+q_3^2 & -(q_1q_2-q_0q_3) & -(q_1q_3+q_0q_2) \\ -(q_1q_2+q_0q_3) & q_1^2+q_3^2 & -(q_2q_3-q_0q_1) \\ -(q_1q_3-q_0q_2) & -(q_2q_3+q_0q_1) & q_1^2+q_2^2 \end{bmatrix}\begin{bmatrix} f_x^p \\ f_y^p \\ f_z^p \end{bmatrix} - \\
&- \begin{bmatrix} 0 & -[V_x^c tg(\varphi)/R_x + 2\omega_{ie}\sin(\varphi)] \\ V_x^c tg(\varphi)/R_x + 2\omega_{ie}\sin(\varphi) & 0 \\ -[V_x^c/R_x + 2\omega_{ie}\cos(\varphi)] & -V_y^c/R_y \end{bmatrix} \\
&\begin{bmatrix} V_x^c/R_x + 2\omega_{ie}\cos(\varphi) \\ V_y^c/R_y \\ 0 \end{bmatrix}\begin{bmatrix} \Delta V_x^c \\ \Delta V_y^c \\ \Delta V_z^c \end{bmatrix} + \begin{bmatrix} \nabla_x^p \\ \nabla_y^p \\ \nabla_z^p \end{bmatrix}
\end{aligned}$$

where $\nabla^p = [\nabla_x^p, \nabla_y^p, \nabla_z^p]^T$ is the accelerometer error vector in the platform frame.

Position Error Equation

The position error vector in the computer frame is decoupled from the quaternions. There are no differences in the position error model between the two cases whether the misalignments of the computer frame and the platform frame are small or large. Let the difference between the INS computed position and the true position in the computer frame ΔR^c be the position error in the computer frame. The position error equation

becomes:

$$\begin{aligned}\Delta\dot{R}^c &= \begin{bmatrix} \Delta\dot{R}_x^c \\ \Delta\dot{R}_y^c \\ \Delta\dot{R}_z^c \end{bmatrix} = \\ &= \Delta V^c - \Omega_{ec}^c \Delta R^c \\ &= \begin{bmatrix} \Delta V_x^c \\ \Delta V_y^c \\ \Delta V_z^c \end{bmatrix} - \begin{bmatrix} 0 & -V_x^c tg(\varphi)/R_x & V_x^c/R_x \\ V_x^c tg(\varphi)/R_x & 0 & V_y^c/R_y \\ -V_x^c/R_x & -V_y^c/R_y & 0 \end{bmatrix} \begin{bmatrix} \Delta R_x^c \\ \Delta R_y^c \\ \Delta R_z^c \end{bmatrix}\end{aligned} \tag{5.17}$$

Quaternion Error Model

The attitude error here is modelled using the quaternion vector $Q_p^c = [q_0, q_1, q_2, q_3]^T$ which represents the misalignment of the platform frame and the computer frame.

Let

$$B = \frac{1}{2} \begin{bmatrix} -q_1 & -q_2 & -q_3 \\ q_0 & -q_3 & q_2 \\ q_3 & q_0 & -q_1 \\ -q_2 & q_1 & q_0 \end{bmatrix} \tag{5.18}$$

Then the quaternion error model can be written:

$$\begin{aligned}
\dot{Q}_p^c &= B[(I - C(Q_c^p))\omega_{ic}^c - \epsilon^p] \\
&= \begin{bmatrix} -q_1 & -q_2 & -q_3 \\ q_0 & -q_3 & q_2 \\ q_3 & q_0 & -q_1 \\ -q_2 & q_1 & q_0 \end{bmatrix} \begin{bmatrix} q_2^2 + q_3^2 \\ -(q_1 q_2 - q_0 q_3) \\ -(q_1 q_3 + q_0 q_2) \end{bmatrix} \\
&\quad \begin{bmatrix} -(q_1 q_2 + q_0 q_3) & -(q_1 q_3 - q_0 q_2) \\ q_1^2 + q_3^2 & -(q_2 q_3 + q_0 q_1) \\ -(q_2 q_3 - q_0 q_1) & q_1^2 + q_2^2 \end{bmatrix} \begin{bmatrix} -V_y^c / R_y \\ \omega_{ie}\cos(\varphi) + V_x^c / R_x \\ \omega_{ie}\sin(\varphi) + V_x^c tg(\varphi)/R_x \end{bmatrix} - \\
&\quad - \frac{1}{2} \begin{bmatrix} -q_1 & -q_2 & -q_3 \\ q_0 & -q_3 & q_2 \\ q_3 & q_0 & -q_1 \\ -q_2 & q_1 & q_0 \end{bmatrix} \begin{bmatrix} \epsilon_x^p \\ \epsilon_y^p \\ \epsilon_z^p \end{bmatrix}
\end{aligned} \tag{5.19}$$

where $\epsilon^p = [\epsilon_x^p, \epsilon_y^p, \epsilon_z^p]^T$ is the gyro error vector in the platform frame.

5.3.3 Filter Process Structure in Continuous Time

The error models and the filter equations are presented in continuous time.

$$\dot{X}(t) = f_c(X, t) + G_c u(t) \tag{5.20}$$

X being the function of the velocity error, the position error and the quaternions, the process model becomes:

$$\begin{bmatrix} \Delta\dot{V}^c \\ \Delta\dot{R}^c \\ \dot{Q}_p^c \end{bmatrix} = \begin{bmatrix} (I_{3\times 3} - C(Q_p^c))f_t^p - (2\Omega_{ie}^c + \Omega_{ec}^c)\Delta V^c \\ \Delta V^c - \Omega_{ec}^c \Delta R^c \\ B(I - C(Q_c^p))\omega_{ic}^c \end{bmatrix} + \begin{bmatrix} \nabla^p \\ 0_{3\times 1} \\ -B\epsilon^p \end{bmatrix} \tag{5.21}$$

where

$$f_c(X, t) = \begin{bmatrix} (I_{3\times 3} - C(Q_p^c))f_t^p - (2\Omega_{ie}^c + \Omega_{ec}^c)\Delta V^c \\ \Delta V^c - \Omega_{ec}^c \Delta R^c \\ B(I - C(Q_c^p))\omega_{ic}^c \end{bmatrix} \tag{5.22}$$

and

$$G_c u(t) = \begin{bmatrix} \nabla^p \\ 0_{3\times 1} \\ -B\epsilon^p \end{bmatrix} \tag{5.23}$$

Rather than model ∇^b and ϵ^b in the body frame as in the psi angle approach, this method handles the IMU errors directly in the platform frame. $\nabla^p = [\nabla^p_x, \nabla^p_y, \nabla^p_z]^T$ and $\epsilon^p = [\epsilon^p_x, \epsilon^p_y, \epsilon^p_z]^T$ are the accelerometer and the gyro error vectors in the platform frame. They are related to the IMU biases in the body frame by:

$$\nabla^p = C(Q^p_b) \times \nabla^b \tag{5.24}$$

$$\epsilon^p = C(Q^p_b) \times \epsilon^b \tag{5.25}$$

where the matrix $C(Q^p_b)$ transforms the vectors from the body frame to the platform frame. It must be noted that the quaternions Q^p_b in (5.24) and (5.25) do not contain the filter state estimate Q^c_p.

Let

$$D^p = -B\epsilon^p = \begin{bmatrix} D^p_1 \\ D^p_2 \\ D^p_3 \\ D^p_4 \end{bmatrix} \tag{5.26}$$

and

$$E = -B \times C(Q^p_b) \tag{5.27}$$

Then

$$D^p = -B\epsilon^p = E \times \epsilon^b \tag{5.28}$$

The turn-on biases of the accelerometers and the gyros in the body frame are removed in the coarse alignment and during the zero velocity stage when the vehicle stops. The remains of the bias ∇^b of the accelerometers and the bias ϵ^b of the gyros in the body frame are considered as white Gaussian noise.

The linear combinations of jointly white Gaussian random variables are also white Gaussian random variables [49]. Therefore ∇^p, D^p and $\begin{bmatrix} \nabla^p \\ D^p \end{bmatrix}$ are also white Gaussian noises.

Let us set the noise $u(t)$ as

$$u(t) = \begin{bmatrix} \nabla^p \\ D^p \end{bmatrix} = \begin{bmatrix} \nabla^p_x \\ \nabla^p_y \\ \nabla^p_z \\ D^p_1 \\ D^p_2 \\ D^p_3 \\ D^p_4 \end{bmatrix} \tag{5.29}$$

This can be projected into the state space using the transformation matrix G_c:

$$G_c = \begin{bmatrix} 1 & 0 & 0 & 0 & 0 & 0 & 0 \\ 0 & 1 & 0 & 0 & 0 & 0 & 0 \\ 0 & 0 & 1 & 0 & 0 & 0 & 0 \\ 0 & 0 & 0 & 0 & 0 & 0 & 0 \\ 0 & 0 & 0 & 0 & 0 & 0 & 0 \\ 0 & 0 & 0 & 0 & 0 & 0 & 0 \\ 0 & 0 & 0 & 1 & 0 & 0 & 0 \\ 0 & 0 & 0 & 0 & 1 & 0 & 0 \\ 0 & 0 & 0 & 0 & 0 & 1 & 0 \\ 0 & 0 & 0 & 0 & 0 & 0 & 1 \end{bmatrix} \tag{5.30}$$

5.3.4 Observation Equations

The observations are the position and the velocity information differences of the INS and the DGPS. Let Z be the measurement vector:

$$
\begin{aligned}
Z &= \begin{bmatrix} \widehat{R}^c_{INS} - \widehat{R}^t_{GPS} \\ \widehat{V}^c_{INS} - \widehat{V}^t_{GPS} \end{bmatrix} \\
&= \begin{bmatrix} \Delta R^c - \Gamma_{gps} \\ \Delta V^c - \Theta_{gps} \end{bmatrix} \\
&= \begin{bmatrix} \Delta R^c_x \\ \Delta R^c_y \\ \Delta R^c_z \\ \Delta V^c_x \\ \Delta V^c_y \\ \Delta V^c_z \end{bmatrix} - \begin{bmatrix} \Gamma_x \\ \Gamma_y \\ \Gamma_z \\ \Theta_x \\ \Theta_y \\ \Theta_z \end{bmatrix}
\end{aligned}
\tag{5.31}
$$

where $\widehat{R}^c_{INS}$ and $\widehat{V}^c_{INS}$ are the INS computed position and velocity. $\widehat{R}^t_{GPS}$ and $\widehat{V}^t_{GPS}$ are the GPS position and velocity outputs respectively. $\Gamma_{gps} = [\Gamma_x, \Gamma_y, \Gamma_z]^T$ is the white noise of the DGPS position measurement and $\Theta_{gps} = [\Theta_x, \Theta_y, \Theta_z]^T$ is the white noise of the DGPS velocity measurement. The observation matrix H is obtained by the relationship between the states and the measurement:

$$
Z = H \begin{bmatrix} \Delta V^c \\ \Delta R^c \\ Q^c_p \end{bmatrix} - \begin{bmatrix} \Gamma_x \\ \Gamma_y \\ \Gamma_z \\ \Theta_x \\ \Theta_y \\ \Theta_z \end{bmatrix}
\tag{5.32}
$$

H is given by:

$$H = \begin{bmatrix} 0 & 0 & 0 & 1 & 0 & 0 & 0 & 0 & 0 & 0 \\ 0 & 0 & 0 & 0 & 1 & 0 & 0 & 0 & 0 & 0 \\ 0 & 0 & 0 & 0 & 0 & 1 & 0 & 0 & 0 & 0 \\ 1 & 0 & 0 & 0 & 0 & 0 & 0 & 0 & 0 & 0 \\ 0 & 1 & 0 & 0 & 0 & 0 & 0 & 0 & 0 & 0 \\ 0 & 0 & 1 & 0 & 0 & 0 & 0 & 0 & 0 & 0 \end{bmatrix} \tag{5.33}$$

5.3.5 The Discrete-Time Filter

The filter process model in continuous time is:

$$\begin{aligned} \dot{X}(t) &= f_c(X,t) + G_c u(t) \\ Z(t) &= HX(t) + w(t) \end{aligned} \tag{5.34}$$

where

$$f_c(X,t) = \begin{bmatrix} (I_{3\times 3} - C(Q_p^c))f_t^p - (2\Omega_{ie}^c + \Omega_{ec}^c)\Delta V^c \\ \Delta V^c - \Omega_{ec}^c \Delta R^c \\ B(I - C(Q_c^p))\omega_{ic}^c \end{bmatrix} \tag{5.35}$$

and

$$G_c u(t) = G_c \times \begin{bmatrix} \nabla_x^p \\ \nabla_y^p \\ \nabla_z^p \\ D_1^p \\ D_2^p \\ D_3^p \\ D_4^p \end{bmatrix} \tag{5.36}$$

with the constant matrix G_c.

The filter accuracy is achieved by using a first order Euler integration scheme at each filter time. Let dt be the data fusion interval. At time t_{k+1} and t_k, $dt = t_{k+1} - t_k$,

we have:

$$\begin{aligned}\dot{X}(t_k) &\approx \frac{X(t_{k+1}) - X(t_k)}{dt} \\ &\approx f_c(X(t_k), t_k) + G_c u(t_k)\end{aligned} \tag{5.37}$$

Therefore the discrete-time process model is:

$$\begin{aligned}X(t_{k+1}) &= X(t_k) + dt \times f_c(X(t_k), t_k) + G_c u(t_k) dt \\ &= f_k(X(t_k)) + G_k u_k\end{aligned} \tag{5.38}$$

where

$$\begin{aligned}f_k(X_k) &= X(t_k) + dt \times f_c(X(t_k), t_k) \\ &= X(t_k) + dt \times \begin{bmatrix} (I_{3X3} - C(Q_p^c)) f_t^p - (2\Omega_{ie}^c + \Omega_{ec}^c)\Delta V^c \\ \Delta V^c - \Omega_{ec}^c \Delta R^c \\ B(I - C(Q_c^p))\omega_{ic}^c \end{bmatrix}_{X(t_k), t_k}\end{aligned} \tag{5.39}$$

and

$$\begin{aligned}G_k &= G_c dt \\ u_k &= u(t_k)\end{aligned} \tag{5.40}$$

The measurement is taken at the GPS sampling time. The discrete observation equation is:

$$Z(t_k) = HX(t_k) + w(t_k) \tag{5.41}$$

with the constant observation matrix H.

For convenience, let $X_k = X(t_k)$, $Z_k = Z(t_k)$ and $w_k = w(t_k)$. The discrete filter is written as

$$\begin{aligned}X_k &= f_k(X_k) + G_k u_k \\ Z_k &= HX_k + w_k\end{aligned} \tag{5.42}$$

5.3.6 Data Fusion - the Distribution Approximation Filter

Introduction

The filter process models of the quaternion approach are nonlinear.

The EKF predicts the state of the system under the assumption that its process and observation models are locally linear. The process model and the observation models are expanded as a Taylor series about the filter's estimated trajectory using Jacobians. The cyclic computation of the state prediction, measurement prediction, innovation, updated state estimation and the state error covariance, state prediction covariance, innovation, filter gain and the updated state covariance are similar to those derived from the procedure using the linear Kalman filter [83, 71].

There are a number of problems with the EKF. The first is the need to analytically evaluate the Jacobian matrices of the process and observation models. The Jacobian is not guaranteed to exist (e.g. at discontinuity), or might not have a finite value. Further, there can be considerable implementation difficulties when the system is composed of many states and is highly non-linear. Finally the linearization can introduce significant errors.

These problems motivated the development of a new filter algorithm called the Distribution Approximation Filter (DAF) jointly by Julier and Uhlmann [21, 19]. The DAF takes a mid-course between the analytical and numerical approaches. Like the numerical methods, it approximates the state distribution rather than the process or observation model.

The DAF uses the intuition that it is easier to approximate a distribution than it is to approximate an arbitrary nonlinear function or transformation. The approach is illustrated in Figure 5.5.

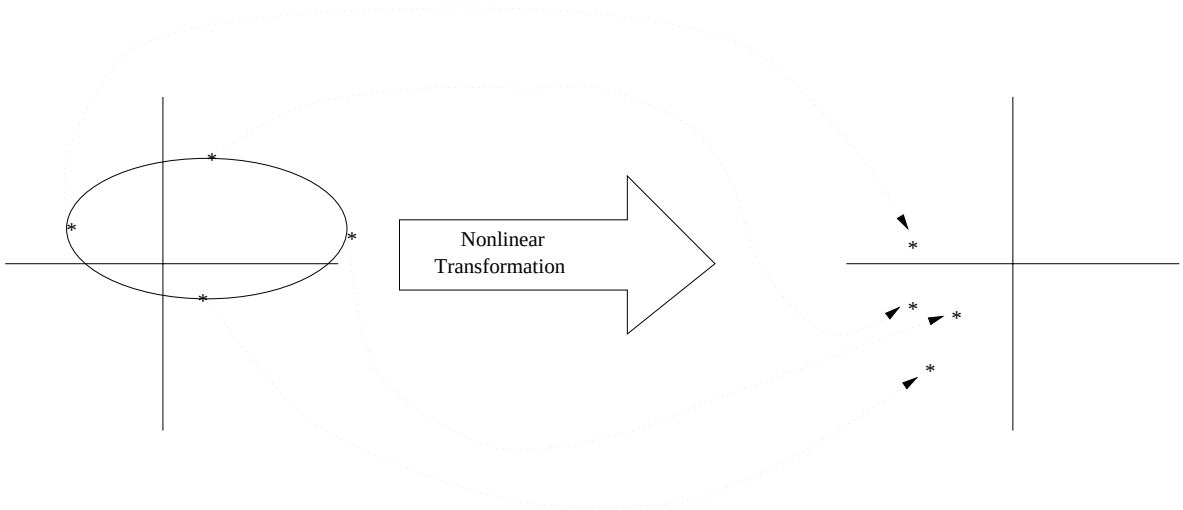

Figure 5.5: The principle of the Distribution Approximation Filter

DAF Principle

If the discrete filter process model and observation model are:

$$X_k = f_k(X_k) + U_k \tag{5.43}$$
$$Z_k = HX_k + w_k$$

it is assumed that the process noise U_k is a Gaussian-distributed, zero mean random variable with covariance Q_k. The process noise at any time is independent of the state of the system.

$$E[U] = 0 \tag{5.44}$$
$$E[U_i U_j^T] = Q_i \delta_{ij}$$
$$E[U_i X_j^T] = 0 \ \forall i, j$$

where δ_{ij} is the Kronecker delta function.

The observation noise w_k encompasses all the unmodelled effects which act on the observations, but not on the underlying state of the system itself. It is assumed to be a zero-mean Gaussian distributed random variable with variance R_k and it is independent

of the observation noises at all previous time steps:

$$E[w] = 0 \tag{5.45}$$
$$E[w_i w_j^T] = R_i \delta_{ij}$$
$$E[w_i X_j^T] = 0 \ \forall i, j$$

The problem of how to solve can be summarized as follows. We have an $n-$dimensional vector random variable X with mean $\overline{x}$ and covariance P_{xx} and we would like to predict the mean $\overline{y}$ and covariance P_{yy} of an $m-$dimensional vector random variable Y where Y is related to X by the non-linear transformation

$$Y = g[X] \tag{5.46}$$

Following the intuition that it is easier to approximate a Gaussian distribution than it is to approximate an arbitrary nonlinear function or transformation, a parameterization could be found which captures the mean and covariance information while at the same time permitting the direct propagation of the information through an arbitrary set of nonlinear equations. This can be accomplished by generating a discrete distribution having the same first and second order moments, where each point in the discrete approximation can be directly transformed. The mean and covariance of the transformed ensemble can then be computed as the estimate of the nonlinear transformation of the original distribution.

The DAF operational principle is explained as follows [19]:

Assume an $n-$dimensional Gaussian distribution having covariance P, a set of $2n$ points having the same sample covariance from the columns (or rows) of the matrices $\pm\sqrt{nP}$ (the positive and negative roots). This set of points is zero mean, but if the original distribution has mean $\overline{x}$, then simply adding $\overline{x}$ to each of the points yields a symmetric set of $2n$ points having the desired mean and covariance. Because the set is symmetric, its odd central moments are zeros, so its first three moments are the same as the original Gaussian distribution. These points are transformed nonlinearly using the transition equation. The transformed points can be used to compute the predicted mean

and covariance. With this approach, there is no need to evaluate Jacobian matrices to compute the estimation of mean and covariance as in the EKF method.

The DAF is summarized as follows:

- The set of translated σ points is computed from the $n \times n$ matrix $P_{k,k}$ as

$$\begin{aligned} \sigma_{k,k} \longleftarrow 2n \text{ columns from } \pm\sqrt{(n+\kappa)P_{k,k}} \\ \chi_{ok,k} = X_{k,k} \\ \chi_{ik,k} = \sigma_{ik,k} + X_{k,k} \end{aligned} \tag{5.47}$$

  which assures that

$$P_{k,k} = \frac{1}{n+\kappa}\sum_{i=1}^{2n}[\chi_{ik,k} - X_{k,k}][\chi_{ik,k} - X_{k,k}]^T \tag{5.48}$$

- The predicted mean is computed as

$$X_{k+1,k} = \frac{1}{n+\kappa}[\kappa\chi_{ok+1,k} + \frac{1}{2}\sum_{i=1}^{2n}\chi_{ik+1,k}] \tag{5.49}$$

- The predicted covariance is computed as

$$\begin{aligned} P_{k+1,k} = \frac{1}{n+\kappa}\{\kappa[\chi_{ok+1,k} - X_{k+1,k}][\chi_{ok+1,k} - X_{k+1,k}]^T + \\ +\frac{1}{2}\sum_{i=1}^{2n}[\chi_{ik+1,k} - X_{k+1,k}][\chi_{ik+1,k} - X_{k+1,k}]^T\} + Q_k \end{aligned} \tag{5.50}$$

  where Q_k is the dynamic noise covariance.

- The predicted observation:

$$Z_{k+1,k} = \frac{1}{n+\kappa}\{\kappa Z_{ok+1,k} + \frac{1}{2}\sum_{i=1}^{2n} Z_{ik+1,k}\} \tag{5.51}$$

The quantity κ is a scaling factor which provides an extra degree of freedom to fine tune the higher order moments of the approximation.

5.3.7 Filter Implementation Using DAF

The filter states are the errors of the INS velocity, position and quaternions. The discrete filter is:

$$X_k = f_k(X_k) + G_k u_k$$

$$Z_k = H X_k + w_k$$

where $f_k(X_k)$, $G_k u_k$ and H are as equations (5.39), (5.40) and (5.33).

The initial filter state starts from $X_{0,0} = [0, 0, 0, 0, 0, 0, q_0(1), q_1(1), q_2(1), q_3(1)]^T$ with zero INS velocity error, zero INS position error and arbitrary initial quaternion error $[q_0(1), q_1(1), q_2(1), q_3(1)]^T$. The initial covariance matrix is set by

$$P_{0,0} = \begin{bmatrix} \sigma_{Vx}^2 & 0 & 0 & 0 & 0 & 0 & 0 & 0 & 0 & 0 \\ 0 & \sigma_{Vy}^2 & 0 & 0 & 0 & 0 & 0 & 0 & 0 & 0 \\ 0 & 0 & \sigma_{Vz}^2 & 0 & 0 & 0 & 0 & 0 & 0 & 0 \\ 0 & 0 & 0 & \sigma_{Rx}^2 & 0 & 0 & 0 & 0 & 0 & 0 \\ 0 & 0 & 0 & 0 & \sigma_{Ry}^2 & 0 & 0 & 0 & 0 & 0 \\ 0 & 0 & 0 & 0 & 0 & \sigma_{Rz}^2 & 0 & 0 & 0 & 0 \\ 0 & 0 & 0 & 0 & 0 & 0 & \sigma_{q0}^2 & 0 & 0 & 0 \\ 0 & 0 & 0 & 0 & 0 & 0 & 0 & \sigma_{q1}^2 & 0 & 0 \\ 0 & 0 & 0 & 0 & 0 & 0 & 0 & 0 & \sigma_{q2}^2 & 0 \\ 0 & 0 & 0 & 0 & 0 & 0 & 0 & 0 & 0 & \sigma_{q3}^2 \end{bmatrix} \tag{5.52}$$

The diagonal terms of $P_{0,0}$ represent variances or mean-squared errors. The off-diagonal terms are set to be zeros.

The initial dynamic process noise is set as Q_0.

$$Q_0 = \begin{bmatrix} \sigma^2_{acc\_x} & 0 & 0 & 0 & 0 & 0 & 0 \\ 0 & \sigma^2_{acc\_y} & 0 & 0 & 0 & 0 & 0 \\ 0 & 0 & \sigma^2_{acc\_z} & 0 & 0 & 0 & 0 \\ 0 & 0 & 0 & \sigma^2_{q\_0} & 0 & 0 & 0 \\ 0 & 0 & 0 & 0 & \sigma^2_{q\_1} & 0 & 0 \\ 0 & 0 & 0 & 0 & 0 & \sigma^2_{q\_2} & 0 \\ 0 & 0 & 0 & 0 & 0 & 0 & \sigma^2_{q\_3} \end{bmatrix} \tag{5.53}$$

where the tuning of the diagonal terms of Q_0 determines the performance of the filter.

The initial measurement noise R_0 is set by

$$R_0 = \begin{bmatrix} r^2_{rx} & 0 & 0 & 0 & 0 & 0 \\ 0 & r^2_{ry} & 0 & 0 & 0 & 0 \\ 0 & 0 & r^2_{rz} & 0 & 0 & 0 \\ 0 & 0 & 0 & r^2_{vx} & 0 & 0 \\ 0 & 0 & 0 & 0 & r^2_{vy} & 0 \\ 0 & 0 & 0 & 0 & 0 & r^2_{vz} \end{bmatrix} \tag{5.54}$$

The diagonal terms of R_0 are initial measurement noises on INS and GPS position and velocity.

The filter is implemented at time t_k using the DAF. Following the DAF procedures (5.47) to (5.51):

- At the data fusion time t_{k-1}, the state estimate is X_{k-1}. The projected covariance matrix is P_{k-1}.
- At the current data fusion time t_k, compute the σ points using the projected covariance P_{k-1}.

$$\sigma = \sqrt{nP_{k-1}} \tag{5.55}$$

where n is the size of P_{k-1}.

- Form the matrix χ_i

$$\chi_{ik,k} = [X_{k-1} + \sigma, X_{k-1} - \sigma] \tag{5.56}$$

- Transform each point through the nonlinear state process model as:

$$\chi_{ik,k-1} = f_k(\chi_{ik,k}) \tag{5.57}$$

- Compute the predicted mean. Then the estimated errors are used to update the states. After the correction, the predicted mean state $X_{k,k-1}$ of the filter should be reset to zero:

$$X_{k,k-1} = [0, 0, 0, 0, 0, 0, 0, 0, 0, 0]^T \tag{5.58}$$

- The predicted covariance $P_{k,k-1}$ is computed as

$$P_{k,k-1} = \frac{1}{2n} \sum_{i=1}^{2n} [\chi_{ik,k-1} - X_{k,k-1}][\chi_{ik,k-1} - X_{k,k-1}]^T + Q_k \tag{5.59}$$

  where Q_k is the dynamic noise covariance.

- Compute the filter gain K_k :

$$K_k = P_{k,k-1} H^T [H P_{k,k-1} H^T + R_k] \tag{5.60}$$

  with R_k being the measurement noise.

- Since the predicted state is zero, the update state estimate X_k is computed as:

$$X_k = K_k Z_k \tag{5.61}$$

  where Z_k is the measurement of this time.

- The update covariance estimate P_k is computed by:

$$P_k = [I - K_k H] P_{k,k-1} \tag{5.62}$$

X_k is then used to correct the INS velocity, position and quaternions.

The quaternion correction is given by:

$$Q_b^p = Q_p^c \otimes Q_b^p \tag{5.63}$$

with $\otimes$ being the quaternion multiplication.

After this filter cycle, the INS will continue to generate navigation data at the IMU sampling rate until the next GPS fix becomes available.

5.4 Summary

In this chapter, the INS algorithm using quaternions for low cost IMUs has been presented.

INS provides navigation data with high frequency in between GPS updating. At each INS navigation step, the INS velocity, position, attitude and quaternions are updated independently. The quaternions are used to represent both the vehicle attitude and the misalignment of the computer frame and the platform frame. Quaternion initialization and update using a 2-step Adams-Bashford method are presented in this approach.

The initial alignment method with unknown initial attitudes is developed using an in-motion alignment filter aided by external velocity or position information. In this approach, the GPS is used as the external information both for alignment and to bound errors. The INS error propagation models developed in the previous chapter are used as process models.

The Distribution Approximation Filter is used to solve the nonlinear filter and its advantages with respect to the EKF are presented.

Experimental results will be presented in the next chapter.

Chapter 6

Experimental Results

6.1 Introduction

This chapter presents the experimental results for the INS algorithms using the psi angle approach, the quaternion approach and the GPS modelling.

The results of the GPS modelling in the frequency domain are presented in Section 6.2. Model parameters are shown. PSDs of raw GPS position data and the calculated PSDs using the model parameters are compared with the experimental data obtained using a standard GPS receiver. Section 6.2.2 validates the GPS model by a set of plots in the frequency domain and the time domain using the feed back de-correlation filter.

Section 6.3 shows the experimental results to verify the psi angle model and the INS algorithm for a low cost IMU. The experiment uses a low cost IMU aided by a DGPS. The results will display how the heading errors are corrected from $\pm 180^{\circ}$ to $\pm 0.1^{\circ}$. INS alignment and calibration results will be presented in this section.

Section 6.4 outlines the experimental results of the quaternion algorithm developed in this thesis. INS errors in acceleration, velocity, position, attitude and quaternions will be presented using this approach.

The experimental procedures were designed based on IEEE standards and other publications [84, 85, 86, 87, 88, 89, 90, 91, 92, 93, 94, 95].

6.2 GPS Position Modelling Results

This section presents the results of the GPS error modelling. The experimental data were obtained using a standard GPS receiver (Ashtech Sensor II).

6.2.1 Model Results

The GPS receiver module processes signals from the Global Positioning System satellite constellation to provide real-time position, velocity and time measurement using twelve dedicated separate and parallel channels for Clear/Acquisition (C/A) code-phase measurement on the $L1$ ($1575MHz$) band. The standard Sensor II is designed for stand-alone range measurement applications. With four locked satellites, Sensor II can determine a three-dimensional position with an accuracy of 100 metres rms. All computations are accomplished relative to the World Geodetic System WGS-84 reference ellipsoid. The direct outputs of the antenna position data are in the WGS-84 earth-centred earth-fixed reference frame.

In order to calculate the position error characteristics, 50 samples of position data were collected from a known position. Each sample contains data of approximately 30 minutes duration. The known position in the WGS-84 frame is (-4.66×10^6, 2.571×10^6, -3.503×10^6) meters. The sampling frequency is $10Hz$.

Figure 6.1 shows the raw position output in three-dimension in the WGS-84 earth-centred earth-fixed reference frame. The position error noise in each axis is calculated by subtracting the known position from the raw data as in Figure 6.2.

The PSDs of 50 ensembles are averaged to obtain the mean PSD. The true models are estimated by fitting curves to these mean PSD curves. The mean PSDs in axes x, y and z are shown in Figure 6.3, 6.4 and 6.5 respectively.

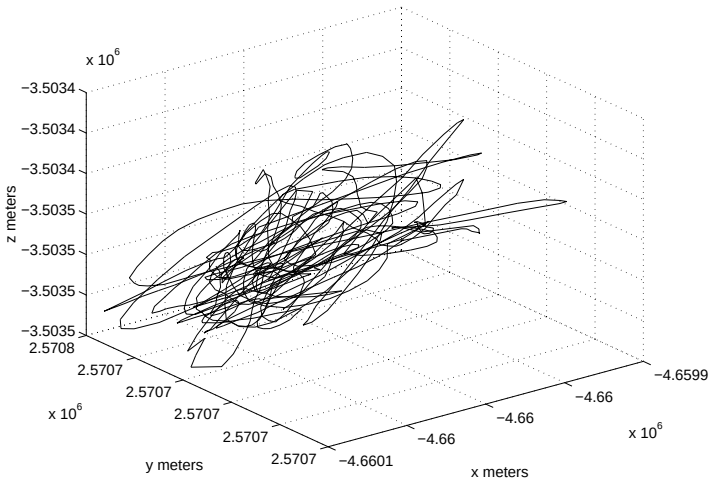

Figure 6.1: Position output from Ashtech Sensor II.

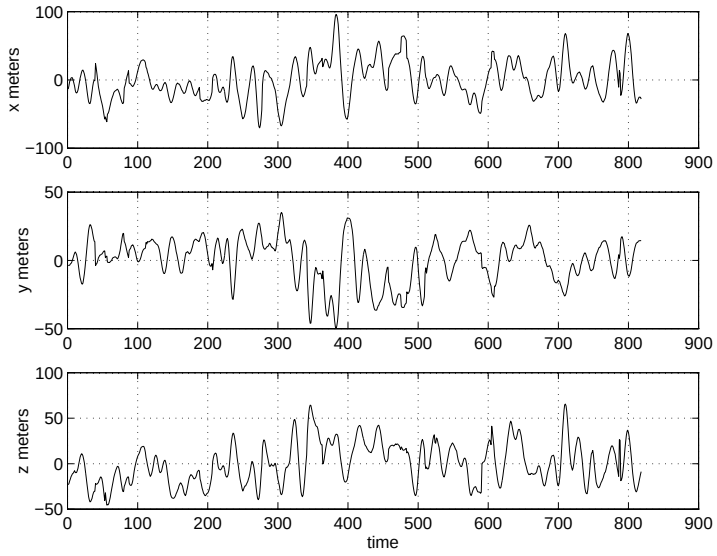

Figure 6.2: Position noise in axes x, y and z.

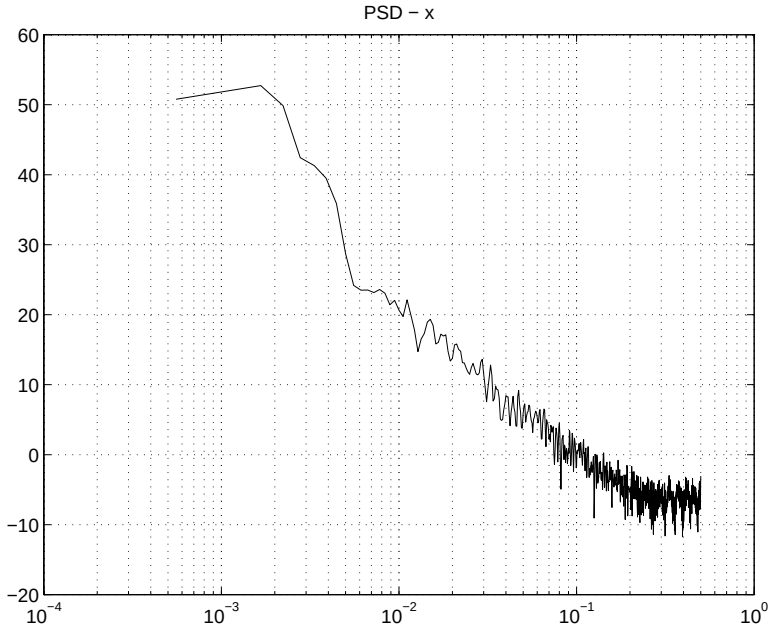

Figure 6.3: Power spectral density of position error in axis x.

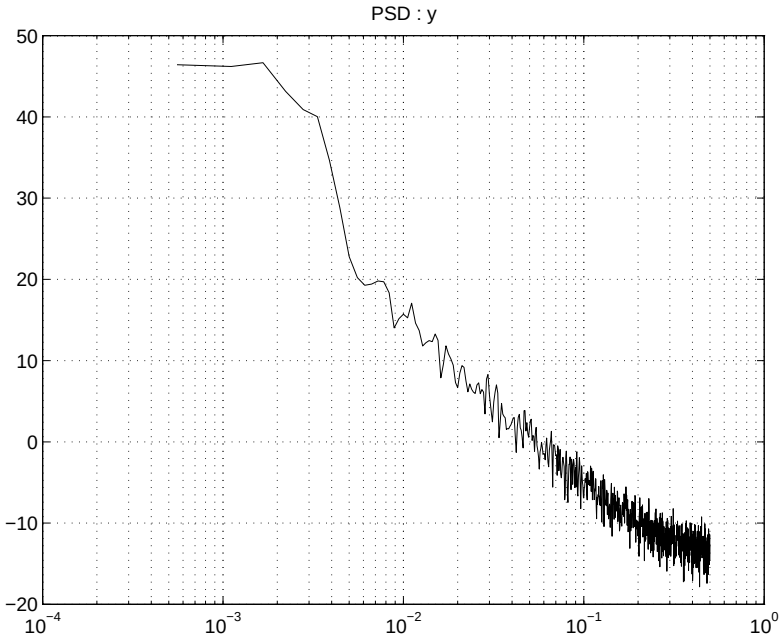

Figure 6.4: Power spectral density of position error in axis y.

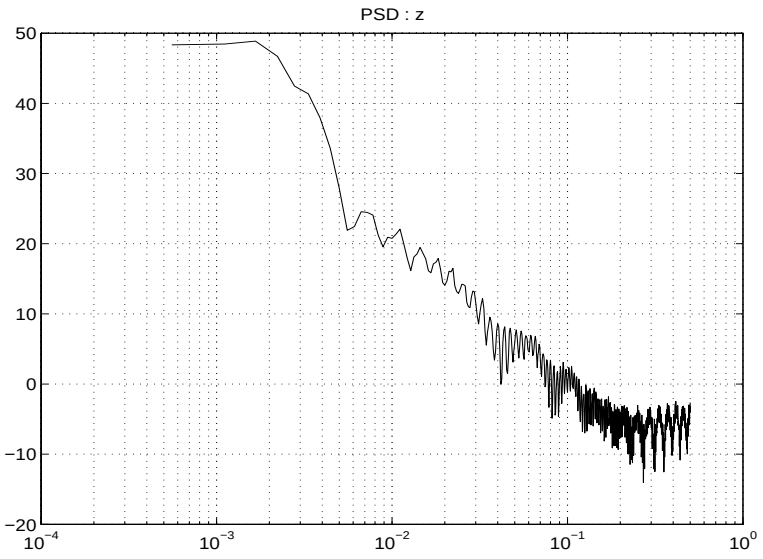

Figure 6.5: Power spectral density of position error in axis z.

The results of the PSD models for position errors in axes x, y and z are:

axis	α	β	k	r
x	0.0018	0.011	0.5	0.0987
y	0.00195	0.015	0.5	0.0523
z	0.00198	0.011	0.5	0.0937

The smooth curves in the Figure 6.6, 6.7 and 6.8 are the estimated PSDs in axes x, y and z using the estimated models. The measured PSDs are plotted with the estimated PSDs.

6.2.2 Model Validation

A feedback de-correlation filter using an INS with a noise variance of $1 \times 10^{-6}(m/s^2)^2$ is used to validate the GPS model. The GPS measurement is basically the entire noise when the vehicle is stationary. Using the estimated model parameters, the bode plots of the transfer function from the GPS measurement to the estimated shaping states in axes x, y and z are shown in Figure 6.9, 6.10 and 6.11 respectively. The gains are $0dB$ for the shaping state estimate before the frequency of $10^{-2} rad/\sec$.

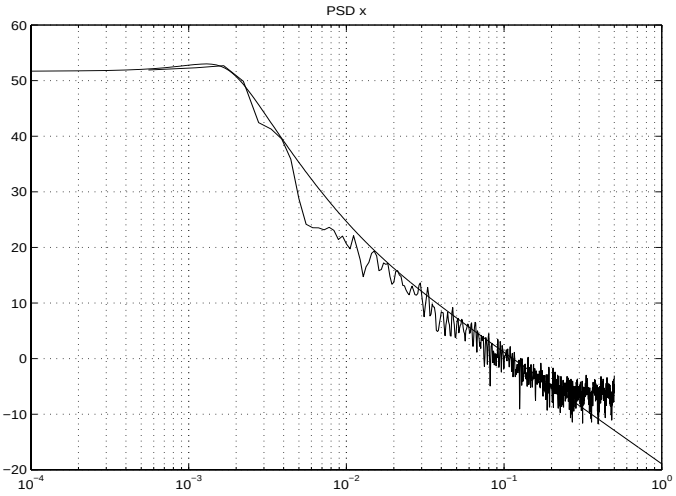

Figure 6.6: Measured PSD and estimated PSD in axis x.

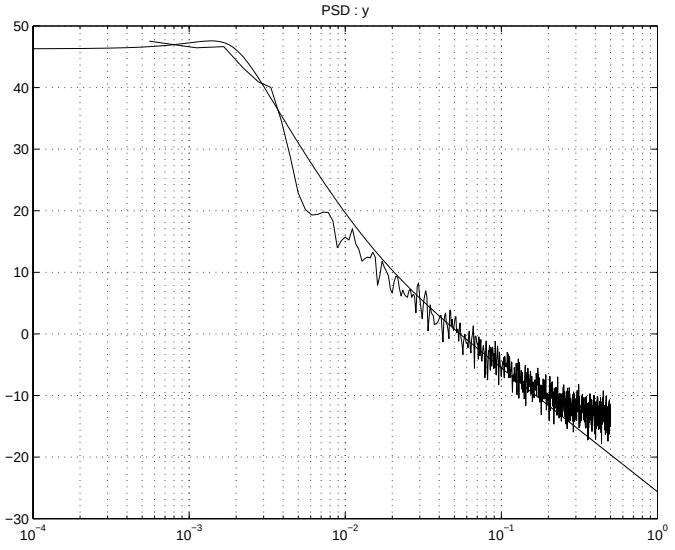

Figure 6.7: Measured PSD and estimated PSD in axis y.

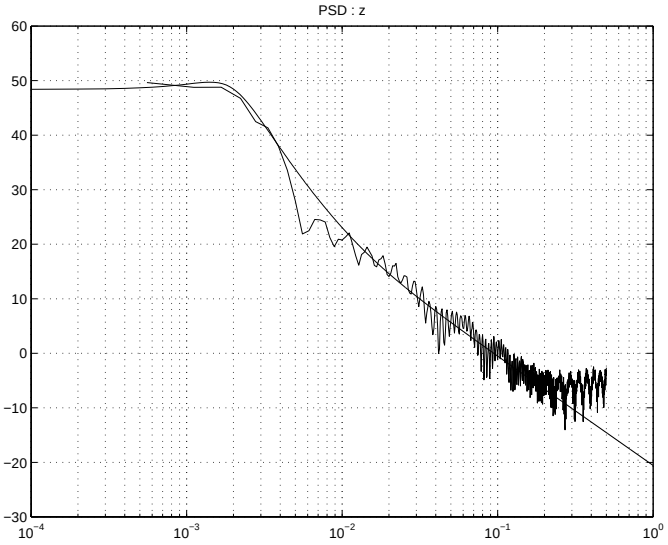

Figure 6.8: Measured PSD and estimated PSD in axis z.

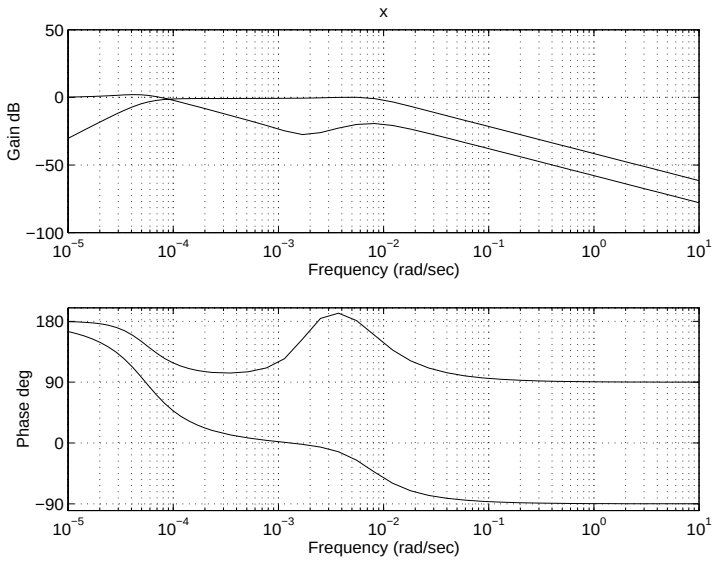

Figure 6.9: Bode plot in axis x.

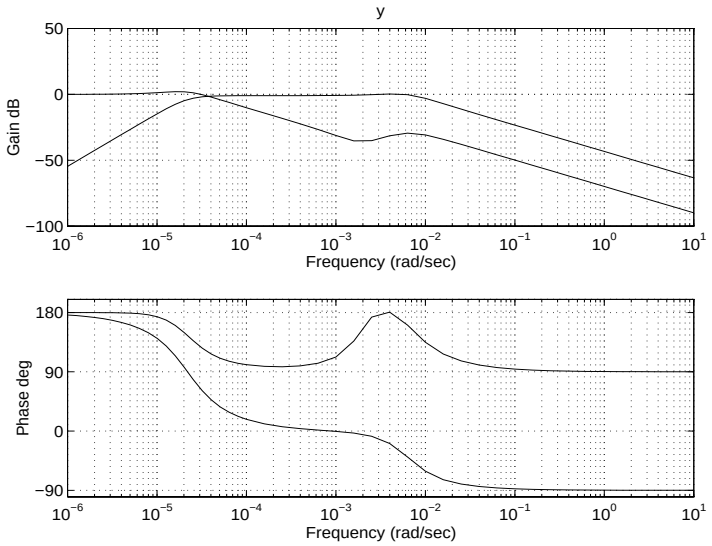

Figure 6.10: Bode plot in axis y.

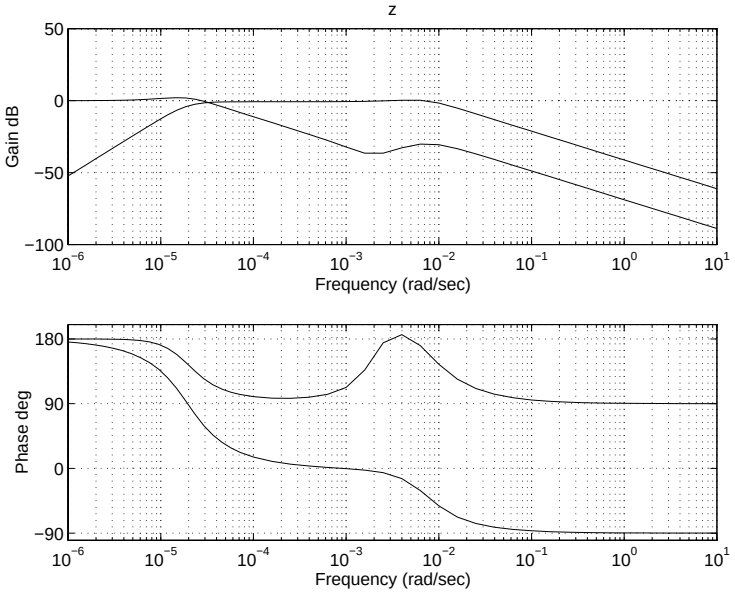

Figure 6.11: Bode plot in axis z.

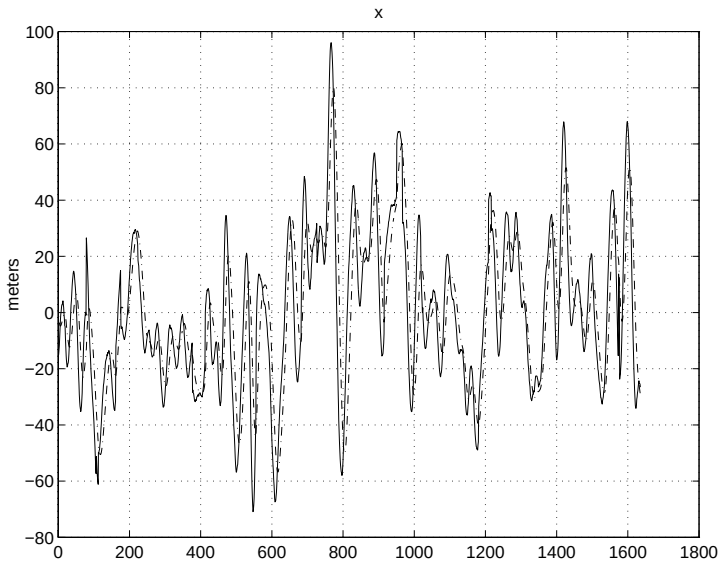

Figure 6.12: Time domain performance in axis x using the estimated model.

The filter performance in the time domain is shown in Figure 6.12, 6.13 and 6.14. It can clearly be seen that the estimated shaping states track the measured GPS noise.

The parameter values of the shaping filter are essential for the de-correlation process. For instance, a change of the parameter α, with $\alpha = 0.003$, will generate the degraded performance shown in Figure 6.15 and 6.16. The dashdot curve in Figure 6.15 is the estimated shaping state. The solid curve is the measured GPS noise. The change of the poles in the model produces a large error in the shaping state estimate.

Similar changes can be seen by changing other parameters:

Figure 6.17	Figure 6.18
axis x	axis z
$r = 0.05$	$b = 0.8, k = 1, r = 0.9$

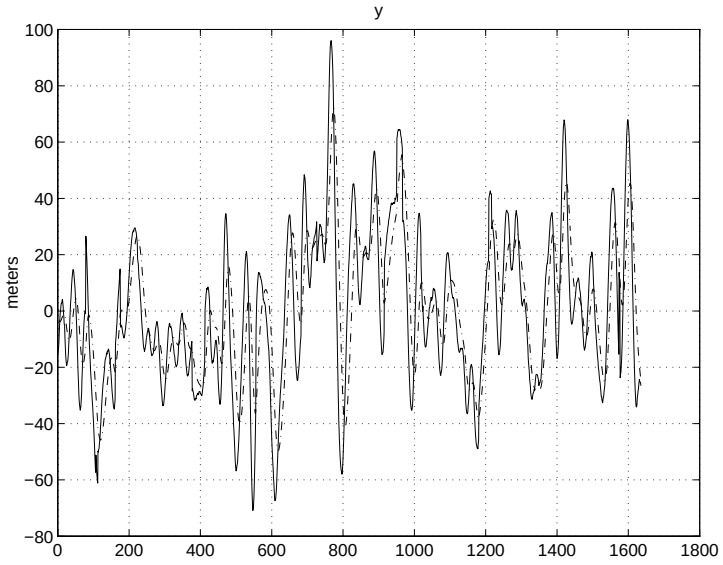

Figure 6.13: Time domain performance in axis y using the estimated model.

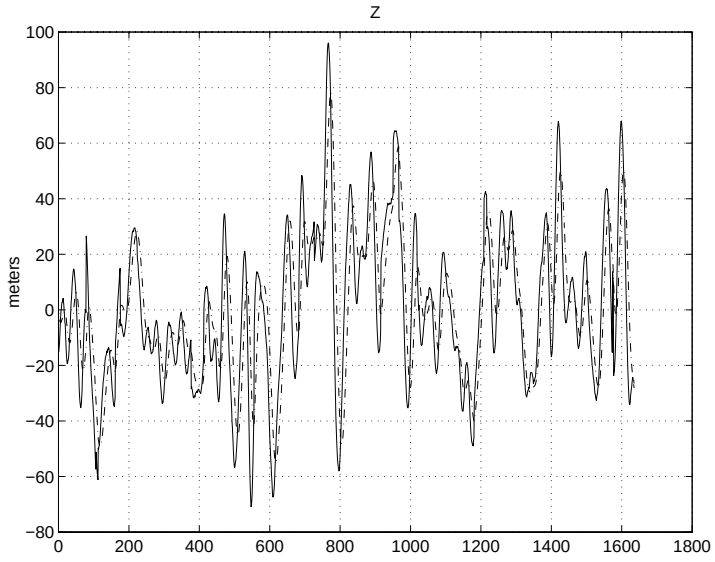

Figure 6.14: Time domain performance in axis z using the estimated model.

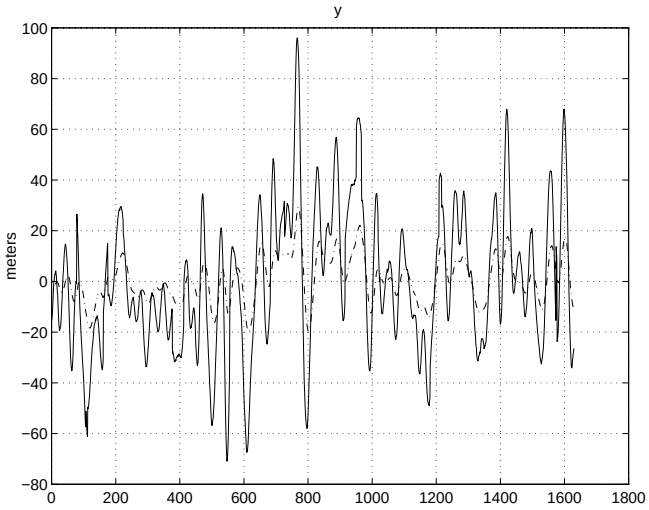

Figure 6.15: Time domain performance in axis y when the poles of the model change.

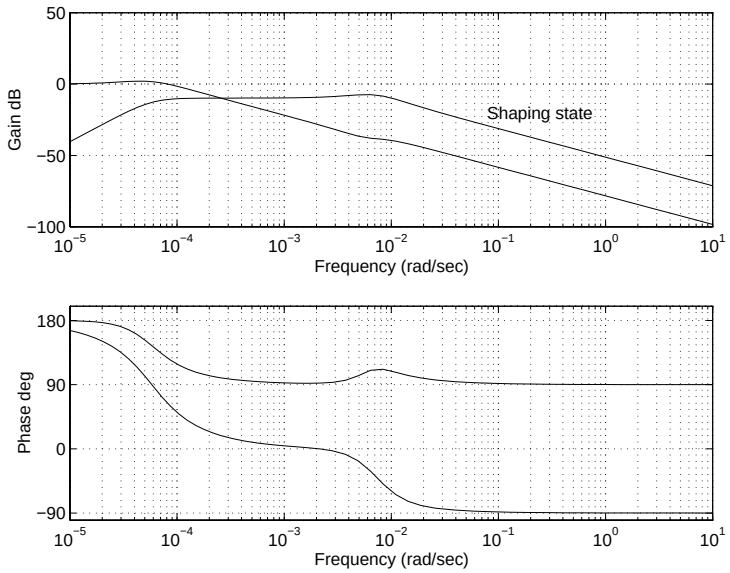

Figure 6.16: Bode plot of the transfer function for axis y when the poles of the model change.

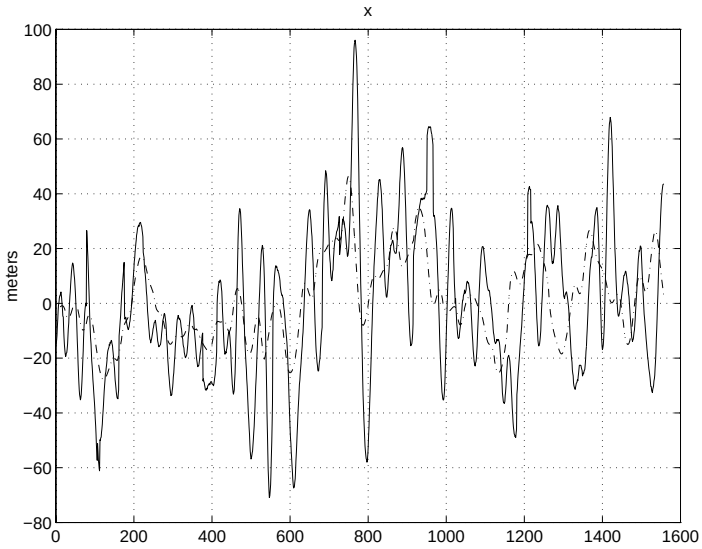

Figure 6.17: Time domain performance in axis x when r is changed.

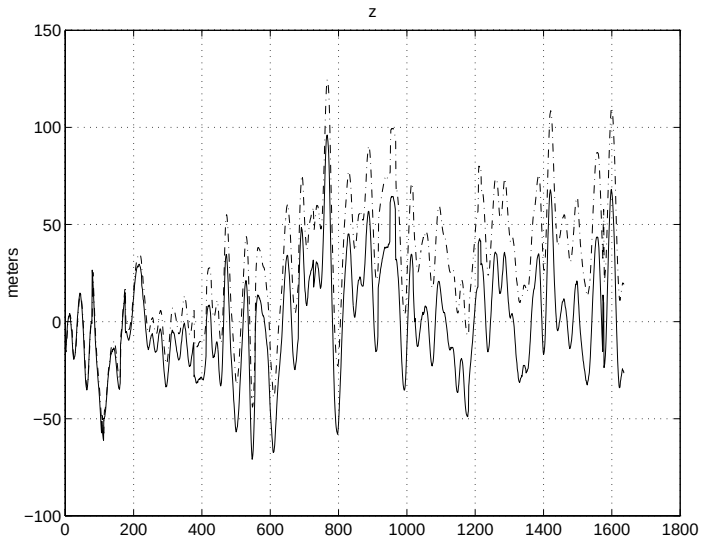

Figure 6.18: Time domain performance in axis z when three parameters are changed.

6.3 Experimental Results of the Psi Angle Approach

This section presents the experiment results to verify the INS algorithm using the psi angle approach for large attitude errors developed in this thesis. The experimental platform consists of a low cost IMU (Watson IMU) aided by a DGPS (Novatel RT2 receiver). The experiment was conducted using a UTE in outdoor enviroment.

The IMU used in this experiment is a strapdown inertial measurement unit [96] which contains three gyros, three accelerometers and two tilt gyros. The IMU is installed directly in the vehicles. The outputs of the IMU are in the body frame of the vehicle whose origin is defined at the IMU mass centre. The vehicle body frame is defined as the IMU body frame. Three accelerometers are called accelerometers x, y and z which are installed in the axes x, y and z of the body frame. The three gyros x, y and z which are installed in the axes x, y and z of the body frame provide the angular rate of the vehicle with respect to the body frame. The accelerometers measure the specific force in the body frame. The tilt gyros provide the bank and the elevation of the vehicle. The data sampling frequency is $84Hz$. The resolution of the IMU is shown in the following table:

Angular Rate Gyros	Accelerometers
$4.3115\times10^{-4}(rad/\sec)$	$0.0024m/s^2$

The resolution and the sensitivity of the angular rate gyros is not enough to measure the earth rate.

The DGPS provides the position and velocity information in the WGS-84 reference with an accuracy of $2cm$ CEP and $2cm/\sec$ CEP respectively. The sampling frequency of the DGPS is $10Hz$.

The vehicle trajectory in the experimentation is shown in Figure 6.19. It starts from $(0,0)$ which is the origin of the local level frame. The vehicle moved from $(0,0)$ after a stationary period of approximately 12 seconds and returned and stopped at the starting position.

The outputs of the three accelerometers x, y and z are shown in Figure 6.20. Figure

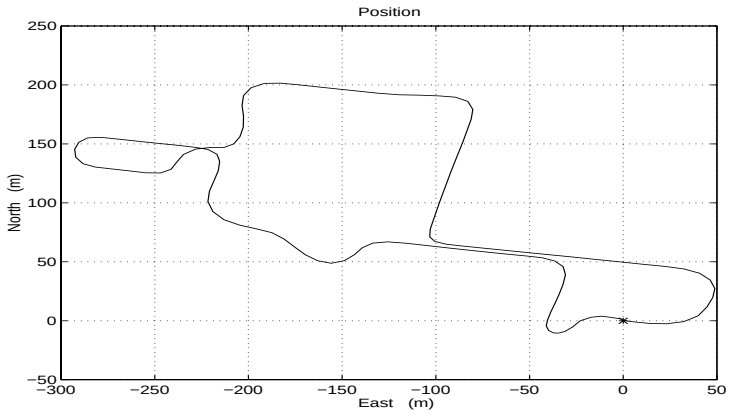

Figure 6.19: The vehicle trajectory.

6.21 is the plot of the raw data of the three gyros. They are all in the body frame.

The noise of the DGPS can be modelled as white noise. The shaping filter is not added to the algorithm. The filter state X using the psi angle approach is defined by:

$$X = [\Delta V_x^c, \Delta V_y^c, \Delta V_z^c, \Delta R_x^c, \Delta R_y^c, \Delta R_z^c, \psi_x, \psi_y, \psi_z, \nabla_x^b, \nabla_y^b, \nabla_z^b, \epsilon_x^b, \epsilon_y^b, \epsilon_z^b]^T \tag{6.1}$$

where $\Delta V^c = [V_x^c, \Delta V_y^c, \Delta V_z^c]^T$ is the INS velocity error vector in the computer frame, $\Delta R^c = [\Delta R_x^c, \Delta R_y^c, \Delta R_z^c]^T$ is the INS position error vector in the computer frame, $\psi = [\psi_x, \psi_y, \psi_z]^T$ is the psi angle vector which is the angle between the computer frame and the platform frame, $\nabla^b = [\nabla_x^b, \nabla_y^b, \nabla_z^b]^T$ is the vector of the accelerometer biases in the body frame and $\epsilon^b = [\epsilon_x^b, \epsilon_y^b, \epsilon_z^b]$ is the vector of the gyro biases in the body frame.

The filter is initialized with an arbitrary heading between $\pm 180°$. The system runs on prediction using IMU data until DGPS information becomes available. At this time the IMU state is updated and the heading is corrected as shown in Figure 6.22.

Figure 6.23 shows how the heading error diminishes to $\pm 1°$ in approximately 15 seconds. After this stage, the system is switched to the small angle form of the filter.

The position outputs of the INS and the GPS are shown in Figure 6.24. The INS continually outputs navigation data between two consecutive GPS sampling times. The GPS information is used to correct the INS velocity, position and DCM at each GPS

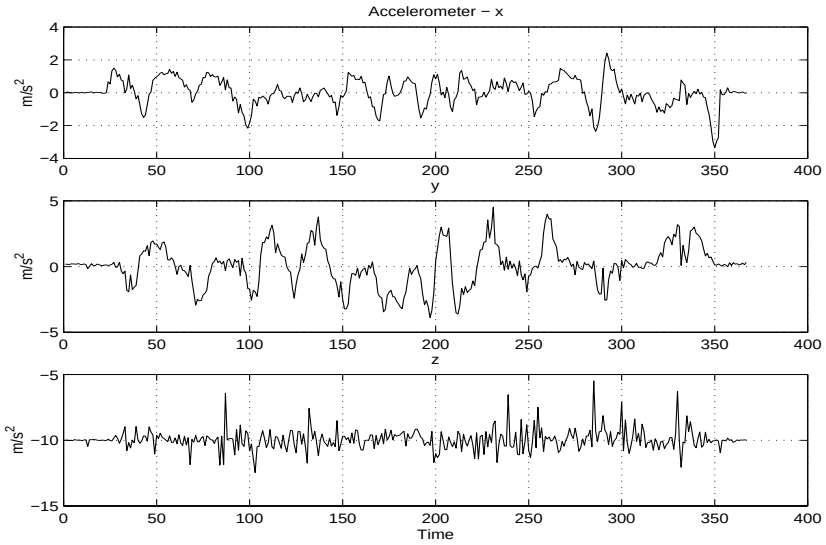

Figure 6.20: Outputs of three accelerometers. The units for the x axes are seconds.

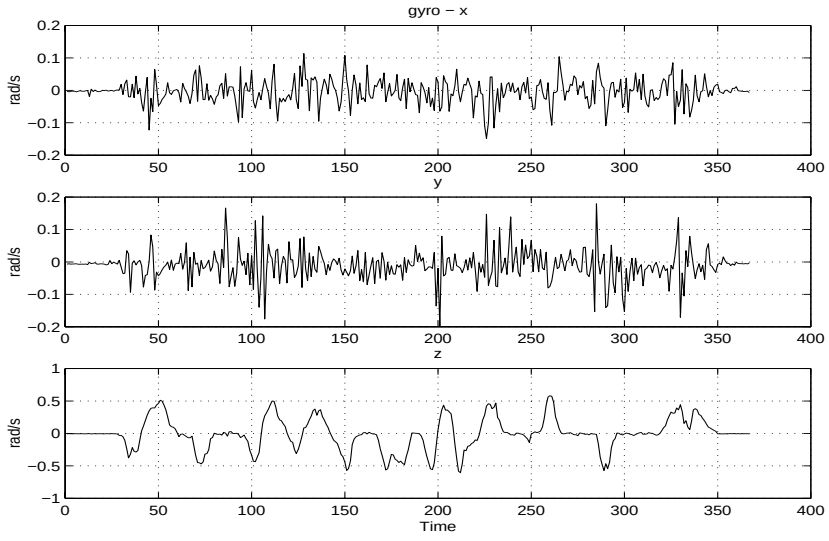

Figure 6.21: Outputs of three gyros. The units for the x axes are seconds.

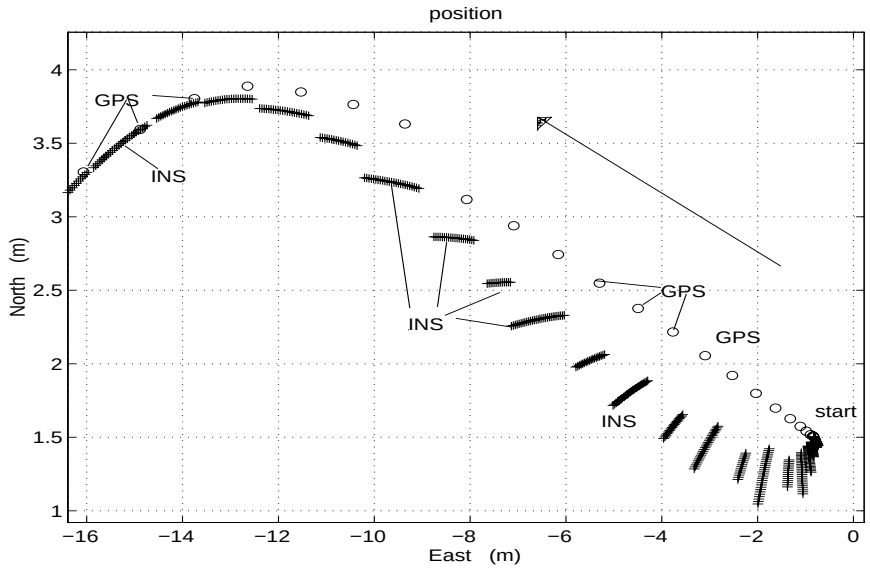

Figure 6.22: INS starts with a wrong heading. The filter corrects the heading in the first 20 seconds.

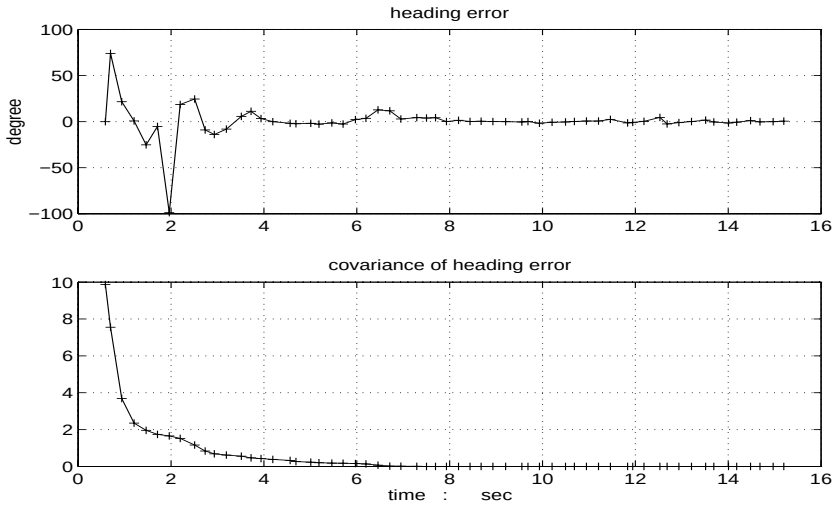

Figure 6.23: Heading error diminishes to small angles in 15 seconds.

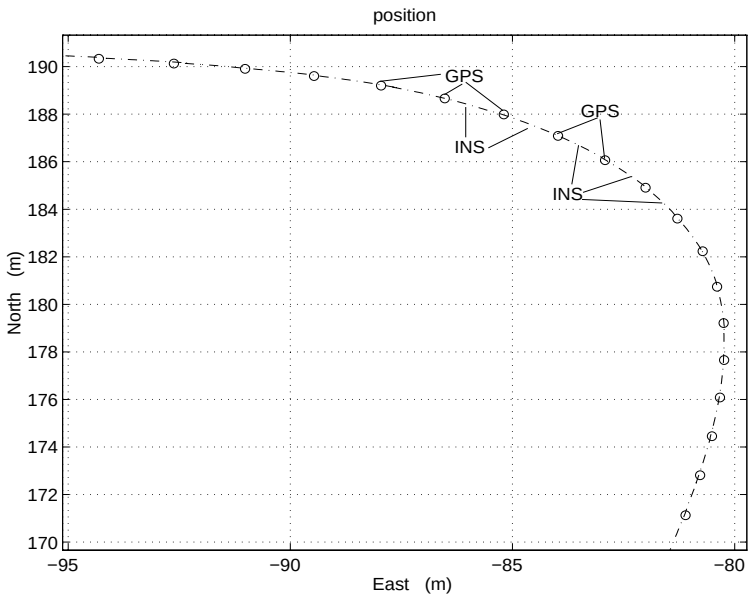

Figure 6.24: Position outputs of the INS and the GPS after attitude correction. The INS continually outputs navigation data between two consecutive GPS sampling times.

sampling time.

Tilt and heading errors are within $\pm 0.05^{\circ}$ as shown in Figure 6.25.

At the end of the run, the vehicle returned to the starting position and stayed stationary for a few seconds. The acceleration and velocity predicted by the INS should be zero during this period. The acceleration outputs in the p-frame are shown in Figure 6.26. It can be seen that the accelerations are very close to zero implying that the alignment procedure is able to correct the transformation matrix or direction cosine matrix (DCM).

Without DCM correction, only position and velocity errors are corrected. In this case, the acceleration is not zero at the end of the run as shown in Figure 6.27.

The drift of one of the gyros used in the IMU is shown in Figure 6.28. It can be appreciated that the random walk is about 0.1 $degree/min$. To degrade the accuracy of the unit, an additional random noise plus drift was added to the IMU sensors. The noise added to the three accelerometers and the three gyros was approximately 3 times

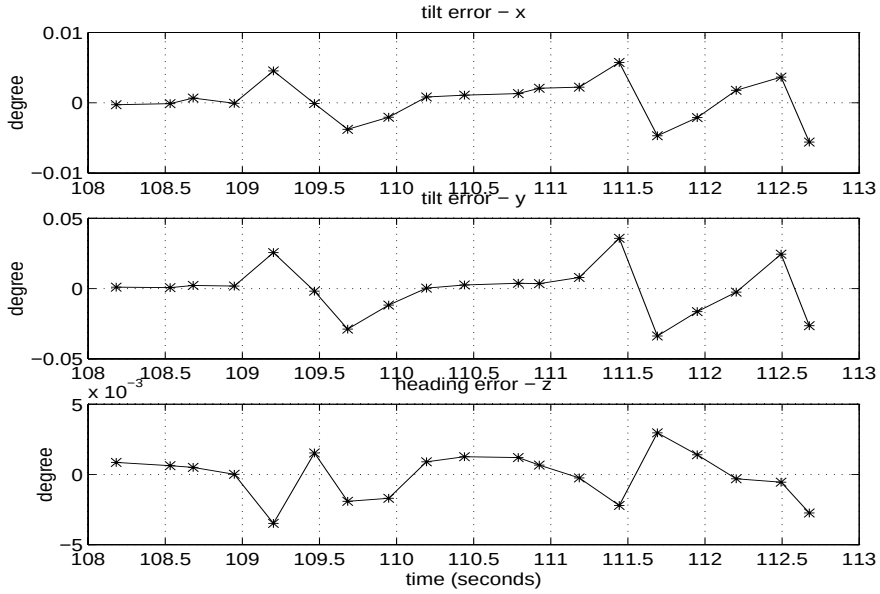

Figure 6.25: Tilt and heading errors diminish to small angles.

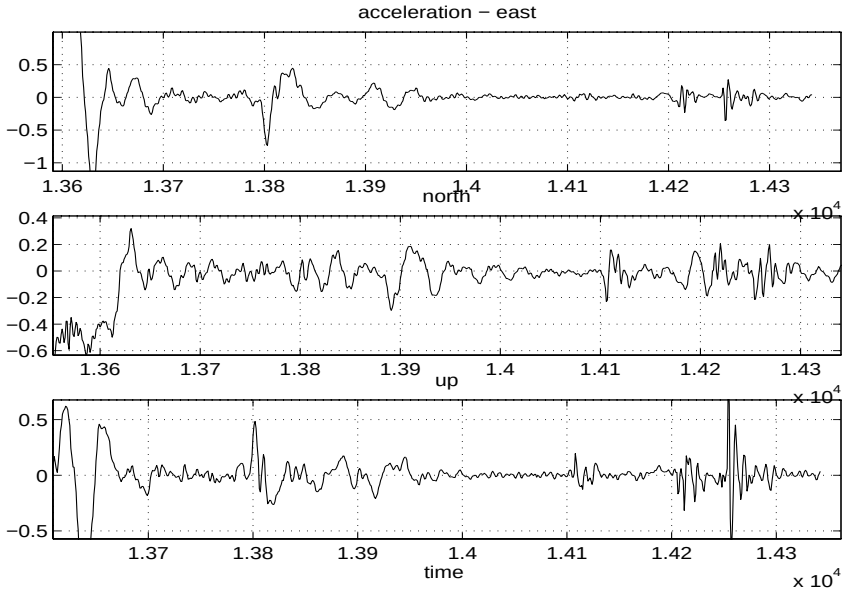

Figure 6.26: At the end of the run, the acceleration of the INS output in the $p-$frame is very close to zero with DCM correction. The unit of the acceleration is m/s^2.

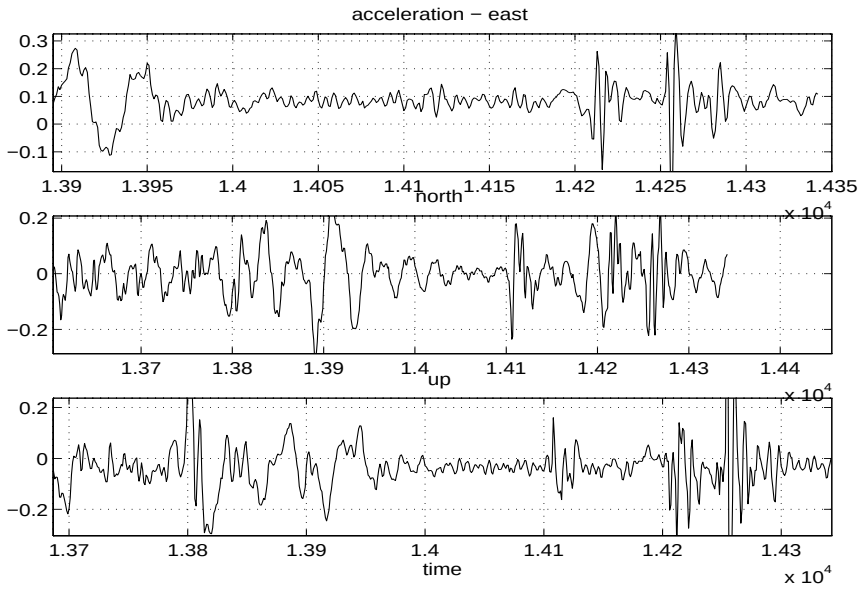

Figure 6.27: The acceleration of the INS output in the end is not zero without DCM correction. The unit in the plot is m/s^2.

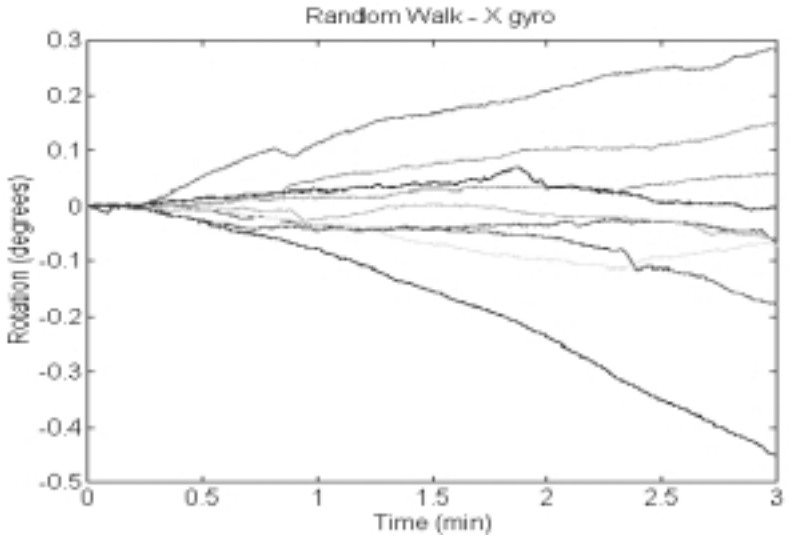

Figure 6.28: Random walk of the gyro x in 3 minutes.

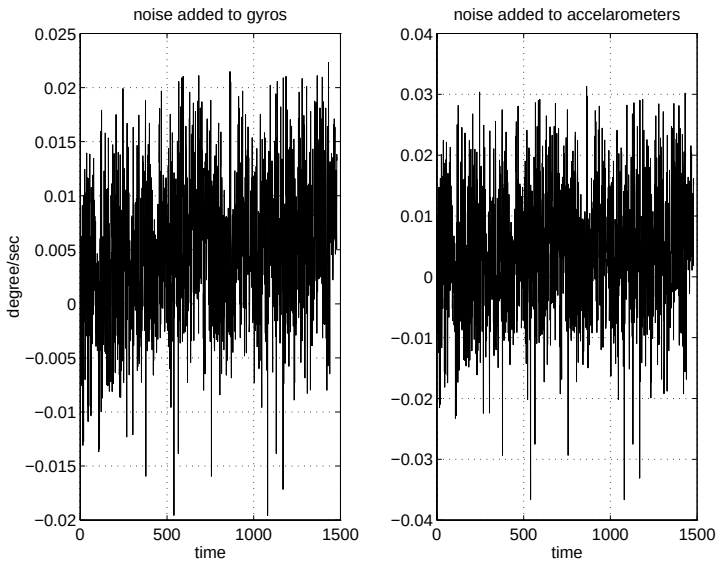

Figure 6.29: The noise added to the three accelerometers and the three gyros was approximately 3 times larger than the standard noise of the Watson IMU. The unit of the acceleration noise is m/s^2.

larger than the standard noise of the Watson IMU. The drift rate of the perturbed gyro noise is shown in Figure 6.29 and is now about 0.3 $degree/\min$.

The alignment results can be seen in Figure 6.30 and Figure 6.31.

At the end of the run, the rotation rate and the acceleration should be close to zero. In Figure 6.30, the rotation rate without filter calibration in 3 gyros is about 0.3 $degree/sec$ while it is approximately zero with the alignment algorithm. Similar results are obtained with acceleration as shown in Figure 6.31. The acceleration in the platform frame at the end is close to zero with the calibration of the filter when the acceleration is perturbed.

These results prove that the biases in gyros and accelerometers are properly estimated.

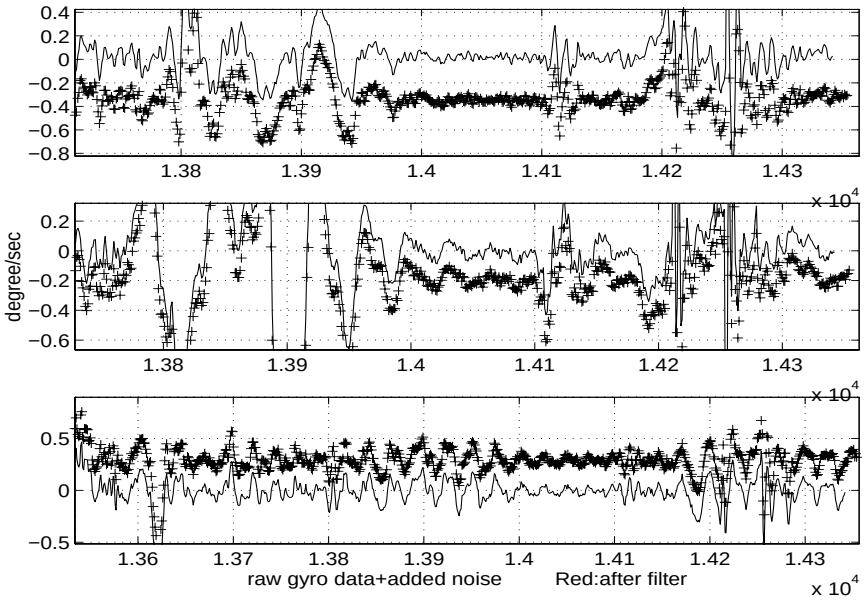

Figure 6.30: The INS rotation rate at the end of the run when the vehicle is stationary should be zero. The solid curve is the rotation rate after calibration by the filter. It is close to zero. The 'plus +' curve is the rotation rate without calibration.

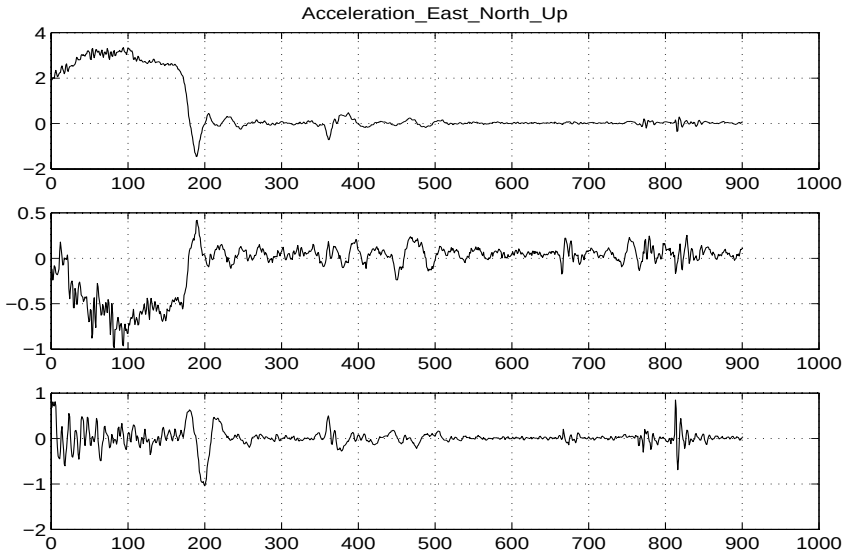

Figure 6.31: With perturbed acceleration, at the end of the run, the acceleration in the platform frame is close to zero after calibration by the filter.

6.4 Experimental Results of the Quaternion Algorithm

The quaternion algorithm developed in this thesis is demonstrated using the experimental results in this section. The experimental data used in the previous section and shown in Figure 6.19, 6.20 and 6.21 were used to test the algorithm.

The filter state X is given by:

$$X = [\Delta V_x^c, \Delta V_y^c, \Delta V_z^c, \Delta R_x^c, \Delta R_y^c, \Delta R_z^c, q_0, q_1, q_2, q_3]^T \tag{6.2}$$

where

$[\Delta V_x^c, \Delta V_y^c, \Delta V_z^c]^T$ is the INS velocity error vector in the computer frame.

$[\Delta R_x^c, \Delta R_y^c, \Delta R_z^c]^T$ is the INS position error vector in the computer frame.

$[q_0, q_1, q_2, q_3]^T$ is the quaternion representing the error between the computer frame and the platform frame.

The Distribution Approximation Filter starts with arbitrary initial quaternions. The vehicle trajectory starts from $(0, 0)$ of the local level frame which is at the right bottom corner of the Figure 6.32. The INS outputs wrong navigation information at the beginning of the run due to incorrect alignment. The position and heading correction can be appreciated in this figure after 60 filter iterations, which is about 20 seconds. The heading error is corrected to less than $\pm 2^\circ$. Figure 6.33 shows this heading correction.

The quaternion errors are shown in Figure 6.34. After 60 filter iterations which is approximately 20 seconds, the quaternion errors become very close to $[1, 0, 0, 0]^T$, which represents a zero rotation between the computer frame and the platform frame. Figure 6.35 is an enhanced view of the four elements of the quaternion errors at around 40 seconds of the vehicle running time.

The accelerations in the three axes of the platform frame are shown in Figure 6.36. At the end of the run, the true acceleration in the platform should be zero. Figure 6.37 is the enhanced view of the calculated acceleration in the platform frame. The

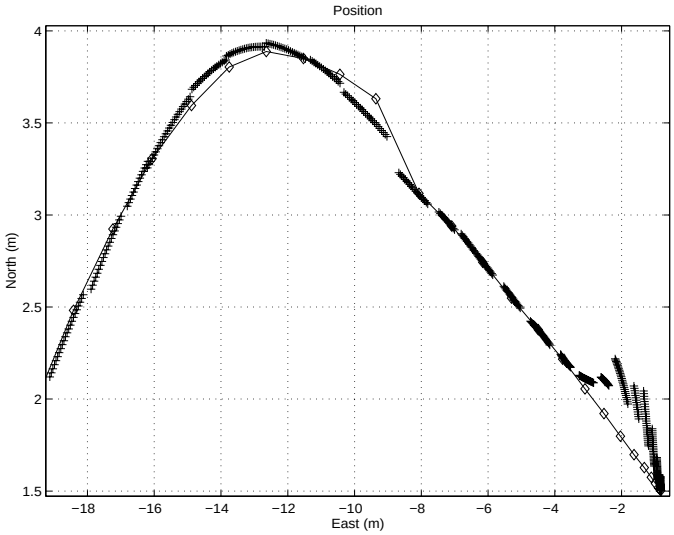

Figure 6.32: At the beginning, the INS is uncertain within $\pm 180^\circ$. After 60 iterations of the filter, the INS heading error is corrected to less than $\pm 5^\circ$.

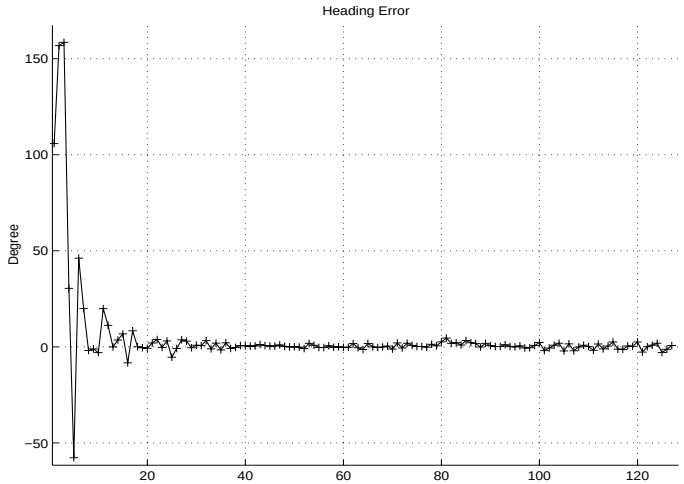

Figure 6.33: The INS heading error is diminished to small angles after 60 iterations of the filter.

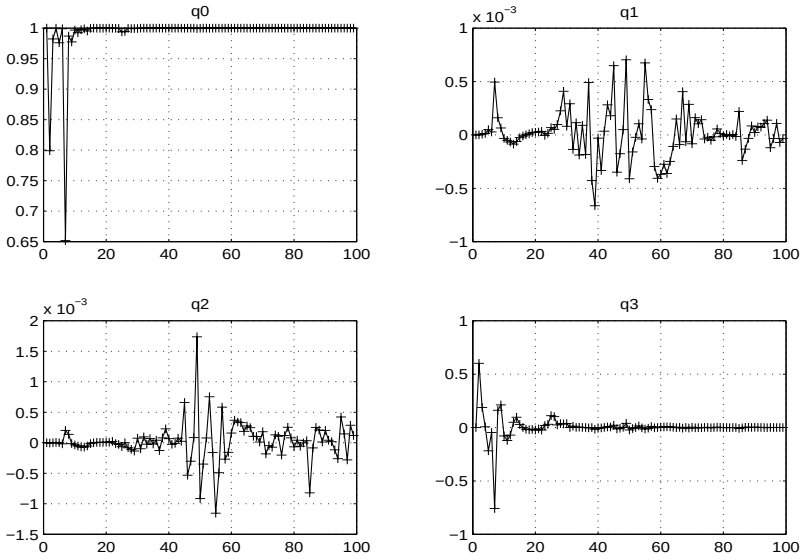

Figure 6.34: Quaternions are corrected after each filter time.

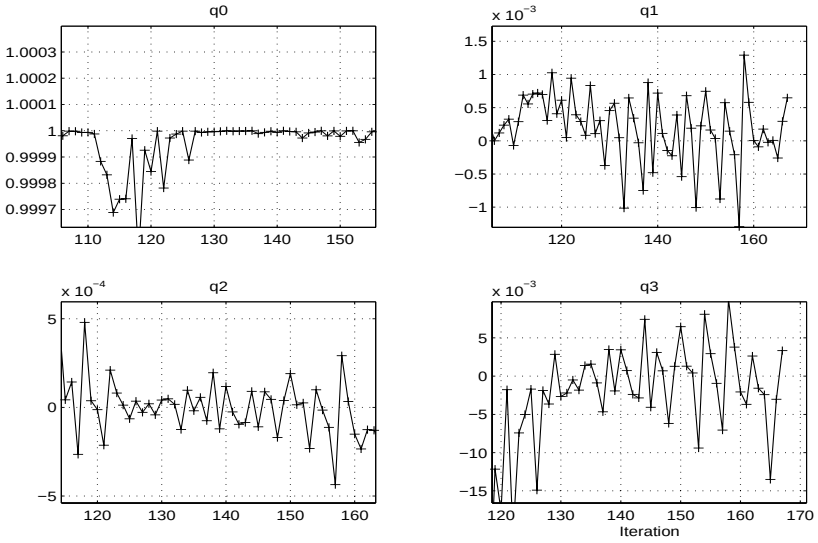

Figure 6.35: The enhanced view of the quaternion errors between the filter iteration 100 to 160 which correspond to the vehicle running time 25 seconds to 45 seconds. The four elements are very close to $[1, 0, 0, 0]^T$ which represents quaternions of a zero rotation from the computer frame to the platform frame.

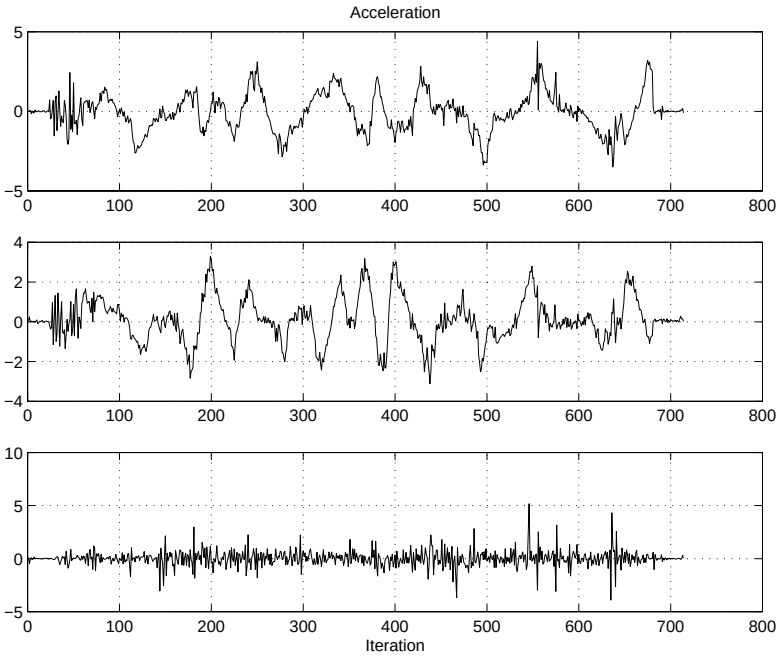

Figure 6.36: Accelerations in the three axes of the platform frame. The unit of the plot is m/s^2.

acceleration in axis x and axis z are very close to zero. The error in axis y is about 0.08 m/s^2.

The attitude errors in the three axes are shown in Figure 6.38. The tilt errors are less than $\pm 0.04°$. The heading errors are within $\pm 0.5°$.

The velocity and position errors at the end of the run can be seen in Figure 6.39. The velocity errors are within $0.5m/s^2$. The position errors are within $0.2m$.

Figure 6.40 shows the position curves of the INS and GPS outputs after 170 seconds of the run. In this run the sampling frequency of the GPS is about 5Hz. The INS position prediction matches the GPS position plot which is the label "o" in the plot.

Figure 6.41 is an enhanced view of this position match. The INS position output is as the solid curve. The GPS position output is as the curve "o".

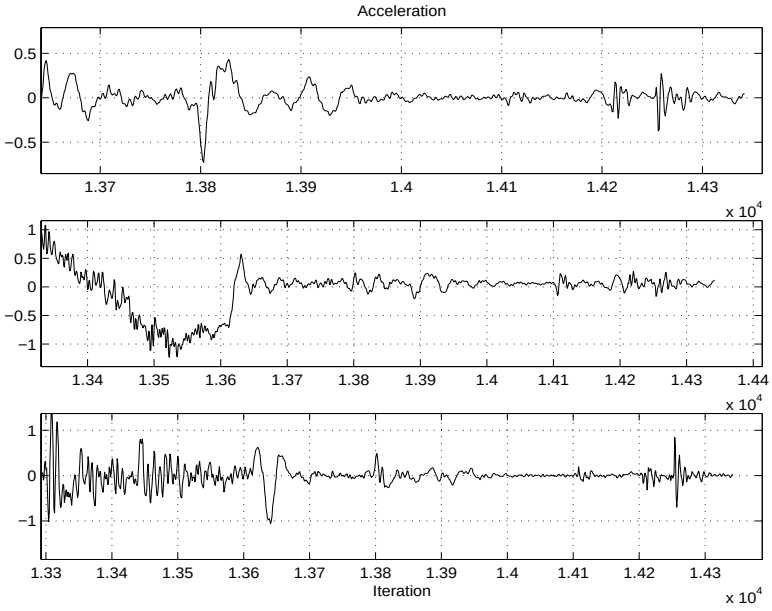

Figure 6.37: At the end of the run, the vehicle is stationary. The accelerations in the three axes of the platform frame are very close to zero.

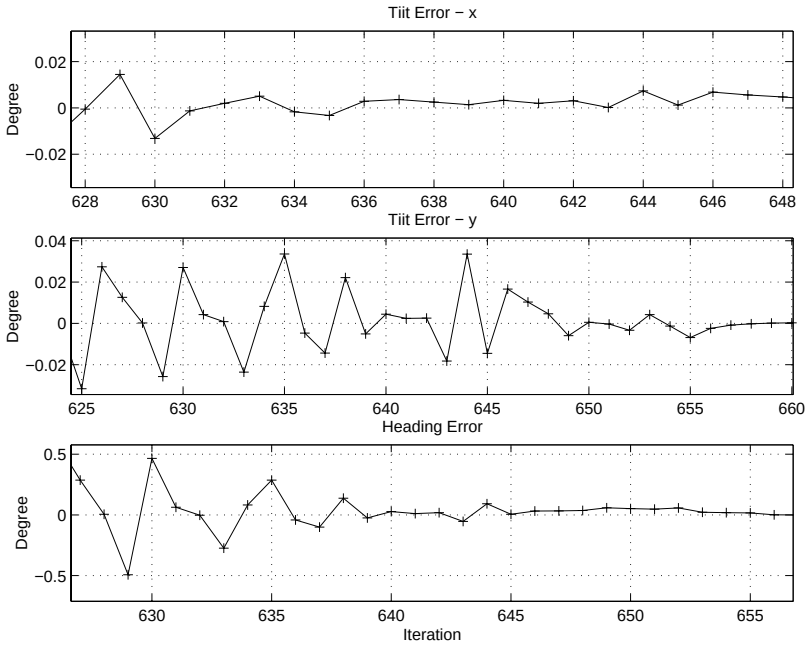

Figure 6.38: Tilt errors are less than $\pm 0.04°$. Heading errors are within $\pm 0.5°$.

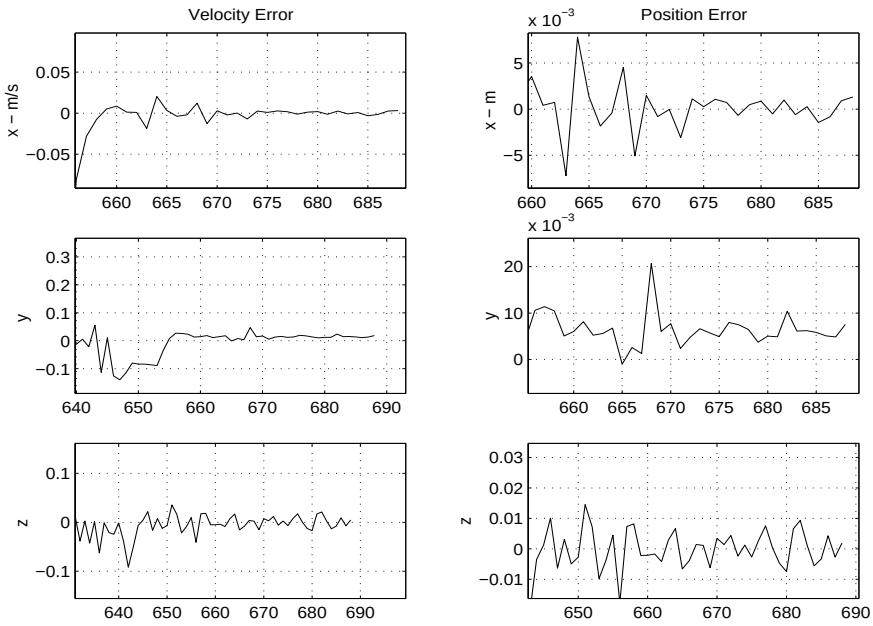

Figure 6.39: The velocity errors are within 0.1 m/s. The position errors are within 0.02 m.

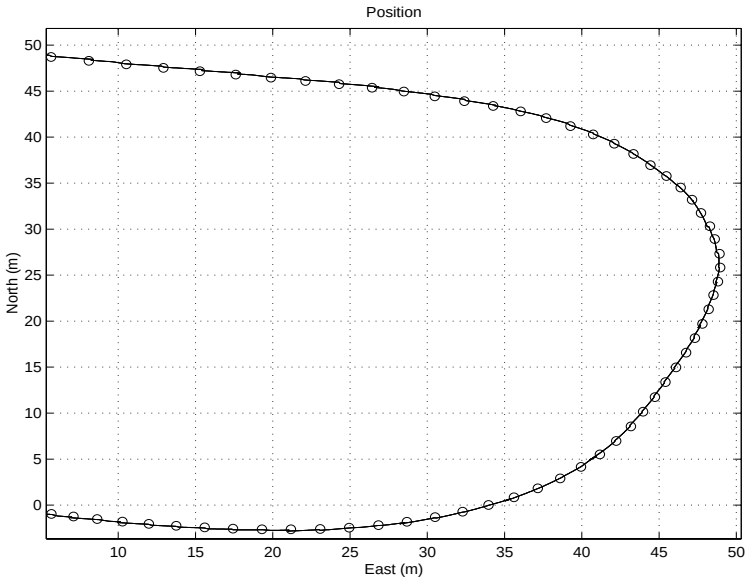

Figure 6.40: The solid curve is the INS position output. Curve "o" is the GPS position output. INS outputs position data with the frequency of $84Hz$ between two GPS position outputs.

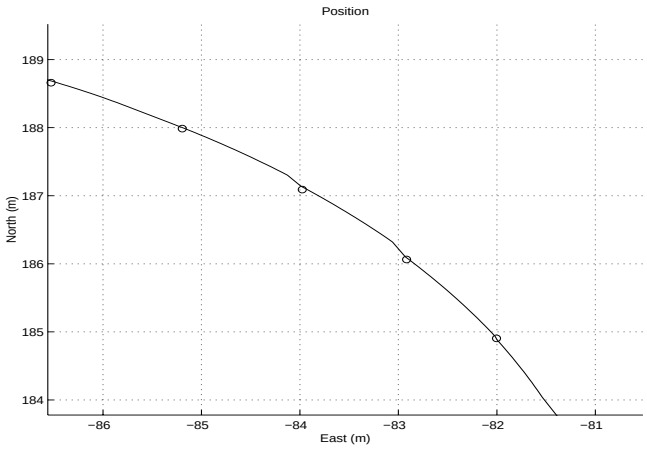

Figure 6.41: INS Position and heading corrections can be seen in the curve between two GPS position outputs.

6.5 Summary

The GPS modelling results have verified the modelling theory and techniques in the frequency domain developed in this thesis.

The experimental results in this chapter have verified the psi angle and the quaternion models for low cost INS developed in this thesis.

These results have shown that for a low cost INS with aiding GPS information, position, velocity and attitude accuracy can be achieved using the INS algorithms in the psi angle approach and the quaternion approach presented in this thesis.

Chapter 7

Summary and Conclusions

7.1 Introduction

This chapter summarizes the major contributions of this thesis, draws conclusions and makes suggestions for future research.

In Section 7.2, a chapter by chapter summary of this thesis is presented. Section 7.3 highlights the major contributions of this thesis. Finally, Section 7.4 reviews some of the limitations of the work and future research in this area is suggested.

7.2 Summary of Each Chapter

Chapter 1 provided the primary motivation for the work carried out in this thesis. It is argued that INS errors determine the behaviour and the accuracy of an INS. The error model is the tool for error analysis. Advanced INS algorithms are based on error modelling. For a low cost INS with less accurate resolution, INS errors are large. INS error models for large attitude errors are needed.

A short survey of INS error models was given in this chapter. The psi angle approach or the computer frame approach and the phi angle approach or the true frame approach are two modelling approaches which were investigated.

This chapter introduced the main research theme of this thesis - the development of

INS error models for large attitude errors in the computer frame approach with both psi angle form and quaternion form, and the development of two integrated INS algorithms for a low cost INS. These two algorithms were aided by the GPS. GPS modelling in the frequency domain was also discussed extensively.

In **Chapter 2,** the generic INS error propagation models for large attitude errors in the psi angle approach and the quaternion approach were presented.

A short survey of INS error models was given in Section 2.2. This survey showed that two approaches have been adopted in the literature: the psi angle approach (or the computer frame approach) and the phi angle approach (or the true frame approach). So far, there are no generic error propagation models for three large attitude errors. All the quaternion error models in the literature are based on small angle assumption.

Section 2.3 developed INS error propagation models for large errors in the psi angle approach. There are three models: the velocity error model, the position error model and the attitude model. The attitude errors were presented using three psi angles. In this case, the three attitude errors can be assumed to be large with uncertainties of $\pm 180^{\circ}$.

It was argued that INS attitude updating using quaternions provides more accuracy, requires less computation and avoids singularity in computation. This motivated the development of another set of INS models in quaternion form for large errors in Section 2.4. The computer frame approach was also used in this model. Quaternion errors were presented using the quaternions between the platform frame and the computer frame. Differing from other quaternion models, these models make no assumption of small angle errors.

Chapter 3 presented the identification of GPS error models using frequency domain techniques.

It is argued that the navigation problem can be generally split into two components: creating a process model of the host vehicle and understanding or modelling the sensors to be used. The process model of a navigation system describes the prediction of states which are typically the position, velocity, attitude and related parameters affecting

these variables. This chapter detailed the modelling of the GPS measurement which is used to aid INS navigation.

Section 3.2 reviewed previous work on GPS modelling in the frequency domain. This review showed that a GPS position error model has not been theoretically developed in the frequency domain. Section 3.3 derived a GPS position error model. It is proved that the transfer function of the GPS position error in any frame has the identical poles and zero as the pseudo-range error. A modelling method using power spectral density of the noise was presented in Section 3.4. Section 3.5 examined the de-correlation of the GPS coloured noise. A shaping filter was introduced to the de-correlation filter. An additional sensor is required for de-correlation. Feedforward filter and feedback filter with the INS and GPS measurements were analyzed in both the frequency domain and the time domain to determine the quality of aiding sensors to perform de-correlation.

Chapter 4 designed a low cost INS algorithm with unknown initial conditions using the psi angle approach in the computer frame.

The INS alignment algorithms were reviewed in Section 4.2. This review showed that the analytic coarse alignment method and gyrocompassing are the major methods for self-alignment. They require the measurements of the gravity vector and the earth rate by three accelerometers and three gyros. In-motion alignment is also used for INS fine alignment and was reviewed. It is shown that most of the applications in the literature for in-motion alignment were based on filters with known initial attitudes. For a low cost IMU with low resolution, the initial attitude errors are large. The algorithms to solve this problem were reviewed.

In this chapter, a new algorithm was developed in the computer frame approach that can be used with unknown initial attitudes.

Section 4.3 described the on ground coarse alignment for low cost IMUs. This algorithm also takes into account the turn-on biases estimation. The coarse initial direction cosine matrix was formulated.

The solution of unknown initial attitudes was presented in Section 4.4 using an in-motion alignment algorithm. A filter with error propagation models for large error

angles in the computer frame was developed. The filter was implemented using the Extended Kalman Filter (EKF).

Chapter 5 dealt with the issue of developing an INS algorithm for a low cost IMU using quaternions in the computer frame.

Section 5.2 described independent INS navigation using quaternions. Quaternion initialization was formulated. A 2-step Adams-Bashford method was introduced for quaternion update.

The quaternion algorithm to deal with unknown initial attitudes was developed in Section 5.3. The quaternion errors were exploited using the misalignment of the computer frame and the platform frame. The entire filter process model structure and the process noise were presented. The process noise vectors were reconstructed using the linear combination of the white noise on the accelerometers and gyros in the body frame. A Distribution Approximation Filter (DAF) was used to implement this algorithm. The principle and the benefit of the DAF were briefly described.

Chapter 6 presented the experimental results for the INS algorithms using the psi angle approach, the quaternion algorithm and the GPS modelling.

The results of GPS modelling in the frequency domain were presented in Section 6.2. The GPS model was validated using a set of plots in the frequency domain and the time domain using a feedback de-correlation filter.

Section 6.3 presented the experimental results to verify the psi angle models and the INS algorithm for low cost IMUs using these models. The experiment used a low cost IMU aided by a DGPS. The results demonstrated how the heading errors were corrected. INS alignment and calibration results were also presented in this section.

Section 6.4 outlined the experimental results of the quaternion algorithm. INS errors in acceleration, velocity, position, attitude and quaternions were examined.

These results have shown that for a low cost INS with aiding GPS information, position, velocity and attitude accuracy can be achieved using the INS algorithms presented in this thesis.

7.3 Contributions

The major contributions of this thesis are the development of the error models and the applications of the models to integrated INS algorithms. This section outlines the individual contributions of this thesis.

7.3.1 INS Error Modelling in Psi Angle Approach

This thesis presents two new INS error propagation models for large angle errors.

Two approaches to generate INS models are investigated in the literature: the psi angle approach or the computer frame approach and the phi angle approach or the true frame approach. The two approaches yield identical results. Most of the models in the literature have assumed that either the three attitude errors are small or the two tilt errors are small and one heading error is large.

The psi angle approach was used in this thesis for the development of the INS models. There are three equations in this psi angle model for large attitude errors: the velocity error propagation equation, the position error propagation equation and the psi angle equation. This model differs from other models in that it does not rely on the small angle assumption and can accommodate three large attitude errors. Three independent states were used to describe the three psi angles in the computer frame. The model with three small attitude errors becomes a special form of this model. The model for one large heading error and two small tilt errors is also a special case of the model.

7.3.2 INS Error Modelling Using the Quaternion Approach

Another important contribution of this thesis is the INS model in quaternion form. The model equations are also in the computer frame. There are three sets of equations: the velocity error propagation equation using quaternions, the position error propagation equation and the quaternion error propagation equation. The model differs from other quaternion models in the literature in that it makes no assumption of small attitude

errors. The model is suitable for both small and large angles.

7.3.3 GPS Modelling in Frequency Domain

GPS modelling in the frequency domain is another contribution of this thesis. Unlike other GPS modelling in previous work that modelled the errors of the pseudo range and the clock offset, this approach models the GPS position error reported by standard GPS. The equations of GPS correlated errors in position were derived as second order systems in the frequency domain. Power spectral density (PSD) plots were used as the tool to obtain the model parameters.

This thesis also presented a feedback filter and a feedforward filter for GPS error de-correlation using INS information. The essential requirement for the variance of the INS noise for de-correlation was presented using frequency domain techniques.

7.3.4 INS Algorithm for Low Cost IMU Using Psi Angle Approach

An important contribution of this thesis is the INS algorithm using the psi angle approach. This algorithm was designed for a low cost INS whose resolution is low to perform INS self-alignment. The main contribution is the in-motion alignment to solve the initial attitude uncertainty.

The algorithm includes raw data process, coarse leveling, in-motion alignment and calibration. A GPS shaping filter is introduced in the filter model. When a high accuracy DGPS was used, the error of the DGPS was modelled as white noise. The filter procedure using the EKF was formulated. After the attitude errors diminish to small angles, the filter still works using the psi angle model in its small angle form which is a special case of the psi angle model. The biases of the accelerometers and gyros were modelled and calibrated in-motion. This algorithm combines INS alignment, calibration and navigation under one filter.

7.3.5 INS Algorithm for Low Cost IMU Using Quaternion Model

Another contribution of this thesis is the INS algorithm using the quaternion model for low cost inertial systems with low resolution which are not able to conduct self-alignment.

It is argued that computing the INS attitude using quaternions has more advantages than using Euler angles and the direction cosine matrix. The INS alignment and calibration were implemented in-motion using a nonlinear filter whose process models were the INS error propagation models using quaternions. To avoid deriving the Jacobian matrices of the filter, the Distribution Approximation Filter was used in this algorithm.

7.4 Future Work

7.4.1 DGPS Modelling

This thesis developed GPS modelling in the frequency domain. A shaping filter was described. This GPS model is useful for a stand alone GPS with a position error of 20-100m. In the experimental implementation of the INS algorithms in this thesis, a high accuracy DGPS was used instead of a stand alone GPS. The accuracy of this DGPS was 2cm. The error of this DGPS was modelled as white noise. Future work could model the DGPS in the frequency domain to achieve higher accuracy of the navigation system.

In this thesis, a "loose-coupling" mode is used to fuse the INS and GPS. In this mode the INS and the GPS are treated as navigation systems. The calculated GPS position and velocity are used. When a "tight-coupling" mode is used, the INS and GPS receiver are treated as individual sensors. The raw data of the GPS pseudo range and carrier phase are used directly. Further modelling of these raw data in the frequency domain could be another interesting area.

7.4.2 Experimental Implementation of the INS Algorithms with Three Unknown Attitudes

The INS algorithms developed in this work are theoretically designed for all unknown attitudes. In the real time experimental implementation, two tilt gyros were available in the IMU to reduce initial tilt errors to small angles. Only one heading error was large in the experiment.

Further experimental work could be extended without using tilt gyros.

7.4.3 Self Tuning Filters

In the experimental implementation for these INS algorithms, the performance of the filters was influenced by the choice of the process noise attributes. Currently, the noise strengths were chosen by engineering judgement and experience. An important area for future work could be to develop methods which are able to identify the strengths of the process noise from the collected raw data. Consequently these future self-tuning filters could lead to consistent and accurate performance in real time implementation.

7.4.4 Phi Angle Model for Large Attitude Errors

The psi angle approach and the phi angle approach are adopted in the literature. The psi angle approach in the computer frame was used to develop the INS models and the integrated algorithms for low cost INS in this thesis.

A phi angle model in the true frame for large attitude errors could be an interesting research area for future work. The quaternion models for large attitude errors in the phi angle approach could also be studied in the future.

Bibliography

[1] D. H. Titterton and J. L. Weston. *Strapdown Inertial Navigation Technology* . Peter Peregrinus on behalf of the Institution of Electrical Engineers, London, 1997.

[2] SAGEM Australasia. Sensor II operating manual and interface guide, 1995.

[3] Drora Goshen-Meskin and Itzhack Y. Bar-Itzhack. Unified approach to inertial navigation system error modeling. *Journal of Guidance, Control and Dynamics*, 15(3):648–653, 1992.

[4] Itzhack Y. Bar-Itzhack, Berman N. Control theoretic approach to inertial navigation systems. *Journal of Guidance and Control*, 11(3):237–245, May-June 1988.

[5] Donald O.Benson. A comparison of two approaches to pure-inertial and doppler-inertial error analysis. *IEEE Aerospace and Electronic Systems*, AES-11(4):447–455, July 1975.

[6] Itzharck Y. Bar-Itzhack. Identity between INS position and velocity error models. *Journal of Guidance and Control*, 4:568–570, Sept-Oct 1981.

[7] Itzharck Y. Bar-Itzhack. Identity between INS position and velocity error equations in the true frame. *Journal of Guidance and Control*, 11(6):590–592, 1988.

[8] S. P. Dmitriyev, O. A. Stepanov and S. V. Shepel. Nonlinear filtering methods application in INS alignment. *IEEE Aerospace and Electronic Systems*, AES-33(1):260–271, January 1997.

[9] Bruno M. Scherzinger and D.Blake Reid. Modified strapdown inertial navigation error models. *Proceedings of 1994 IEEE Position, Location and Navigation Symposium - PLANS'94. Las Vegas, NV, USA. IEEE Aerosp. and Electron. Syst. Soc.* , pages 426–430, 1994.

[10] Bruno M. Scherzinger. Inertial navigation error models for large heading uncertainty. *Proceedings of PLANS*, pages 477–484, 1996.

[11] B. Barshan and H. F. Durrant-Whyte. Inertial navigation systems for mobile robots. *IEEE Trans. on Robotics and Automation*, 11(3):328–342, June 1995.

[12] J. Vaganay and M. J. Aldon. Attitude estimation for a vehicle using inertial sensors. *Proceedings the 1st IFAC International Workshop on Intelligent Autonomous Vehicles*, pages 89–94, April 1993.

[13] Hyung Keun Lee, Jang Gyu Lee, Yong Kyu Roh and Chan Gook Park. Modeling quaternion errors in SDINS: computer frame approach. *IEEE Transactions on Aerospace and Electronic Systems*, 34(1):289–297, January 1998.

[14] Bernard Friedland. Analysis strapdown navigation using quaternions. *IEEE Transactions on Aerospace and Electronic Systems*, AES-14(5):764–768, September 1978.

[15] S. Vathsal. Optimal control of quaternion propagation in spacecraft navigation. *Journal of Guidance, Control and Dynamics*, 9(3):382–384, May-June 1986.

[16] Phillip J. Fenner. Requirements, application and result of strapdown inertial technology to commercial airplanes. Technical Report AD-P003 622, Boeing Commercial Airplane Company.

[17] Steven Scheding. *High Integrity Navigation.* PhD thesis, The University of Sydney, 1997.

[18] C. K. Chui and G. Chen. *Kalman Filtering with real-time applications.* Springer-Verlag, 1987.

[19] Simon J. Julier. *Process Models for the Navigation of High Speed Land Vehicles.* PhD thesis, University of Oxford, 1997.

[20] S. J. Julier, J. K. Uhlmann and H. F. Durrant-Whyte. A new approach for filtering nonlinear systems. *Proceedings of the 1995 American Control Conference, Seattle, Washington*, pages 1628–1632, 1995.

[21] S. J. Julier, J. K. Uhlmann and H. F. Durrant-Whyte. A new approach for the nonlinear transformation of means and covariances in linear filters. *IEEE Transactions on Automatic Control*, 1996.

[22] S. J. Julier and J. K. Uhlmann. A new extension of the Kalman filter to nonlinear systems. *The Proceedings of AeroSense: The 11th International Symposium on Aerospace/Defense, Session: Multi Sensor Fusion, Tracking and Resource Management II*, 1997.

[23] S. J. Julier and J. K. Uhlmann. A consistent, debiased method for converting between polar and cartesian coordinate systems. *The Proceedings of AeroSense: The 11th International Symposium on Aerospace/Defense Sensing, Simulation and Controls, Orlando, Florida. Session: Acquisition, Tracking and Pointing XI*, 1997.

[24] Abraham Weinred and Itzhack Y.Bar-Itzhack. The psi-angle error equation in strapdown inertial navigation systems. *IEEE Aerospace and Electronic Systems*, AES-14(3):539–542, May 1978.

[25] N. Lovren and J. K. Pieper. Error analysis of direction cosine and quaternion parameters techniques for aircraft attitude determination. *IEEE Transactions on Aerospace and Electronic Systems*, 34(3):983–989, July 1998.

[26] George Arshal. Error equations of inertial navigation. *Journal of Guidance, control and dynamics*, 10:351–358, July-Aug 1987.

[27] Kenneth R. Britting. *Inertial Navigation System Analysis.* Wiley-Interscience, 1971.

[28] Tuan Manh Pham. Kalman filter mechanization for INS airstart. *IEEE AES System Magazine*, pages 3–11, January 1992.

[29] Stergios I. Roumeliotis, Gaurav S. Sukhatme and George A. Bekey. Smoother based 3d attitude estimation for mobile robot localization. *Proceedings of the 1999 IEEE International Conference on Robotics and Automation*, pages 1979–1986, May 1999.

[30] John L. Crassidis and F. Landis Markley. Minimum model error approach for attitude estimation. *Journal of Guidance, Control and Dynamics*, 20(6):1241–1247, November-December 1997.

[31] Xiaoying Kong, E. Nebot and H. Durrant-Whyte. Development of a non-linear psi-angle model for large misalignment errors and its application in INS alignment and calibration. *Proceedings of IEEE International Conference on Robotics and Automation*, pages 1430–1435, May 10-15 1999. Detroit, MI, USA.

[32] Chen Zhe. *Principle of Strapdown Inertial Navigation System.* Beijing University of Aeronautics and Astronautics, 1985.

[33] R. J. Milleken and C. J. Zoller. Principle of operation of NAVSTAR and system characteristics. *Global positioning system : papers published in Navigation*, 1:3–14, 1993.

[34] E. M. Nebot, H. Durrant-Whyte, S. Scheding. Frequency domain modeling of aided GPS with application to high-speed vehicle navigation. *IEEE International Conference on Robotics and Automation, New Mexico*, pages 1892–1897, April 1997.

[35] Institute of Navigation. *Global positioning system : papers published in Navigation*, volume 1-4. Washington, D.C. Institute of Navigation, 1980-1993.

[36] Bertrand Merminod. *The use of Kalman filters in GPS navigation.* PhD thesis, The University of New South Wales, Australia, 1989.

[37] Clifford Meth. With GPS, you can get there from here. *Electronic Design*, November 1995.

[38] G. D'este R. Zito and M. A. Taylor. Global positioning system in the time domain: How useful a tool for intelligent vehicle-highway systems. Technical Report 4, University of South Australia, 1995.

[39] Bertil Ekstrand. Analytical steady state solution for a Kalman tracking filter. *IEEE Transactions on Aerospace and Electronic Systems*, 19(6):815–819, November 1983.

[40] Steven R. Rogers. Alpha-Beta filter with correlated measurement noise. *IEEE Transactions on Aerospace and Electronic Systems*, 23(4):592–594, July 1987.

[41] Steven R. Rogers. Continuous-time ECV and ECA track filters with colored measurement noise. *IEEE Transactions on Aerospace and Electronic Systems*, 26(4):663–666, July 1990.

[42] C. C. Arcasoy, B. Koc. Analytical solution for continuous-time Kalman tracking filters with colored measurement noise in frequency domain. *IEEE Transactions on Aerospace and Electronic Systems*, 30(4):1059–1063, October 1994.

[43] Ralph Mason Joe M. Toth and Ken J. Runtz. Precise navigation using adaptive FIR filtering and time domain spectral estimation. *IEEE Transactions on Aerospace and Electronic Systems*, 30(4):1071–1076, October 1994.

[44] R. A. Walker and K. Kubik. Parabolic equation modelling of GPS signal propagation and RF communication links in the open mining enviroment. *Proceedings of Fourth International Symposium on Mine Mechanisation and Automation*, 2:B6–47–B6–55, July 1997.

[45] Simon Cooper. *A frequency response method for sensor suite selection with an application to high-speed vehicle navigation.* PhD thesis, Oxford University, June 1996.

[46] H. Lichtenegger B. Hofmann-Wellenhof and J. Collins. *Global Positioning System : Theory and Practice.* Wien ; New York : Springer, 1993.

[47] D. K. Anand. *Introduction to Control Systems*, volume 8 of *International series on system and control.* Pergamon Press, University of Maryland,USA, 2nd edition, 1984.

[48] Benjamin C. Kuo. *Automatic Control Systems.* Englewood Cliffs, N.J. : Prentice-Hall, 3rd edition, 1975.

[49] Peter S. Maybeck. *Stochastic models, estimation and control*, volume 141 of *Mathematics in science and engineering.* New York : Academic Press, 1979-1982.

[50] Paul G. Savage. Strapdown inertial navigation integration algorithm design Part 1: Attitude algorithm. *Journal of Guidance and Control*, 21(1):19–28, January-February 1998.

[51] Paul G. Savage. Strapdown inertial navigation integration algorithm design Part 2: Velocity and position algorithm . *Journal of Guidance and Control*, 21(2):208–221, March-April 1998.

[52] Itzhack Y. Bar-Itzhack. Azimuth observability enhancement during inertial navigation system in-flight alignment. *Journal of Guidance and Control*, 2(4):337–344, July-August 1980.

[53] Yeon Fuh Jiang and Yu Ping Lin. Error estimation in ground alignment through observation analysis. *IEEE Transactions on Aerospace and Electronic Systems*, 28(1):92–97, January 1992.

[54] Yeon Fuh Jiang. Error analysis of analytic coarse alignment methods. *IEEE Transactions on Aerospace and Electronic Systems*, 34(1):334–337, January 1998.

[55] Heung Won Park, Jang Gyu Lee and Chan Gook Park. Multiposition alignment of strapdown inertial navigation system. *IEEE Transactions on Aerospace and Electronic Systems*, AES-29(4):1323–1328, October 1993.

[56] Heung Won Park, Jang Gyu Lee and Chan Gook Park. Covariance analysis of strapdown INS considering gyrocompass characteristics. *IEEE Transactions on Aerospace and Electronic Systems*, AES-31(1):320–328, January 1995.

[57] J. C. Huang, H. V. White. Self-alignment techniques for inertial measurement units. *IEEE Transactions on Aerospace and Electronic Systems*, AES-11(6):1232–1247, November 1975.

[58] Frank D. Jurenka and Cornnelius T. Leondes. Optimum alignment of an inertial autonavigator. *IEEE Transactions on Aerospace and Electronic Systems*, AES-3(6):880–888, November 1967.

[59] Itzhack Y. Bar-Itzhack. Two misconceptions in the theory of inertial navigation systems. *Journal of Guidance and Control*, 18(4):908–911, 1990.

[60] Itzhack Y. Bar-Itzhack. The enigma of false bias detection in a strapdown system during transfer alignment. *Journal of Guidance and Control*, 8(2):175–180, March-April 1985.

[61] Cristopher C. Ross and Timothy F. Elbert. A transfer alignment algorithm study based on actual flight test data from a tactical air-to-ground weapon launch. *Proceedings of IEEE PLANS*, pages 431–438, 1994.

[62] Boaz Porat, Itzhack Y. Bar-Itzhack. Effect of acceleration switching during INS in-flight alignment. *Journal of Guidance and Control*, 4(4):385–389, July-August 1981.

[63] Itzhack Y. Bar-Itzhack. Optimal updating of INS using sighting devices. *Journal of Guidance and Control*, 1(5):305–312, Sept.-Oct. 1978.

[64] Averil B. Chatfield. *Fundamentals of High Accuracy Inertial Navigation*, volume 174 of *Progress in Astronautics and Aeronautics*. American Institute of Aeronautics and Astronautics, Inc., 1997.

[65] Shmuel Merhav. *Aero Sensor System and Applications.* Springer-Verlag New york,Inc., 1996.

[66] Yeon Fuh Jiang, Yu Ping Lin. Error estimation of ground alignment to arbitrary azimuth. *IFAC*, (AIAA-93-3823-CP):1088–1093, 1993.

[67] R. M. Rogers. IMU in-motion alignment without benefit of attitude initialization. *Navigation*, 44(3):301–311, Fall 1997.

[68] Xiaoying Kong, Eduardo Nebot and Hugh Durrant-Whyte. Use quaternions in a low cost strapdown INS unit. *Proceedings of the International Conference on Field and Service Robotics, Canberra, Australia*, pages 286–291, 1997.

[69] Fan Yaozu and Xu Dahua. *Test and Modeling of Inertial Sensors.* Aerospace Press: Beijing, 1985.

[70] Richard P.Wishner Michael Athans and Anthony Bertolini. Suboptimal state estimation for continuous-time nonlinear system from discrete noisy measurements. *IEEE Transaction on Automatic Control*, AC-13(5):504–514, October 1968.

[71] Robert Grover Brown and Patrick Y.C. Hwang. *Introduction to random signals and applied Kalman filtering : with Matlab exercises and solutions.* New York : Wiley, 1997.

[72] Jonh E. Bortz. A new mathematical formulation for strapdown inertial navigation. *IEEE Transactions on Aerospace and Electronic Systems*, AES-7(1):61–66, January 1971.

[73] R. E. Mortensen. Strapdown guidance error analysis. *IEEE Transactions on Aerospace and Electronic Systems*, AES-10(4):451–457, July 1974.

[74] James C. Wilcox. A new algorithm for strapped-down inertial navigation. *IEEE Transactions on Aerospace and Electronic Systems*, AES-3(5):796–802, September 1967.

[75] Yeon Fui Jiang and Yu Ping Lin. Error analysis of quaternion transformations. *IEEE Transactions on Aerospace and Electronic Systems*, 27(4):634–638, July 1991.

[76] Francois Martel, Parimal K. Pal, Mark L. Psiaki. Three-axis attitude determination via Kalman Filtering of magnetometer data. NASA Technical Reports N89-15951, 1989.

[77] Henderson D. M. Shuttle Program. Euler angles, quaternions, and transformation matrices working relationships. NASA Technical Reports NASA-TM-74839, McDonnell Douglas Tech. Services Co., Inc., 1977.

[78] Paul G. Savage. Strapdown system algorithms. NASA Technical Reports 19840017626 N (84N25694), Strapdown Associates, Inc., 1984.

[79] J. L. Michelin and P. Masson. Strapdown inertial system for tactical missiles using mass unbalanced two-axis rate gyros. NASA Technical Reports AD-P003 623.

[80] Edward Pervin and Jon A. Webb. Quaternions in computer vision and robotics. CMU Report CMU-CS-82-150, Carnegie Mellon University, 1982.

[81] Dohyoung Chung, Jang Gyu Lee, Chan Gook Park and Heung Won Park. Equivalence of the quaternion error model for strapdown INS. *Proceedings of Intelligent Autonomous Control in Aerospace Conference. Beijing, PRC*, pages 179–183, 1995.

[82] Arieh Iserles. *A First Course in the Numerical Analysis.* Cambridge University Press, 1996.

[83] Anh Tuan Le. *Modelling and Control of Tracked Vehicles.* PhD thesis, The University of Sydney, 1999.

[84] Blaha R. J. and Gilmore J. P. Strapdown system performance optimization test evaluation. NASA Technical Reports NASA-CR-135484, MIT, 1973.

[85] Peter A. Grundy. Error source recovery INS test flight data. NASA Technical Reports AD-A012 359, Intermetrics, Incorporated, 1975.

[86] Ebner R. Brown A. and Mark J. A calibration technique for a laser gyro strapdown inertial navigation system. *Proceedings of DGON symposium on Gyro technology, Stuttgart, Germany*, 1982.

[87] T. G. Smithson. A review of the mechanical design and development of a high performance accelerometer. *Proceedings of Institute of Mechanical Engineering Conference on Mechanical Technology of Inertial Sensors*, pages C49–87, 1987.

[88] The Institute of Electrical and Electronics Engineers, Inc. IEEE Standard Inertial Sensor Terminology. (IEEE Std 528-1984).

[89] The Institute of Electrical and Electronics Engineers, Inc. IEEE Specification Format for Single-Degree-of-Freedom Spring-Restrained Rate Gyros [Description]. (IEEE Std 292-1969).

[90] The Institute of Electrical and Electronics Engineers, Inc. IEEE Standard Specification Format Guide and Test Procedures for Linear, Single-Axis, Pendulous, Analog Torque Balance Accelerometer [Description]. (IEEE Std 337-1972).

[91] The Institute of Electrical and Electronics Engineers, Inc. IEEE Standard Specification Format Guide and Test Procedure for Single-Degree-of-Freedom Rate-Integrating Gyro [Description]. (IEEE Std 517-1974).

[92] The Institute of Electrical and Electronics Engineers, Inc. IEEE Supplement for Strapdown Applications to IEEE Standard Specification Format Guide and Test Procedure for Single-Degree-of-Freedom Rate-Integrating Gyros. (IEEE Std 529-1980).

[93] The Institute of Electrical and Electronics Engineers, Inc. IEEE Standard Specification Format Guide and Test Procedure for Linear, Single-Axis, Digital, Torque-Balance Accelerometer [Description]. (IEEE Std 530-1978, R1992).

[94] The Institute of Electrical and Electronics Engineers, Inc. IEEE Standard Specification Format Guide and Test Procedure for Single-Axis Laser Gyros[Description]. (IEEE Std 647-1995).

[95] The Institute of Electrical and Electronics Engineers, Inc. IEEE Recommended Practice for Precision Centrifuge Testing of Linear Accelerometers [Description]. (IEEE Std 836-1991 (R1997)).

[96] Watson Industries INC. Inertial measurement unit owner's manual, 1995.